

For Reference

NOT TO BE TAKEN FROM THIS ROOM

Ex LIBRIS
UNIVERSITATIS
ALBERTAENSIS



THE UNIVERSITY OF ALBERTA

A THEORY OF OSCILLATOR NOISE AND ITS
APPLICATION TO IMPATT DIODE OSCILLATORS

by



JOSEF LUDVIK FIKART

A THESIS

SUBMITTED TO THE FACULTY OF GRADUATE STUDIES AND RESEARCH
IN PARTIAL FULFILMENT OF THE REQUIREMENTS FOR THE DEGREE
OF DOCTOR OF PHILOSOPHY

DEPARTMENT OF ELECTRICAL ENGINEERING

EDMONTON, ALBERTA

SPRING, 1973

ABSTRACT

A large-signal theory of oscillator noise is presented, which is applicable to oscillators employing active elements that can be described by a time-dependent differential equation with a Langevin noise source. The method uses a modified quasistationary perturbation theory with an RF amplitude-dependent perturbing noise voltage (current) source, which has been mathematically expressed in terms of the "initial" (pre-oscillation) amplitude- and phase noise modulation rates. The usual requirement that this noise voltage (current) be a member of a normal random process, which results in equality of the two initial power spectra, is not invoked here. The RF amplitude dependence of the open-circuit perturbing noise voltage (short-circuit noise current) has been obtained from the differential equation of the active element, under the condition of sinusoidal current (voltage) excitation at the frequency at which it would normally oscillate. Upon linearizing in stochastic quantities, expanding the deterministic terms by means of Fourier series and Fourier transforming the result, a system of linear equations in the frequency domain is obtained for the noise voltages (currents) at frequencies about multiples of the excitation frequency and at the baseband frequency. In this way, most of the conversion processes in the active element can be taken into account. The Fourier transforms and power spectra of the initial modulation rates have been determined in terms of the upper- and lower sideband noise voltages (currents); they are used in the modified formulas of a quasistationary perturbation theory to obtain the AM-and FM noise spectra of the oscillator output.

The theory has been applied to IMPATT diode oscillators and the computed spectra have been compared with various experimental data. To supplement data already available in the literature, a sensitive noise-measuring system has been assembled, carefully tested and used for amplitude- and frequency noise measurements on IMPATT diodes. The experimental data have been found to be in good agreement with the theoretical predictions.

Additional insight into IMPATT diode noise has been provided, since the above method made it possible to evaluate the individual (and generally different) dependence of the AM-and FM noise spectra on the RF output power of the oscillator as well as on other diode- and circuit parameters. As a result of the theoretical and experimental studies, guidelines have been obtained for determining the optimum parameters of an IMPATT diode oscillator, for minimum noise.

Appreciation is also extended to the following organizations: URE-CIAY (Institute of Radioengineering and Electronics of the Czechoslovak Academy of Sciences), Prague, Czechoslovakia, for enabling the author to study at the University of Alberta.

The financial assistance of the National Research Council of Canada and of the Department of Electrical Engineering, University of Alberta, for the award of a Research Assistantship, and of the University of Alberta for the award of a University of Alberta Graduate Fellowship and for an L.M. Kittum Memorial Fellowship are gratefully appreciated.

The support in part of this research by the Defense Research Board of Canada, under Grant No. 1510-76, is also gratefully acknowledged.

ACKNOWLEDGEMENTS

The author wishes to express his appreciation for the assistance of the following persons during the course of this research:

Dr. P.A. Goud, for his advice and encouragement during the supervision of this work.

Dr. J.R. Ashley, Dr. J. Nigrin and Dr. M.T. Vlaardingerbroek, for advice and stimulating discussions.

Dr. C.G. Englefield, Dr. J. Nigrin, Dr. K. Stromsmoe and Dr. S. Woods, for serving on the Ph.D. Candidacy Committee.

Mr. J. Fearn, for his skillful technical assistance.

Mrs. M.K. Mounteer, for her excellent work in typing this thesis.

Sincere thanks are extended to all the members of the Microwave Electronics Group for helpful discussions and assistance.

The author also thanks his wife, Inka, for her patience, encouragement and help.

Appreciation is also extended to the following organizations: URE-CSAV (Institute of Radioengineering and Electronics of the Czechoslovak Academy of Sciences), Prague, Czechoslovakia, for enabling the author to study at the University of Alberta.

The financial assistance of the National Research Council of Canada and of the Department of Electrical Engineering, University of Alberta, for the award of a Research Assistantship, and of the University of Alberta for the award of a University of Alberta Graduate Fellowship and for an I.W. Killam Memorial Fellowship are greatly appreciated.

The support in part of this research by the Defence Research Board of Canada, under Grant No. 9510-76, is also gratefully acknowledged.

TABLE OF CONTENTS

	Page
I INTRODUCTION	1
1-1 Brief Review of Pertinent Oscillator Noise Theories	1
1-2 Purpose of this Study	7
1-3 Organization of this Thesis	8
II QUASISTATIONARY PERTURBATION THEORY OF NOISE IN FREE- RUNNING OSCILLATORS: MODIFICATION FOR LARGE-SIGNAL CONDITIONS	10
2-1 Principles of the Perturbation Method in Oscillators	10
2-1-1 Oscillator Model with Perturbing Noise Source	10
2-1-2 Representation of the Output Signal and Noise Source; Output Noise Modulation Rates	13
2-1-3 Quasistationary Perturbation Equations	15
2-2 Properties of the Perturbing Noise Source	20
2-2-1 Introduction of the Initial Modulation Rates	20
2-2-2 Properties of Initial Modulation Rates under Small- and Large Signal Conditions	22
2-3 A Review of the Quasistationary Perturbation Theories of Thaler <i>et al.</i> and Vlaardingerbroek	25
2-4 Large-Signal Modification of the Theories of Vlaardingerbroek and Thaler	30
2-5 Simplified Large-Signal Version of Thaler's Theory	33
III SPECTRA OF INITIAL (PRE-OSCILLATION) NOISE MODULATION RATES: LARGE-SIGNAL CALCULATION	37
3-1 Excitation of the Active Element	37

3-2	Mathematical Description of the Active Element; Generalized Langevin Equation for Stochastic Quantities	40
3-3	Fourier Transform of Langevin Equation; Open-Circuit Noise Voltage (Short-Circuit Noise Current)	41
3-4	Fourier Transform and Power Spectral Densities of the Initial Noise Modulation Rates	46
3-5	Computation of Oscillator Noise: General Procedure	48
IV	APPLICATION OF THE NOISE THEORY TO IMPATT DIODE OSCILLATORS	52
4-1	IMPATT Diode Model	53
4-1-1	Avalanching P-N Junction	53
4-1-2	The Read Diode	54
4-1-3	Approximation of Real IMPATT Diodes by Read Diode Equations	60
4-2	Derivation of the Open-Circuit Noise Voltage	62
4-2-1	Excitation of the Diode	62
4-2-2	Langevin Equation for Stochastic Quantities	63
4-2-3	Fourier Transform of Langevin Equation; Open-Circuit Noise Voltage	64
4-3	Computed Noise Spectra	68
4-3-1	Computation: Input Data, Conditions, Procedure	68
4-3-2	Plots of Computed Spectra and Discussion	79
V	NOISE MEASUREMENTS ON IMPATT DIODE OSCILLATORS	93
5-1	The Noise-Measuring System	93
5-1-1	Small-Signal Measuring Principles	93
5-1-2	Threshold and Accuracy	97
5-1-3	Complete Measuring System	99

5-2	Auxiliary Data: IMPATT Diodes, Coaxial Resonator, and General Measurement Procedure Used.	103
5-3	Comparison of the Computed Noise Spectra with Experimental Data	107
VI	SUMMARY AND CONCLUSIONS	116
	REFERENCES	120
APPENDIX-A	Derivation of Some Read Diode Relations in a Normalized Form	124
APPENDIX-B	Large-Signal Analysis of the Read Diode	132
APPENDIX-C	Derivation of the Coefficients $a_{p-l,l}$ in the Conversion Matrix (4.44)	135

LIST OF TABLES

	Page
TABLE 4-1: SOME PARAMETERS OF REPRESENTATIVE IMPATT DIODES AT 6 GHz	70
TABLE 5-1: PARAMETERS OF MEASURED IMPATT DIODES AT 6 GHz	104

LIST OF FIGURES

	Page
Fig. 2-1a: OSCILLATOR EQUIVALENT CIRCUIT WITH NOISE VOLTAGE SOURCE	12
Fig. 2-1b: OSCILLATOR EQUIVALENT CIRCUIT WITH NOISE CURRENT SOURCE	12
Fig. 2-2: OSCILLATOR NOISE INTERACTION DIAGRAM	19
Fig. 3-1a: EXCITATION OF THE ACTIVE ELEMENT BY CURRENT SOURCE	39
Fig. 3-1b: EXCITATION OF THE ACTIVE ELEMENT BY VOLTAGE SOURCE	39
Fig. 3-2: COMPLETE OSCILLATOR NOISE CONVERSION DIAGRAM	50
Fig. 4-1: READ DIODE; STRUCTURE, DOPING PROFILE, ELECTRIC FIELD DISTRIBUTION AND AVALANCHE REGION DEFINITION	55
Fig. 4-2a: OPEN-CIRCUIT NOISE VOLTAGE SPECTRUM AS A FUNCTION OF RF ELECTRIC FIELD	81
Fig. 4-2b: OPEN-CIRCUIT NOISE VOLTAGE SPECTRUM, NORMALIZED TO ITS SMALL-SIGNAL VALUE, AS A FUNCTION OF RF ELECTRIC FIELD	81
Fig. 4-3: DEPENDENCE OF INITIAL SPECTRA ON DIODE RF VOLTAGE	83
Fig. 4-4: DEPENDENCE OF THE SPECTRA S_{bb} AND $ S_{mb} $ ON DIODE RF VOLTAGE	84

Fig. 4-5:	DEPENDENCE OF INITIAL SPECTRA ON BIAS CIRCUIT CONDUCTANCE	86
Fig. 4-6:	DEPENDENCE OF THE SPECTRA S_{bb} AND $ S_{mb} $ ON BIAS CIRCUIT CONDUCTANCE	87
Fig. 4-7a:	INITIAL SPECTRA S_{mm} AND $S_{\phi\phi}$ AS FUNCTIONS OF DRIFT TRANSIT ANGLE	89
Fig. 4-7b:	INITIAL SPECTRA S_{mm} AND $S_{\phi\phi}$ AS FUNCTIONS OF EQUIVALENT AVALANCHE-TO-DRIFT REGION LENGTH RATIO	89
Fig. 4-8:	AMPLITUDE NOISE COMPARISON OF Si, Ge, AND GaAs DIODES	90
Fig. 4-9:	FREQUENCY NOISE COMPARISON OF Si, Ge AND GaAs DIODES	91
Fig. 5-1:	BASIC SYSTEM FOR OSCILLATOR AM-AND FM NOISE MEASUREMENTS	95
Fig. 5-2:	INACCURACY OF NOISE MEASUREMENTS IN THE "DOUBLE CHANNEL MODE", FOR TYPICAL DEVIATIONS OF CIRCUIT PARAMETERS FROM IDEAL AND FOR SEVERAL VALUES OF AM-AND FM OSCILLATOR NOISE	100
Fig. 5-3:	COMPLETE AM- AND FM NOISE-MEASURING SYSTEM	101
Fig. 5-4:	DETECTOR OUTPUT PROCESSING AND SWITCHING	102
Fig. 5-5:	COAXIAL RESONATOR	105
Fig. 5-6a:	FM NOISE AS A FUNCTION OF RF DIODE VOLTAGE	108
Fig. 5-6b:	AM NOISE AS A FUNCTION OF RF DIODE VOLTAGE	108
Fig. 5-7:	FM NOISE AS A FUNCTION OF DRIFT TRANSIT ANGLE	110
Fig. 5-8a:	FM NOISE AS A FUNCTION OF OUTPUT POWER	111
Fig. 5-8b:	AM NOISE AS A FUNCTION OF OUTPUT POWER	111

Fig. 5-9:	FM-AND AM NOISE AS A FUNCTION OF BIAS CURRENT	113
Fig. 5-10:	BASEBAND NOISE VOLTAGE SPECTRUM AS A FUNCTION OF OUTPUT POWER	113
Fig. 5-11:	MEASURED AM-AND FM NOISE AS A FUNCTION OF BASEBAND FREQUENCY	114

CHAPTER I

INTRODUCTION

The subject of oscillator noise, its theoretical description and experimental assessment is not only an interesting problem per se, but is also one of direct practical importance. The amount of oscillator-generated noise determines to an important extent the quality of a telecommunications system. The invention of a new electron device that is capable of operating as an oscillator has therefore generally been followed by noise studies of the active element itself and of the oscillator unit in which the latter is used. This has been especially true in the case of recent semiconductor devices, such as Gunn diodes, IMPATT diodes and BARITT diodes, all of which are capable of oscillating in the microwave frequency range. Specifically, IMPATT diodes with their strong nonlinearities spurred the interest in large-signal studies of oscillator noise. In this thesis, it has been attempted to develop a large-signal theory of oscillator noise that would take into account most of the conversion processes existing in high-level oscillators, while at the same time yielding a clearly defined procedure for actual computation of the oscillator noise spectra, the results of which could be compared with measured data.

1-1 Brief Review of Pertinent Oscillator Noise Theories

The theory of noise in free-running oscillators was first established

by Bernstein¹. From the studies that followed, the ones most often cited and actually used for oscillator noise assessment are those of Edson², Mullen³ and Kurokawa^{4,5}. These theories provide relatively simple analytic expressions for the amplitude (AM)-and frequency (FM) noise spectra.

In order to obtain these simple analytic expressions, the following basic assumptions needed to be made in the above studies: 1) the amplitude- and phase fluctuations are small, so that a quasilinear approximation is possible about the operating point of the active element, 2) the random amplitude and phase vary slowly with time (quasistationarity), 3) the perturbing noise voltage source used in the oscillator equivalent circuit is independent of the amplitude of oscillation in a small region near the operating point, and 4) the perturbing noise voltage is decomposed into two components at the frequency of oscillation, one in-phase and the other in quadrature with the oscillator periodic signal; the slowly varying random amplitudes of these components are assumed to be uncorrelated and to have equal power spectra. In addition, the influence of the oscillation frequency harmonics on the noise is neglected.

A more rigorous and systematic study by Lax⁶ has shown that, while the quasilinear approximation is valid for amplitude fluctuations (if this approximation is made in the correct variable), phase fluctuations should not be treated in this manner, since they may be quite large in self-sustained oscillators. Beside other results, Lax's paper contains comparisons of spectral linewidths obtained by different procedures. Hempstead and Lax⁷ go further in this by exactly solving the appropriate

Fokker-Planck equation, which is probably the most rigorous approach to take when the fluctuations are so large that a quasilinear approximation is not warranted.

Although the above considerations are of fundamental importance, they do not have a crucial effect in the practical application of a noise theory to typical oscillators in the radio-frequency and microwave range. This is because, even under large-signal conditions, the fluctuations in phase and in amplitude are rarely so large at these frequencies as to seriously invalidate the quasilinear approximation. While this approximation is incorrect in *principle* for phase fluctuations, its *quantitative* effect is manifested strongly mainly in the spectral linewidth, and much less so in the spectral density of frequency fluctuations; this quantity is predominantly used for frequency noise characterization of the above class of oscillators. It has been estimated by this author, using the appropriate formulas of Lax⁶, that in a microwave oscillator at 10 GHz, a 3 dB difference in the spectral density of frequency noise caused by the quasilinear approximation will typically occur at very low baseband frequencies, 100 Hz - 1 kHz. This is a negligible portion of the baseband frequency region of interest. In other respects, Lax's theory⁶ is not fundamentally different from the previously mentioned methods; it uses the assumption of quasistationarity and that of a spectrally pure oscillator. The perturbing noise voltage is formally dependent on a controlling parameter, associated with the amplitude of oscillation; understandably, since the theory is a general one, no details are given as to how this dependence arises in a specific case.

As a consequence of the lack of a complete and computationally applicable large-signal theory, the assessment of noise in typical oscillators used for telecommunications purposes has so far been based on Edson's and Kurokawa's results, in which the perturbing noise voltage is normally replaced by the noise voltage present across the active element open-circuited at the frequency of oscillation and dc-excited only. For devices having a weak dependence of the open-circuit noise voltage on the ac voltage and current that are present in the circuit under oscillatory conditions, this approach is satisfactory.

With the commencement of noise studies on IMPATT diode oscillators, it soon became apparent that some of the noise properties of oscillators employing such a highly nonlinear element will defy description by the existing theories. A rather extensive literature has developed, dealing with both small-signal and large-signal noise properties of IMPATT diodes. After the fundamental studies of Tager⁸, Hines⁹, Haitz¹⁰ and Gummel and Blue¹¹ on dc-excited IMPATT diodes, attention shifted to the phenomenon of up-conversion and its different influence on the amplitude-and frequency spectra, first treated by Scherer¹², and to the means of suppressing the frequency noise by injection locking (Kurokawa⁴ and Hines *et al.*¹³) or by high-Q cavity stabilization (Ashley and Searles¹⁴). Many other authors studied various aspects of the IMPATT noise problem. Rather than present the extensive list of references here, we refer the reader to the review paper by Gupta¹⁵, where most of the contributions in this field are briefly discussed and a list of references is given. However, some of these studies, considered by the present author to be of direct importance to the subject of this thesis, will now be briefly reviewed.

Thaler *et al.*,¹⁶ presented a quasistationary perturbation theory, based on Kurokawa's work, in which the influence of bias current fluctuations on the diode impedance at the oscillation frequency is introduced. This permitted the expression of amplitude- and frequency noise in terms of primary- and modulation noise. Although this theory is a small-signal one, since the perturbing noise voltage is assumed to be independent of the amplitude of oscillation, it yields some interesting suggestions on minimizing the internal phase-to-amplitude conversion in the oscillator (or phase-to-amplitude coupling, as mentioned by Lax⁶).

Convert¹⁷ is probably the first to have pointed out that the perturbing noise voltage in IMPATT diode oscillators may be strongly dependent on the amplitude of oscillation and that its two components, in- and out-of-phase with the oscillator signal, may be cross-correlated. His derivations were carried out specifically for the Read diode. The disadvantage of this rather involved treatment is that it puts aside some of the circuit aspects; also, no computational results are available that would permit comparisons with measured data. The theory uses a previously published large-signal study of the Read diode by Delagebeaudeuf¹⁸.

Vlaardingerbroek¹⁹ modified the quasistationary perturbation theory of Kurokawa^{4,5} by including the effect of down-conversion by demodulation. The resulting system of equations is the most complete one in the literature as of this writing, and provides a sound basis for a large-signal generalization if the noise source voltages can be computed in dependence on the amplitude of oscillation. In such a generalization, the amplitude dependence of the noise source voltages and their cross spectra, normally neglected in the small-signal approach, would have to be considered.

A very important step in the analysis of the amplitude dependence of noise in IMPATTs is the study of Kuvás²⁰. First, the statistics of the basic noise-generating process, namely that of random ionization in the avalanche region, are derived in dependence on the amplitude of the driving current at the frequency at which the device would normally oscillate. He concluded that, for the usual range of excitation, this influence is negligible and the spectrum density of this basic noise process depends only on the magnitude of the bias (dc) current, as first derived in the small-signal treatment of Tager⁸. Next, the transformation of this random process into its external form, the open-circuit noise voltage, is described mathematically under conditions of large-signal excitation. It is shown that the open-circuit noise voltage is strongly dependent on the magnitude of the periodic driving force, although the basic noise process in the avalanche region is little influenced by it. Alternatively, the noise measure and power-to-noise ratio are calculated in dependence on the oscillator RF power. All calculations are carried out for an infinite impedance in the bias circuit of the IMPATT diode, so that modulation noise caused by random noise current at low frequencies is excluded. It is suggested by the author that some information on the AM-and FM noise spectra can be obtained from his theory in conjunction with perturbation theories of oscillator noise, such as those in Refs.2, 4, and 5.

This author wishes to emphasize that the use of noise measure gives correct results for AM-and FM noise only in the case where the slowly-varying amplitudes of the in- and out-of-phase components of the perturbing noise voltage have equal spectra. This is typical for low-level oscillators.

If this concept is used as suggested in Ref. 20, the increase in noise measure with the amplitude of oscillation will be reflected in AM-and FM noise spectra in a precisely identical manner. This would be in complete disagreement with experimental data, e.g., in Ref. 21, where the AM noise of IMPATT diodes has been found to change much less with the RF voltage across the diode than FM noise, in the region of high RF voltage. The explanation rests on the fact that AM-and FM noise spectra are uniquely determined by both the random amplitude and phase of the perturbing noise voltage sidebands *above* and *below* the frequency of oscillation. However, Kuvás' procedure computes only the spectrum density of the noise voltage at the oscillation frequency, i.e., at *zero* modulation frequency. With this approach, it is impossible to distinguish between the generally different RF amplitude dependence of the in- and out-of-phase components of the perturbing noise voltage, and that of their auto- and cross spectra. As a consequence, the AM-and FM noise spectra of the oscillator output cannot be correctly computed. To obtain separate expressions for AM-and FM noise spectra, a different approach must be employed right at the beginning of large-signal derivations, although some of Kuvás' ideas, such as application of Fourier transform and linearization in noise amplitudes can be successfully utilized.

1-2 Purpose of this Study

A critical assessment of the available oscillator noise theories shows the need for a complete large-signal theory that would bridge the

existing gaps and provide a tool for a sufficiently accurate calculation of noise in typical radio-frequency oscillators. It is the purpose of this study to develop a theory of oscillator noise that will consistently take into account the joint influence of the amplitude of oscillation and that of the higher harmonics, of the active element parameters and that of external circuitry on the output amplitude-and frequency noise.

The theory is intended to be applied to IMPATT diode oscillators and the computed spectra will be compared with experimental data. Results of the measurements of other authors will be supplemented by the experimental data of the present author which were obtained on IMPATT diode oscillators by means of a sensitive noise-measuring system, which was assembled specifically for this project. It is hoped that this work will help elucidate some of the noise phenomena in IMPATT diodes which are already known, and also provide a more general insight into IMPATT oscillator noise. Finally, the quantitative comparisons of the computed and measured spectra should yield answers as to the viability of the proposed theory.

1-3 Organization of this Thesis

The main part of the original material is contained in Chapters II to VI and some auxiliary work is presented in Appendices A to C. Chapter II is devoted to the discussion- and large-signal modification of the existing quasistationary perturbation theories of oscillator noise. The concept of pre-oscillation modulation rates is introduced in this chapter. In Chapter III, a general large-signal procedure is developed

for the computation of the open-circuit noise voltage and of the pre-oscillation modulation rates for the active element. Chapter IV contains the explicit application of the above general procedures to IMPATT diodes, complete with the plots and discussion of the computed amplitude-and phase (frequency) noise spectra. Some auxiliary derivations and formulas supporting the developments of Chapter IV are given in Appendices A to C.

A comparison of the computed spectra with experimental data is carried out in Chapter V; the noise-measuring system used is also described here.

A summary and conclusions are presented in Chapter VI.

CHAPTER II

QUASISTATIONARY PERTURBATION THEORY OF NOISE IN FREE-RUNNING OSCILLATORS: MODIFICATION FOR LARGE-SIGNAL CONDITIONS

One of the aims of the large-signal treatment of oscillator noise proposed in this thesis is the removal of certain restrictions imposed on the perturbing noise source in the theories cited in Chapter I. A suitable "small-signal" perturbation theory can then be modified accordingly so that the resulting expressions for oscillator output noise can accept, as an input, quantities characterizing the amplitude dependence of the perturbing noise source. The above concept is elaborated on in this Chapter, utilizing the "state of the art" in quasistationary perturbation theory as represented by Thaler *et al.*¹⁶ and Vlaardingerbroek¹⁹, whose contributions are based on the fundamental paper of Kurokawa⁵.

2-1 Principles of the Perturbation Method in Oscillators

2-1-1 Oscillator Model with Perturbing Noise Source

For purposes of noise analysis in general, the equivalent circuit of an oscillator should include both the high-frequency (RF) part as well as the low-frequency (baseband) part, through which the bias voltage and current are also supplied to the active element. Such a combined circuit for oscillator noise analysis has been introduced only recently

by Vlaardingebroek¹⁹. This circuit is shown, in a somewhat modified form, in Fig. 2-1a. The impedance of the active element in the RF circuit is, in general, dependent on the frequency $\omega(t)$ and the amplitude $A^i(t)$ of high-frequency oscillations as well as on the bias current $I_b(t)$. In the low-frequency circuit, the impedance of the active element depends also on the frequency Ω . The perturbing voltage source $v(t)$ is taken to represent the noise process in the active element. For the present purpose this source may be separated into two sources, one for the baseband frequency range and, the other for the oscillation frequency range. These two voltages may, in general, be correlated (see Sec. 2-2-2).

For completeness, we note that the active element can also be represented by the dual of Fig. 2-1a, an admittance in parallel with a current noise source; the corresponding equivalent circuit is in Fig. 2-1b. The behaviour of these two circuits is similar as far as the frequency region around the fundamental frequency of oscillation is concerned; the main difference is that, for oscillators with a sufficient quality factor Q , the RF circuit in Fig. 2-1a contains voltage components at higher harmonics but only one current component (at the fundamental frequency) whereas, in Fig. 2-1b, the situation is reversed. This difference is of no importance in a small-signal noise analysis, where the perturbing noise source is independent of the magnitude of the deterministic current or voltage at the active element. However, as will become apparent in Chapter III, in a large-signal calculation of the perturbing noise voltage or current the differences in harmonic content may play a significant role. It is, therefore, important to choose the correct equivalent circuit for the oscillator to be investigated. In this thesis we shall

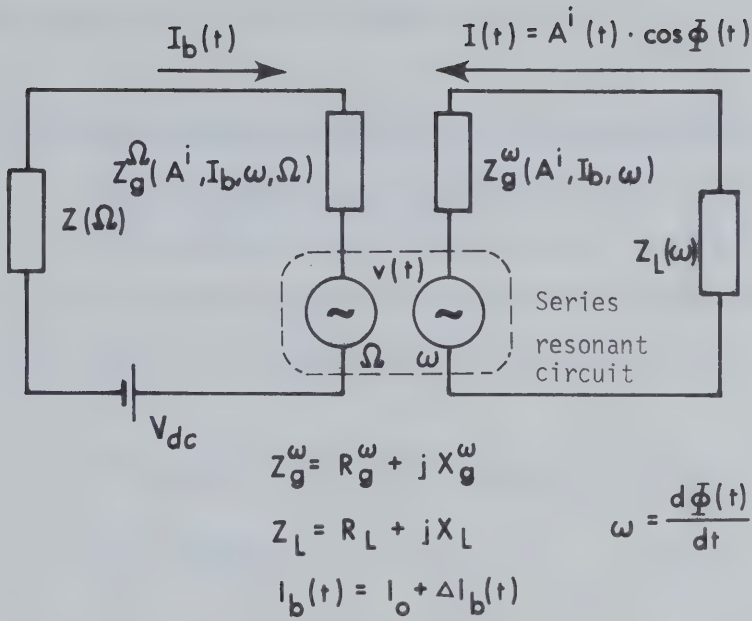


Fig. 2-1a OSCILLATOR EQUIVALENT CIRCUIT WITH NOISE VOLTAGE SOURCE

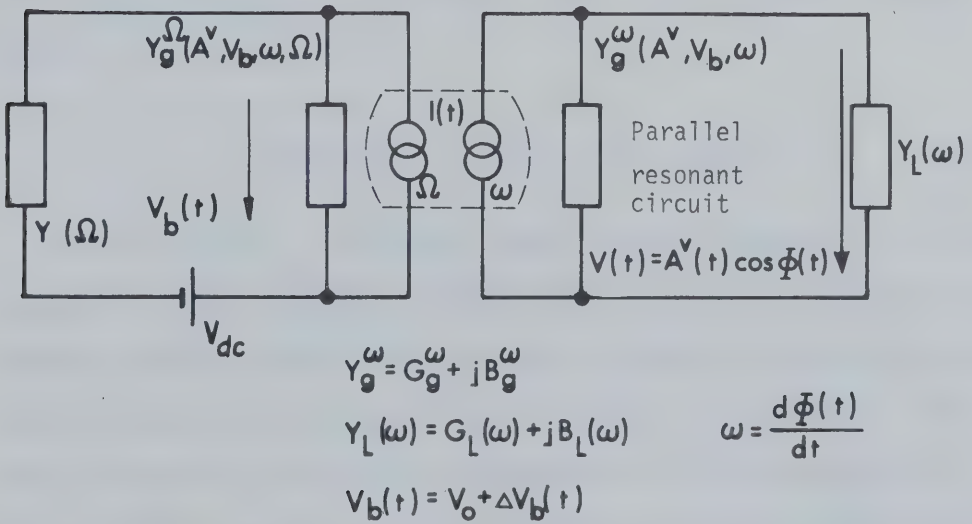


Fig. 2-1b OSCILLATOR EQUIVALENT CIRCUIT WITH NOISE CURRENT SOURCE

give specific relations only for the circuit in Fig. 2-1a, as this is the one of importance for our intended application.

2-1-2 Representation of the Oscillator Output Signal and of the Perturbing Noise Source; Output Noise Modulation Rates

The current in the RF loop of the oscillator circuit in Fig. 2-1a is assumed to be concentrated in frequency around a fixed frequency of oscillation ω_c and it can therefore be expressed as follows:

$$\begin{aligned} I(t) &= A^i(t) \cos \Phi(t) = [A_c^i + \Delta A^i(t)] \cos[\omega_c t + \Delta \Phi(t)] \\ &= A_c^i [1 + M(t)] \cos[\omega_c t + \Delta \Phi(t)] \quad , \end{aligned} \quad (2.1)$$

where

$$M(t) = \Delta A^i(t) / A_c^i \quad . \quad (2.2)$$

The output voltage, i.e., the voltage across the real part of the load impedance, is then given by

$$V_{R_L} = V_c [1 + M(t)] \cos[\omega_c t + \Delta \Phi(t)] \quad ; \quad V_c = A_c^i R_L(\omega_c) \quad . \quad (2.3)$$

The frequency ω_c is commonly called "carrier frequency". For the purpose of a noise analysis, no intentional deterministic modulation is assumed; both $M(t)$ and $\Delta \Phi(t)$ are stochastic quantities representing the random fluctuations of the amplitude and phase of the oscillator signal. These fluctuations are caused by the presence of the noise sources in the oscillator circuit. We shall call $M(t)$ and $\Delta \Phi(t)$ the output amplitude- and phase noise modulation rates, respectively. The power spectra of

these quantities are extensively used for the noise characterization of oscillators and are referred to as "double-sideband amplitude (AM) noise-to-carrier ratio" and "double-sideband phase (PM) noise-to-carrier ratio", both evaluated in a certain specified frequency band, e.g., 100 Hz (located at a specified "distance" from ω_c).

In the important quasistationary limit, i.e., for $M(t)$ and $\Delta\phi(t)$ varying slowly with time, the output signal can be expressed in the form

$$V_{R_L} = V_c [1 + M(t)] \cos\{[\omega_c + \Delta\omega(t)]t\} \quad , \quad (2.4)$$

where $\Delta\omega(t)$ is the random frequency deviation due to noise. The square root of its power spectrum is also extensively used and is referred to as the rms frequency deviation in a certain specified frequency band. Note that, in general,

$$\Delta\omega(t) = \frac{d[\Delta\phi(t)]}{dt} \quad , \quad (2.5)$$

or in the frequency domain,

$$\Delta\omega(\Omega) = j\Omega\Phi(\Omega) \quad , \quad (2.6)$$

so that the power spectra $S_{\omega\omega}(\Omega)$ and $S_{\phi\phi}(\Omega)$ of $\Delta\omega(t)$ and $\Delta\phi(t)$, respectively, are related by

$$S_{\omega\omega}(\Omega) = \Omega^2 S_{\phi\phi}(\Omega) \quad . \quad (2.7)$$

For completeness, we note that relations similar to Eqs. (2.1) - (2.4) can be written for the circuit in Fig. 2-1b.

In correspondence with the mathematical form used for the output signal, the perturbing noise voltage (current) in the RF region is conveniently expressed by means of the well-known narrowband representation¹⁶

$$\begin{aligned} v^\omega(t) &= v_c(t)\cos\omega_c t - v_s(t)\sin\omega_c t \\ &= \operatorname{Re}\{[v_c(t) + jv_s(t)]\exp j\omega_c t\} \quad , \end{aligned} \quad (2.8)$$

where $v_c(t)$ and $v_s(t)$ are small stochastic quantities slowly varying in time. A detailed examination of the properties of these quantities will be carried out in Sec. 2-2.

2-1-3 Quasistationary Perturbation Equations

The conditions of quasistationarity can be stated as follows¹⁶:

$$\frac{d[\Delta A^i(t)]}{dt} \ll A_c^i \omega_c \quad ; \quad \frac{d}{dt} \Delta\omega(t) \ll \omega_c^2 \quad . \quad (2.9)$$

This means that $\Delta A^i(t)$ and $\Delta\omega(t)$ are assumed to vary only slowly with time. Such a restriction can be imposed if the region of interest is confined to low modulation frequencies in the power spectra of $\Delta A^i(t)$ and $\Delta\omega(t)$.

This quasistationary approximation makes it possible in the RF region to express the voltage across (current through) the active element as the product of current (voltage) and active element impedance (admittance) at the instantaneous amplitude and frequency and also bias current. Similarly, the voltage across (current through) the load

impedance (admittance) is given as the product of current (voltage) and load impedance (admittance) at the instantaneous frequency¹⁶. As a consequence, the voltage balance equation in the RF loop of Fig. 2-1a reduces from a differential equation to the simple relation

$$\{A^i(t)\exp j[\omega_c + \Delta\omega(t)]t\} \cdot \{Z_g^\omega[A^i(t), I_b(t), \omega(t)] + Z_L[\omega(t)]\} + [v_c(t) + jv_s(t)]\exp j\omega_c t = 0 \quad (2.10)$$

Now the deviations $\Delta A^i(t)$, $\Delta I_b(t)$ and $\Delta\omega(t)$ from the stable operating point given by A_c^i , I_o and ω_c are assumed small and the impedances in Eq. (2.10) are expanded into Taylor series, stopping with the linear terms. The following general perturbation equation results:

$$\begin{aligned} & \{[A_c^i + \Delta A^i(t)]\exp j[\omega_c + \Delta\omega(t)]t\} \cdot \left\{ \left. \frac{\partial Z_g^\omega}{\partial A^i} \right|_{A^i=A_c^i} \cdot \Delta A^i(t) + \left. \frac{\partial Z_g^\omega}{\partial I_b} \right|_{I_b=I_o} \cdot \Delta I_b(t) \right. \\ & \left. + \left[\left. \frac{\partial Z_g^\omega}{\partial \omega} \right|_{\omega=\omega_c} + \left. \frac{dZ_L}{d\omega} \right|_{\omega=\omega_c} \right] \Delta\omega(t) \right\} + [v_c(t) + jv_s(t)]\exp j\omega_c t = 0 \quad (2.11) \end{aligned}$$

Using the condition for steady-state oscillations

$$Z_g^\omega(A_c^i, I_o, \omega_c) + Z_L(\omega_c) = 0 \quad (2.12)$$

neglecting the higher-order terms (products of small stochastic quantities) in Eq. (2.11) and separating Eq. (2.11) into real and imaginary parts yields two perturbation equations

$$\frac{\partial R_g^\omega}{\partial A_c^i} \Delta A^i(t) + \frac{\partial R_g^\omega}{\partial I_o} \Delta I_b(t) + \left[\frac{\partial R_g^\omega}{\partial \omega_c} + \frac{dR_L}{d\omega_c} \right] \Delta \omega(t) = - \frac{v_c(t)}{A_c^i} \quad (2.13)$$

$$\frac{\partial X_g^\omega}{\partial A_c^i} \Delta A^i(t) + \frac{\partial X_g^\omega}{\partial I_o} \Delta I_b(t) + \left[\frac{\partial X_g^\omega}{\partial \omega_c} + \frac{dX_L}{d\omega_c} \right] \Delta \omega(t) = - \frac{v_s(t)}{A_c^i} \quad (2.14)$$

In these equations, the following notation has been introduced for convenience:

$$\left. \frac{\partial R_g^\omega}{\partial A_c^i} \right|_{A_c^i = A_c^i} = \frac{\partial R_g^\omega}{\partial A_c^i} ; \quad \left. \frac{\partial R_g^\omega}{\partial I_b} \right|_{I_b = I_o} = \frac{\partial R_g^\omega}{\partial I_o} , \quad (2.15)$$

etc.

Eqs. (2.13) and (2.14), transformed into the frequency domain, have the form

$$\frac{\partial R_g^\omega}{\partial A_c^i} \Delta A^i(\Omega) + \frac{\partial R_g^\omega}{\partial I_o} \Delta I_b(\Omega) + \left[\frac{\partial R_g^\omega}{\partial \omega_c} + \frac{dR_L}{d\omega_c} \right] \Delta \omega(\Omega) = - \frac{v_c(\Omega)}{A_c^i} \quad (2.16)$$

$$\frac{\partial X_g^\omega}{\partial A_c^i} \Delta A^i(\Omega) + \frac{\partial X_g^\omega}{\partial I_o} \Delta I_b(\Omega) + \left[\frac{\partial X_g^\omega}{\partial \omega_c} + \frac{dX_L}{d\omega_c} \right] \Delta \omega(\Omega) = - \frac{v_s(\Omega)}{A_c^i} , \quad (2.17)$$

where $v_c(\Omega)$, $v_s(\Omega)$, $\Delta A^i(\Omega)$... are the Fourier transforms of the corresponding quantities in the time domain, with the implicit assumption that the latter are truncated on a finite time interval $(-T, T)$ and that they satisfy all the other requirements for the existence of the Fourier transform²².

To complete the description of the oscillator circuit in Fig. 2-1a, a bias circuit equation is introduced¹⁹:

$$I_b(\Omega)\{Z_g^\Omega(A^i, I_b, \omega, \Omega) + Z(\Omega)\} + v(\Omega) + V_{dc} = 0 \quad (2.18)$$

The meaning of the quantities contained in Eq. (2.18) is apparent from Fig. 2-1a. Again, the impedance of the active element is expanded into a Taylor series around the operating point and, after removing the dc part, the following perturbation equation is obtained:

$$\begin{aligned} I_o \frac{\partial Z_g^\Omega}{\partial A_c^i} \Delta A^i(\Omega) + [Z_g^\Omega(A_c^i, I_o, \omega_c, \Omega) + \frac{\partial Z_g^\Omega}{\partial I_o} I_o + Z(\Omega)] \Delta I_b(\Omega) \\ + I_o \frac{\partial Z_g^\Omega}{\partial \omega_c} \Delta \omega(\Omega) = -v(\Omega) \end{aligned} \quad (2.19)$$

The first and third terms in this equation represent the effect of demodulation¹⁹.

It may be useful at this point, and for future reference also, to depict the interaction between the individual quantities in Eqs. (2.16), (2.17) and (2.19) graphically. This is illustrated in the "interaction diagram", Fig. 2-2, which shows the links between physical causes and effects. Note that, if modulation is nonexistent ($\partial Z_g^\omega / \partial I_o = 0$), $\Delta A^i(\Omega)$ and $\Delta \omega(\Omega)$ are independent of $v(\Omega)$. Similarly, $v_c(\Omega)$ or $v_s(\Omega)$ can influence $\Delta I_b(\Omega)$ only via demodulation.

If the equivalent circuit in Fig. 2-1b were used, the system corresponding to Eqs. (2.16), (2.17) and (2.19) would be completely analogous. The noise voltage sources would be replaced by noise current sources, the bias current fluctuations $\Delta I_b(t)$ by voltage fluctuations $\Delta V_b(t)$ and all impedances by admittances.

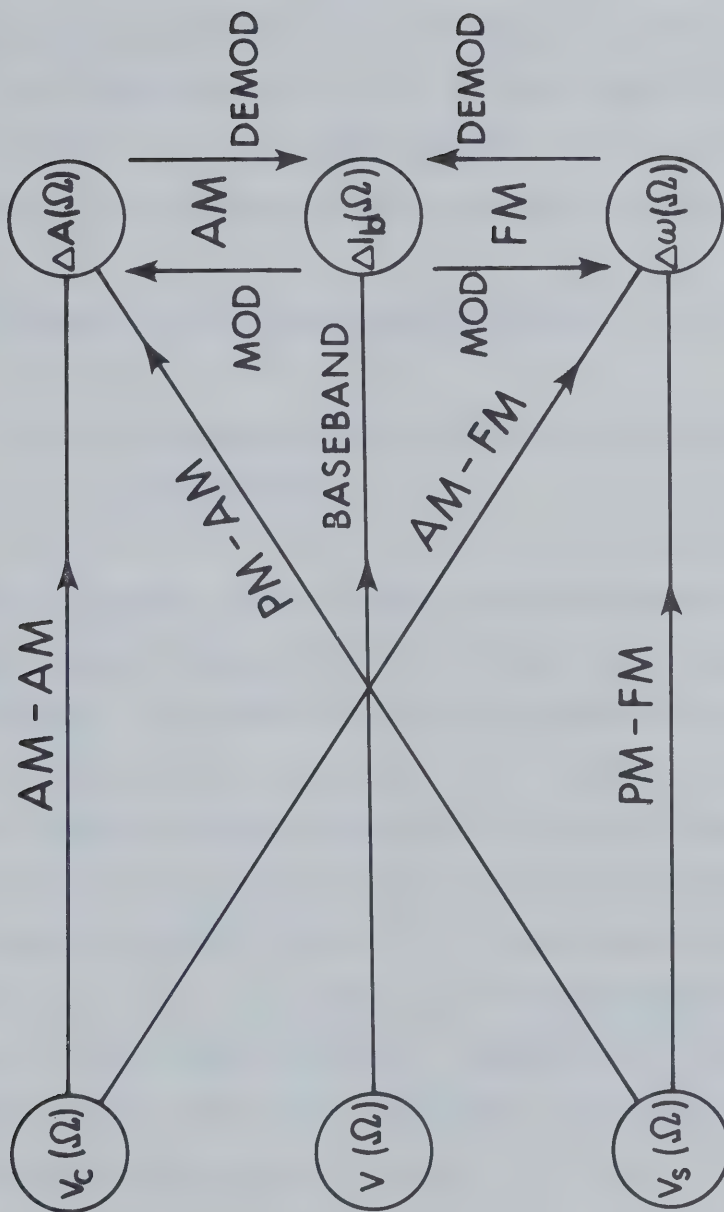


Fig. 2-2 OSCILLATOR NOISE INTERACTION DIAGRAM

Mathematically, Eqs. (2.16), (2.17) and (2.19) form a linear system that can be solved for $\Delta A^i(\Omega)$, $\Delta\omega(\Omega)$ and $\Delta I_b(\Omega)$ in terms of the perturbing voltages $v_c(\Omega)$, $v_s(\Omega)$ and $v(\Omega)$. This has been carried out by Thaler *et al.*¹⁶ and Vlaardingerbroek¹⁹, using different simplifying assumptions; a brief review of this is given in Sec. 2-3. Prior to this, the spectral properties of the perturbing noise source must be investigated.

2-2 Properties of the Perturbing Noise Source

2-2-1 Introduction of the Initial (pre-oscillation) Noise

Modulation Rates

The form of Eq. (2.8) indicates that the perturbing noise voltage could be expressed by means of some equivalent modulation rates or indices characterizing the initial (pre-oscillation) amplitude-and phase fluctuations. This would also formally complement the introduction of noise modulation rates in the output noise characterization, Eqs. (2.1-2.3). Let us therefore introduce the initial amplitude-and phase noise modulation rates $m(t)$ and $\phi(t)$, varying slowly in time and such that $m(t) \ll 1$ (small amplitude fluctuations) and $\phi(t) \ll \pi/2$ (small phase deviations), where both $m(t)$ and $\phi(t)$ are assumed to be truncated sample functions of wide-sense stationary random processes. Furthermore, let us express the perturbing noise voltage near the carrier frequency by means of these rates and the output carrier voltage V_c as follows:

$$\begin{aligned}
 v^{(w)}(t) &= \text{Re}\{V_c[1 + m(t)]\exp j[\omega_c t + \phi(t)]\}_s \\
 &\doteq |V_c|m(t)\cos[\omega_c t + \arg(V_c)] - |V_c|\phi(t)\sin[\omega_c t + \arg(V_c)] \quad , \\
 &\hspace{25em} (2.20)
 \end{aligned}$$

where the subscript s denotes the stochastic part. Comparing Eqs. (2.20) and (2.8) and realizing that V_c has been chosen to be a real number in the oscillator model of Fig. 2-1a, we obtain

$$v_c(t) = V_c m(t) \quad ; \quad v_s(t) = V_c \phi(t) \quad . \quad (2.21)$$

Hence any conclusions regarding the statistical or spectral properties of $m(t)$ or $\phi(t)$ are equally valid for $v_c(t)$ and $v_s(t)$, respectively.

The Fourier transform of Eq. (2.20) yields

$$v(\omega)_{\omega \neq \omega_c} = \frac{1}{2} V_c [m(\omega - \omega_c) + j\phi(\omega - \omega_c)] + \frac{1}{2} V_c [m(\omega + \omega_c) - j\phi(\omega + \omega_c)] \quad . \quad (2.22)$$

Since $m(t)$ and $\phi(t)$ are restricted to low modulation frequencies, the upper and lower sidebands of $v(t)$ for a particular modulation frequency $\Omega \ll \omega_c$ are

$$v(\omega_c + \Omega) = \frac{1}{2} V_c [m(\Omega) + j\phi(\Omega)] \quad (2.23)$$

$$v(\omega_c - \Omega) = \frac{1}{2} V_c [m^*(\Omega) + j\phi^*(\Omega)] \quad . \quad (2.24)$$

The Fourier transform of the initial modulation rates can now be determined from Eqs. (2.23) and (2.24) in terms of the sidebands:

$$m(\Omega) = v(\omega_c + \Omega)/V_c + v^*(\omega_c - \Omega)/V_c^* \quad (2.25)$$

$$\phi(\Omega) = -j\{v(\omega_c + \Omega)/V_c - v^*(\omega_c - \Omega)/V_c^*\} \quad . \quad (2.26)$$

(The asterisks in Eqs. (2.24 - 2.26) denote complex conjugate quantities).

If the equivalent circuit in Fig. 2-1b is used in place of that in Fig. 2-1a, $v(\omega)$ in the above formulas would be replaced by $i(\omega)$ and V_c by I_c , i.e., by the fundamental current amplitude through the real part of the load admittance.

Since the quantities $v_c(\Omega)$ and $v_s(\Omega)$ in Eqs. (2.16) and (2.17) can be replaced by $m(\Omega)$ and $\phi(\Omega)$, it also seems proper to normalize $v(\Omega)$ in Eq. (2.19) so as to obtain a completely normalized right-hand side of the system (2.16), (2.17) and (2.19). This can be done by relating $v(\Omega)$ to V_0 , the dc voltage across the active element. Denoting the new quantity by $b_v(\Omega)$ and combining it with Eqs. (2.25) and (2.26), we obtain in matrix form

$$\begin{bmatrix} m(\Omega) \\ b_v(\Omega) \\ \phi(\Omega) \end{bmatrix} = \begin{bmatrix} 1/V_c & 0 & 1/V_c^* \\ 0 & 1/V_0 & 0 \\ -j/V_c & 0 & j/V_c^* \end{bmatrix} \cdot \begin{bmatrix} v(\Omega + \omega_c) \\ v(\Omega) \\ v(\Omega - \omega_c) \end{bmatrix}, \quad (2.27)$$

where the property $v(\Omega - \omega_c) = v^*(\omega_c - \Omega)$ is used.

2-2-2 Statistical and Spectral Properties of the Initial Noise

Modulation Rates and of the Perturbing Noise Voltage under Small-and Large Signal Conditions

Since $m(t)$, $\phi(t)$ and $b_v(t)$ are assumed to be truncated sample functions of stochastic processes, the power spectral densities $S_{mm}(\Omega)$, $S_{\phi\phi}(\Omega)$ and $S_{bb}(\Omega)$ of $m(t)$, $\phi(t)$ and $b_v(t)$, respectively, can be calculated

from the corresponding Fourier transforms as follows^{22,23}:

$$S_{mm}(\Omega) = \lim_{T \rightarrow \infty} E\{|m(\Omega)|^2/2T\} \quad (2.28)$$

$$S_{\phi\phi}(\Omega) = \lim_{T \rightarrow \infty} E\{|\phi(\Omega)|^2/2T\} \quad (2.29)$$

$$S_{bb}(\Omega) = \lim_{T \rightarrow \infty} E\{|b_v(\Omega)|^2/2T\} \quad , \quad (2.30)$$

where E denotes the expectation integral and T is the time boundary used in the truncation of $m(t)$, $\phi(t)$ and $b_v(t)$. Similarly, the cross-spectral densities are given by

$$S_{m\phi} = \lim_{T \rightarrow \infty} E\{m(\Omega)\phi^*(\Omega)/2T\} = S_{\phi m}^* \quad (2.31)$$

$$S_{mb} = \lim_{T \rightarrow \infty} E\{m(\Omega)b_v^*(\Omega)/2T\} = S_{bm}^* \quad (2.32)$$

$$S_{\phi b} = \lim_{T \rightarrow \infty} E\{\phi(\Omega)b_v^*(\Omega)/2T\} = S_{b\phi}^* \quad . \quad (2.33)$$

Substitution of Eqs. (2.27) into Eqs. (2.28) - (2.33) yields expressions for the auto-and cross spectra of $m(t)$, $\phi(t)$ and $b_v(t)$ in terms of the spectra $S_{vv}(\omega)$ of $v(t)$:

$$\begin{aligned} S_{mm}(\Omega) = & [S_{vv}(\omega_c + \Omega) + S_{vv}(\omega_c - \Omega)]/|V_c|^2 \\ & + \lim_{T \rightarrow \infty} E\{\text{Re}[v(\omega_c + \Omega)v(\omega_c - \Omega)/V_c^2]/T\} \end{aligned} \quad (2.34)$$

$$S_{\phi\phi}(\Omega) = [S_{VV}(\omega_c + \Omega) + S_{VV}(\omega_c - \Omega)]/|V_c|^2 \\ - \lim_{T \rightarrow \infty} E\{\text{Re}[v(\omega_c + \Omega)v(\omega_c - \Omega)/V_c^2]/T\} \quad (2.35)$$

$$S_{bb}(\Omega) = S_{VV}(\Omega)/V_o^2 \quad (2.36)$$

$$S_{m\phi}(\Omega) = \lim_{T \rightarrow \infty} E\{\text{Im}[v(\omega_c + \Omega)v(\omega_c - \Omega)/V_c^2]/T\} \\ + j[S_{VV}(\omega_c + \Omega) - S_{VV}(\omega_c - \Omega)]/|V_c|^2 \quad (2.37)$$

$$S_{mb}(\Omega) = \lim_{T \rightarrow \infty} E\{v(\omega_c + \Omega)v^*(\Omega)/V_o V_c + v^*(\omega_c - \Omega)v^*(\Omega)/V_o V_c^*\} \quad (2.38)$$

$$S_{\phi b}(\Omega) = \lim_{T \rightarrow \infty} E\{-j[v(\omega_c + \Omega)v^*(\Omega)/V_o V_c - v^*(\omega_c - \Omega)v^*(\Omega)/V_o V_c^*]\}. \quad (2.39)$$

As mentioned in Chapter I, the perturbing voltage $v(t)$ is normally postulated to be independent of the amplitude of oscillations. It is then reasonable to assume that $v^\omega(t)$, i.e., $v(t)$ around the frequency ω_c , is a sample function of a wide-sense stationary, normal, narrowband noise process. Also, the low and high frequency part of $v(t)$ are assumed to be uncorrelated. Alternatively, the total perturbing voltage is often assumed to have a white spectrum. All these assumptions imply the statistical independence of the Fourier transforms $v(\omega_c + \Omega)$, $v(\omega_c - \Omega)$ and $v(\Omega)$, so that all the cross-spectral terms in Eqs. (2.34) - (2.39) become zero. Then

$$S_{mm}(\Omega) = S_{\phi\phi}(\Omega) = [S_{VV}(\omega_c + \Omega) + S_{VV}(\omega_c - \Omega)]/|V_c|^2 \quad (2.40)$$

$$S_{m\phi}(\Omega) = -S_{\phi m}(\Omega) = j[S_{vv}(\omega_c + \Omega) - S_{vv}(\omega_c - \Omega)]/|V_c|^2 \quad (2.41)$$

$$S_{mb}(\Omega) = S_{\phi b}(\Omega) = 0 \quad . \quad (2.42)$$

Under large-signal conditions, the noise voltage $v(t)$ may be amplitude dependent. In view of the existence of nonlinear transformations of the basic noise process in the active element, which manifest themselves in the form of frequency conversions, the requirement of wide-sense stationarity, let alone normality for $v(t)$, appears to be too restrictive. Incidentally, even with $m(t)$ and $\phi(t)$ wide-sense stationary (these assumptions will be kept throughout this study), $v^\omega(t)$ as expressed by Eq. (2.20) is generally non-stationary²³. As a result, the two auto spectra $S_{mm}(\Omega)$ and $S_{\phi\phi}(\Omega)$ are not necessarily equal and the cross spectra $S_{m\phi}(\Omega)$ and $S_{\phi m}(\Omega)$ are not purely imaginary. Furthermore, the spectra $S_{mb}(\Omega)$ and $S_{\phi b}(\Omega)$ do not, in general, vanish. The practical consequence of this generalization is that all the auto-and cross spectra must generally appear in the final formulas such as those that may be obtained from the perturbation equations (2.16), (2.17) and (2.19). This is shown in Sec. 2-4. Furthermore, these auto-and cross spectra must be obtained by applying the general formulas (2.28) - (2.33), as shown in Sec. 3-4, rather than from any simplified relations such as Eqs. (2.40) - (2.42).

2-3 A Review of the Quasistationary Perturbation Theories of Thaler *et al.*, and Vlaardingerbroek

Thaler *et al.*¹⁶ oriented their theory towards IMPATT diode oscillators.

For this reason, they included the effect of bias current fluctuations in perturbation equations, which had not been included before in such an explicit form. The resulting perturbation equations are of the form of Eqs. (2.13) and (2.14) with the frequency dependence of the active element impedance neglected. Furthermore, the bias current fluctuations $\Delta I_b(t)$ were assumed uncorrelated with the perturbing voltage $v^\omega(t)$ near the carrier and therefore uncorrelated with the components $v_c(t)$ and $v_s(t)$. Such an assumption is certainly justifiable at low oscillation amplitudes, i.e., in a small-signal theory. As a consequence, no bias circuit equation such as Eq. (2.19) is really needed and the system of equations (2.13), (2.14) is simply solved for $\Delta A^i(t)$ and $\Delta\omega(t)$ in terms of $v_c(t)$, $v_s(t)$ and $\Delta I_b(t)$ as the known quantities. In our notation, Thaler *et al.* obtained¹⁶

$$\Delta A^i(t) = - \frac{v_c(t) \frac{dX_L}{d\omega_c} - v_s(t) \frac{dR_L}{d\omega_c} + \Delta I_b(t) A_C^i \left[\frac{\partial R_g^\omega}{\partial I_0} \frac{dX_L}{d\omega_c} - \frac{\partial X_g^\omega}{\partial I_0} \frac{dR_L}{d\omega_c} \right]}{A_C^i \left[\frac{\partial R_g^\omega}{\partial A_C^i} \frac{dX_L}{d\omega_c} - \frac{\partial X_g^\omega}{\partial A_C^i} \frac{dR_L}{d\omega_c} \right]} \quad (2.43)$$

$$\Delta\omega(t) = \frac{v_c(t) \frac{\partial X_g^\omega}{\partial A_C^i} - v_s(t) \frac{\partial R_g^\omega}{\partial A_C^i} + \Delta I_b(t) A_C^i \left[\frac{\partial R_g^\omega}{\partial I_0} \frac{\partial X_g^\omega}{\partial A_C^i} - \frac{\partial X_g^\omega}{\partial I_0} \frac{\partial R_g^\omega}{\partial A_C^i} \right]}{A_C^i \left[\frac{\partial R_g^\omega}{\partial A_C^i} \frac{dX_L}{d\omega_c} - \frac{\partial X_g^\omega}{\partial A_C^i} \frac{dR_L}{d\omega_c} \right]} \quad (2.44)$$

To simplify these relations, the following notation is introduced:

$$\frac{dR_L}{d\omega_C} + j \frac{dX_L}{d\omega_C} = \left| \frac{dZ_L}{d\omega_C} \right| \exp(j\theta) \quad (2.45)$$

$$\frac{\partial R_g^\omega}{\partial A_C} + j \frac{\partial X_g^\omega}{\partial A_C} = \left| \frac{\partial Z_g^\omega}{\partial A_C} \right| \exp(j\eta) \quad (2.46)$$

$$\frac{\partial R_g^\omega}{\partial I_0} + j \frac{\partial X_g^\omega}{\partial I_0} = \left| \frac{\partial Z_g^\omega}{\partial I_0} \right| \exp(j\psi) \quad (2.47)$$

Furthermore, the small-signal assumptions (2.40) - (2.42) are used so that relatively simple expressions result for the noise spectra $S_{AA}(\Omega)$ and $S_{\omega\omega}(\Omega)$ of $\Delta A^i(t)$ and $\Delta\omega(t)$, respectively:

$$S_{AA}(\Omega) = S_{CC}(\Omega) \{ (A_C^i) \left| \frac{\partial Z_g^\omega}{\partial A_C} \right| \sin(\theta-\eta) \}^{-2} + K_{AM}^2 S_{II}(\Omega) \quad (2.48)$$

$$S_{\omega\omega}(\Omega) = S_{SS}(\Omega) \{ (A_C^i) \left| \frac{dZ_L}{d\omega_C} \right| \sin(\theta-\eta) \}^{-2} + K_{FM}^2 S_{II}(\Omega) \quad , \quad (2.49)$$

where $S_{CC}(\Omega) = S_{SS}(\Omega)$ are the power spectral densities of $v_C(t)$ and $v_S(t)$, respectively, where $S_{II}(\Omega)$ is the power spectral density of the bias current fluctuations $\Delta I_b(t)$, and where K_{AM} , K_{FM} are given by

$$K_{AM} = \left| \frac{\partial Z_g^\omega}{\partial I_0} \right| \sin(\psi-\theta) / \left\{ \left| \frac{\partial Z_g^\omega}{\partial A_C} \right| \sin(\theta-\eta) \right\} \quad (2.50)$$

$$K_{FM} = \left| \frac{\partial Z_g^\omega}{\partial I_0} \right| \sin(\eta-\psi) / \left\{ \left| \frac{dZ_L}{d\omega_C} \right| \sin(\theta-\eta) \right\} \quad (2.51)$$

The second term on the right-hand side of each of Eqs. (2.48) and (2.49)

is usually referred to as "up-conversion noise" or "modulation noise", the latter being more appropriate for reasons given in Sections 2-4 and 2-5. Eqs. (2.48) - (2.51) are the fundamental results of the theory of Thaler *et al.* and, in this thesis, we shall not comment on the detailed influence of the angles θ , η and ψ .

Vlaardingerbroek¹⁹ introduced a bias circuit equation in a form similar to Eq. (2.18). This was done partly in an effort to obtain some information on the large-signal behaviour of oscillator noise, since the effect of down-conversion by rectification [as represented in Eq. (2.19) by the terms proportional to $\Delta A^i(\Omega)$ and $\Delta\omega(\Omega)$] is likely to take place at quite large amplitudes of oscillation. The bias current fluctuations $\Delta I_b(t)$ are taken as the unknown quantity and the system of Eqs. (2.16), (2.17) and (2.19) is solved for the three measurable quantities $\Delta A^i(\Omega)$, $\Delta\omega(\Omega)$ and $\Delta I_b(\Omega)$:

$$\begin{bmatrix} \Delta A^i(\Omega) \\ \Delta\omega(\Omega) \\ \Delta I_b(\Omega) \end{bmatrix} = \begin{bmatrix} \frac{\partial R_g^\omega}{\partial A_c^i}, \frac{dR_L}{d\omega_c}, \frac{\partial R_g^\omega}{\partial I_o} \\ \frac{\partial X_g^\omega}{\partial A_c^i}, \frac{dX_L}{d\omega_c}, \frac{\partial X_g^\omega}{\partial I_o} \\ I_o \frac{\partial Z_g^\omega}{\partial A_c^i}, I_o \frac{\partial Z_g^\omega}{\partial \omega_c}, Z_T(\Omega) \end{bmatrix}^{-1} \begin{bmatrix} -v_c(\Omega)/A_c^i \\ -v_s(\Omega)/A_c^i \\ -v(\Omega) \end{bmatrix}, \quad (2.52)$$

where $Z_T(\Omega)$ is the total impedance (diode + external circuit) in the bias circuit.

The inverse of the matrix in Eq. (2.52) is not given in Ref. 19 for the general case. Rather, the inversion is carried out after the intro-

duction of the following simplifying assumptions, valid specifically for Impatt diodes:

$$\frac{\partial R_g^\omega}{\partial A_c} \frac{\partial X_g^\omega}{\partial I_o} - \frac{\partial R_g^\omega}{\partial I_o} \frac{\partial X_g^\omega}{\partial A_c} = 0 \quad (2.53)$$

$$\frac{\partial Z_g^\omega}{\partial \omega_c} \neq 0; \quad \frac{\partial R_g^\omega}{\partial A_c} = - \frac{\partial R_g^\omega}{\partial I_o} \frac{dI_o}{dA_c}, \quad \frac{\partial X_g^\omega}{\partial A_c} = - \frac{\partial X_g^\omega}{\partial I_o} \frac{dI_o}{dA_c} \quad (2.54)$$

Furthermore, the total bias circuit impedance $Z_T(\Omega)$ is assumed real, $Z_T(\Omega) = R_T(\Omega)$. Eq. (2.52) then assumes the form

$$\begin{bmatrix} \Delta A^i(\Omega) \\ \Delta \omega(\Omega) \\ \Delta I_b(\Omega) \end{bmatrix} = \frac{R_T}{A_c^i D} \begin{bmatrix} -\frac{dX_L}{d\omega_c}, \frac{dR_L}{d\omega_c}, -\frac{1}{R_T} \left(\frac{dR_L}{d\omega_c} \frac{\partial X_g^\omega}{\partial I_o} - \frac{\partial R_g^\omega}{\partial I_o} \frac{dR_L}{d\omega_c} \right) \\ -\frac{\partial X_g^\omega}{\partial I_o} \beta(1+\gamma), \frac{\partial R_g^\omega}{\partial I_o} \beta(1+\gamma), 0 \\ \beta\gamma \frac{dX_L}{d\omega_c}, -\beta\gamma \frac{dR_L}{d\omega_c}, -\frac{\beta}{R_T} \left(\frac{dR_L}{d\omega_c} \frac{\partial X_g^\omega}{\partial I_o} - \frac{\partial R_g^\omega}{\partial I_o} \frac{dX_L}{d\omega_c} \right) \end{bmatrix} \cdot \begin{bmatrix} v_c(\Omega) \\ v_s(\Omega) \\ A_c^i v(\Omega) \end{bmatrix}, \quad (2.55)$$

where

$$\beta = \frac{dI_o}{dA_c}, \quad \gamma = \beta^{-1} I_o \frac{\partial Z_g^\omega}{\partial A_c} R_T^{-1}, \quad 0 \geq \gamma \geq -1, \quad (2.56)$$

$$D = R_T \beta(1+\gamma) \left(\frac{dR_L}{d\omega_c} \frac{\partial X_g^\omega}{\partial I_o} - \frac{\partial R_g^\omega}{\partial I_o} \frac{dX_L}{d\omega_c} \right).$$

A number of conclusions based on Eq. (2.55) are drawn in Ref. 19. One of them is of particular interest to this study; Eq. (2.55) shows that the amplitude noise $\Delta A^i(\Omega)$ increases as the signal level, and therefore

$|\gamma|$, increases, while the FM noise $\Delta\omega(\Omega)$ is independent of the signal level if $v_c(\Omega)$ and $v_s(\Omega)$ are assumed to be amplitude independent. According to experiment however²¹, the FM noise does depend on the amplitude of oscillation; this can be accounted for only if $v_c(\Omega)$ and $v_s(\Omega)$ are amplitude dependent and, possibly, cross-correlated. This indicates again that a truly large-signal theory must take this RF amplitude dependence and cross-correlation into account in some systematic manner.

2-4 Large-signal Modification of the Theories of Vlaardingerbroek and Thaler

Vlaardingerbroek¹⁹ has not given any explicit expressions for the power spectral densities of the quantities in Eq. (2.52). However, his approach is implicitly a large-signal one and all that needs to be done is to calculate the required spectral densities and allow for the RF amplitude dependence of, and cross-correlation between, the noise voltages $v_c(\Omega)$, $v_s(\Omega)$ and $v(\Omega)$.

Let us first normalize Eq. (2.52) by substituting into it both the output- and initial noise modulation rates. For this reason we will also normalize $\Delta I_b(\Omega)$ to the dc bias current I_0 :

$$B_I(\Omega) = \Delta I_b(\Omega)/I_0 \quad . \quad (2.57)$$

Eq. (2.52) then assumes the form

$$\begin{bmatrix} M(\Omega) \\ B_I(\Omega) \\ \phi(\Omega) \end{bmatrix} = \begin{bmatrix} P^i \end{bmatrix} \begin{bmatrix} m(\Omega) \\ b_V(\Omega) \\ \phi(\Omega) \end{bmatrix}, \quad (2.58)$$

where the matrix P^i is the inverse of the perturbation matrix P given by

$$P = - \begin{bmatrix} \frac{A_C^i}{R_L} \frac{\partial R_g^\omega}{\partial A_C^i}, \frac{I_O}{R_L} \frac{\partial R_g^\omega}{\partial I_O}, \frac{\Omega}{R_L} \frac{dR_L}{d\omega_C} \\ \frac{A_C^i}{Z_O} \frac{\partial Z_g^\Omega}{\partial A_C^i}, \frac{Z_T(\Omega)}{Z_O}, \frac{\Omega}{Z_O} \frac{\partial Z_g^\Omega}{\partial \omega_C} \\ \frac{A_C^i}{R_L} \frac{\partial X_g^\omega}{\partial A_C^i}, \frac{I_O}{R_L} \frac{\partial X_g^\omega}{\partial I_O}, \frac{\Omega}{R_L} \frac{dX_L}{d\omega_C} \end{bmatrix}, \quad (2.59)$$

with $Z_O = V_O/I_O =$ dc impedance (resistance) of the active element.

The power spectral densities $S_{MM}(\Omega)$, $S_{BB}(\Omega)$ and $S_{\phi\phi}(\Omega)$ corresponding to $M(\Omega)$, $B_I(\Omega)$ and $\phi(\Omega)$ are given in terms of the initial auto- and cross spectra as follows:

$$\begin{bmatrix} S_{MM}(\Omega) \\ S_{BB}(\Omega) \\ S_{\phi\phi}(\Omega) \end{bmatrix} = \begin{bmatrix} |P_{11}^i|^2 \\ |P_{21}^i|^2 \\ |P_{31}^i|^2 \end{bmatrix} S_{mm}(\Omega) + \begin{bmatrix} |P_{12}^i|^2 \\ |P_{22}^i|^2 \\ |P_{32}^i|^2 \end{bmatrix} S_{bb}(\Omega) + \begin{bmatrix} |P_{13}^i|^2 \\ |P_{23}^i|^2 \\ |P_{33}^i|^2 \end{bmatrix} S_{\phi\phi}(\Omega) + 2\text{Re} \left\{ \begin{bmatrix} P_{11}^i P_{12}^{i*} \\ P_{21}^i P_{22}^{i*} \\ P_{31}^i P_{32}^{i*} \end{bmatrix} S_{mb}(\Omega) + \begin{bmatrix} P_{11}^i P_{13}^{i*} \\ P_{21}^i P_{23}^{i*} \\ P_{31}^i P_{33}^{i*} \end{bmatrix} S_{m\phi}(\Omega) + \begin{bmatrix} P_{12}^{i*} P_{13}^i \\ P_{22}^{i*} P_{23}^i \\ P_{32}^{i*} P_{33}^i \end{bmatrix} S_{\phi b}(\Omega) \right\}. \quad (2.60)$$

The coefficients of the inverse matrix P^i are, in general, complicated expressions and it is not practical to present them here in analytical form. If the general formula (2.60) is to be used, it is better to first compute the coefficients of P numerically and then to invert the matrix.

If the effect of demodulation is neglected, as in the study of Thaler *et al.*¹⁶, considerable simplification can be achieved as far as the coefficients of P^i are concerned. Yet the final result is still in the form of Eq. (2.60) since under large-signal conditions the cross-spectra cannot, in general, be neglected. From the point of view of accuracy, it may be expected that a large-signal theory neglecting demodulation will be satisfactory up to very large amplitudes where demodulation becomes strong. In the case of a large impedance in the bias circuit, the demodulation terms in Eq. (2.59) become insignificant and the generalized Thaler's theory is then applicable at all amplitudes.

The effect of demodulation is represented by P_{21} and P_{23} in the matrix (2.59). If these are set to zero, the matrix can be easily inverted and the coefficients for calculating $S_{MM}(\Omega)$ and $S_{\Phi\Phi}(\Omega)$ in Eq. (2.60), using the definitions (2.45) - (2.47), are

$$P_{11}^i = - \frac{dX_L}{d\omega_c} \left[\frac{A_c^i}{R_L} \left| \frac{dZ_L}{d\omega_c} \right| \left| \frac{\partial Z_g^\omega}{\partial A_c^i} \right| \sin(\theta - \eta) \right]^{-1} \quad (2.61)$$

$$P_{31}^i = \frac{\partial X_{gT}^\omega}{\partial A_c^i} \left[\frac{A_c^i}{R_L} \left| \frac{dZ_L}{d\omega_c} \right| \left| \frac{\partial Z_g^\omega}{\partial A_c^i} \right| \sin(\theta - \eta) \right]^{-1} \quad (2.62)$$

$$P_{12}^i = I_0 \frac{Z_0}{Z_T(\Omega)} \frac{\partial Z_g^\omega}{\partial I_0} \sin(\theta - \psi) \left[A_c^i \left| \frac{\partial Z_g^\omega}{\partial A_c^i} \right| \sin(\theta - \eta) \right]^{-1} \quad (2.63)$$

$$P_{32}^i = I_0 \frac{Z_0}{Z_T(\Omega)} \frac{\partial Z_g^\omega}{\partial I_0} \sin(n-\psi) \left[\Omega \frac{dZ_L}{d\omega_c} \sin(\theta-n) \right]^{-1} \quad (2.64)$$

$$P_{13}^i = \frac{dR_L}{d\omega_c} \left[\frac{A_c^i}{R_L} \left| \frac{dZ_L}{d\omega_c} \right| \left| \frac{\partial Z_g^\omega}{\partial A_c^i} \right| \sin(\theta-n) \right]^{-1} \quad (2.65)$$

$$P_{33}^i = - \frac{\partial R_L^\omega}{\partial A_c^i} \left[\frac{\Omega}{R_L} \left| \frac{dZ_L}{d\omega_c} \right| \left| \frac{\partial Z_g^\omega}{\partial A_c^i} \right| \sin(\theta-n) \right]^{-1} \quad (2.66)$$

The auto- and cross spectral densities of the initial modulation rates, needed in Eq. (2.60), can be determined from the equations describing the active element. This will be shown in Chapter III. Prior to that however, a simplified version of the above generalized theory is presented in the next section.

2-5 Simplified Large-signal Version of Thaler's Theory

The large-signal generalization in the previous section resulted in an equation which contains a large number of terms compared with the small-signal approximation. It is almost certain that some of them will be relatively unimportant; intuitively one would expect that the amplitude dependence of the two auto-spectra $S_{mm}(\Omega)$ and $S_{\phi\phi}(\Omega)$ will contribute much more to the amplitude dependence of $S_{MM}(\Omega)$ and $S_{\Phi\Phi}(\Omega)$ than will that of the cross-spectrum $S_{m\phi}(\Omega)$. The decisive factor here is the behaviour of the active element impedance with respect to RF amplitude and frequency and the external circuit properties.

It turns out that a very simple approximation can be obtained if the following restrictions are imposed on the oscillator:

1) The frequency dependence of the load resistance is negligible compared

to that of the load reactance, near the carrier frequency ω_c :

$$\left| \frac{dR_L}{d\omega_c} \right| \ll \left| \frac{dX_L}{d\omega_c} \right| \text{ so that } \frac{dX_L}{d\omega_c} \cong \left| \frac{dZ_L}{d\omega_c} \right| \text{sign}\left(\frac{dX_L}{d\omega_c}\right) . \quad (2.67)$$

2) The reactance of the active element changes much less with the RF amplitude than its negative resistance:

$$\left| \frac{\partial X_g^\omega}{\partial A_c} \right| \ll \left| \frac{\partial R_g^\omega}{\partial A_c} \right| \text{ so that } \left| \frac{\partial Z_g^\omega}{\partial A_c} \right| \cong - \frac{\partial R_g^\omega}{\partial A_c} . \quad (2.68)$$

The first restriction is in good agreement with reality if a simple external circuit is used. The other restriction is an idealization; altogether they characterize the simplest oscillator conceivable. Its active element would be represented by an amplitude dependent negative resistance with either no reactance at all or with an amplitude independent reactance that can be included in the external circuit. The external circuit itself is a series combination of a frequency independent resistance and the necessary reactance to form a high Q selective circuit.

With the above assumptions, the output noise spectra can be written as follows:

$$S_{MM}(\Omega) = |P_{11}^i|^2 S_{mm}(\Omega) + 2\text{Re}(P_{11}^i P_{12}^{i*}) S_{mb}(\Omega) + |P_{12}^i|^2 S_{bb}(\Omega) \quad (2.69)$$

$$S_{\phi\phi}(\Omega) = |P_{33}^i|^2 S_{\phi\phi}(\Omega) + 2\text{Re}(P_{32}^{i*} P_{33}^i) S_{\phi b}(\Omega) + |P_{32}^i|^2 S_{bb}(\Omega) , \quad (2.70)$$

where

$$P_{11}^i = \left\{ \frac{A_C^i}{R_L} \left| \frac{\partial Z^\omega}{\partial A_C} \right| \right\}^{-1} \quad (2.71)$$

$$P_{33}^i = \left\{ \frac{\Omega}{R_L} \left| \frac{dZ_L}{d\omega_C} \right| \right\}^{-1} \quad (2.72)$$

and P_{12}^i and P_{32}^i are of the same form as in Eqs. (2.63) and (2.64). We note that Eqs. (2.69) and (2.70) with the coefficients as given by Eqs. (2.63), (2.64), (2.71) and (2.72) are very similar to the small-signal equations (2.48) and (2.49). The main difference is that $S_{mm}(\Omega)$ and $S_{\phi\phi}(\Omega)$ are assumed to be amplitude dependent and are not declared equal. Also, the cross-spectral term is missing in Eqs. (2.48) and (2.49).

The first terms on the right-hand side of Eqs. (2.69) and (2.70) may be called "primary noise", whereas the third terms represent modulation noise. The latter contribution is often called up-conversion noise in the small-signal theory. It should be understood however, that under large-signal conditions even the primary noise may contain up-converted components because of the amplitude dependence of the initial spectra $S_{mm}(\Omega)$ and $S_{\phi\phi}(\Omega)$. It is therefore suggested here that the term modulation noise is more suitable for the third terms in Eqs. (2.69) and (2.70).

The primary noise contribution in Eq. (2.70) can be also rewritten in terms of the quality factor of the external circuit:

$$S_{\Phi\Phi}^0(\Omega) = S_{\phi\phi}(\Omega) / \{Q_{ex}(\Omega/\omega_C)\}^2 \quad (2.73)$$

The often used "rms frequency deviation" is given by

$$\Delta f_{\text{rms}}(\Omega) = (\Omega/2\pi)[S_{\phi\phi}(\Omega)]^{1/2} \quad , \quad (2.74)$$

which for primary noise only gives the well-known formula

$$\Delta f_{\text{rms}}^0(\Omega) = (f_c/Q_{\text{ex}})[S_{\phi\phi}(\Omega)]^{1/2} \quad . \quad (2.75)$$

In summary, in the simple oscillator characterized by the conditions (2.67) and (2.68), the internal amplitude-to-phase or phase-to-amplitude conversion, as indicated by the diagonal lines in Fig. 2-2, is so small that the primary amplitude (phase) noise at the output can be expressed in terms of the initial amplitude (phase) noise only.

The above approach yields the simplest large-signal approximation of oscillator noise. The reason for introducing and discussing this simple model rests in the fact that the general model, described by Eq. (2.60), may sometimes reduce to the former even if the condition (2.68) is not satisfied. This depends on the relative magnitudes of the initial spectra. This fact is utilized in some of the calculations of the output noise spectra presented in Chapter V.

CHAPTER III

SPECTRA OF INITIAL (PRE-OSCILLATION) NOISE MODULATION RATES: LARGE SIGNAL
CALCULATION

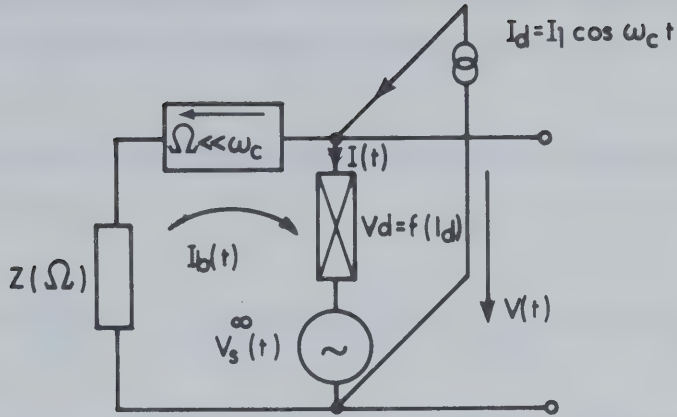
In the previous chapter, formulas have been derived that employ the spectral densities of initial noise modulation rates or, alternatively, the spectral densities of the two orthogonal noise voltage components $v_c(t)$ and $v_s(t)$ in the representation of the perturbing noise voltage. As shown in Sec. 2-2-1, these quantities can be determined from the sidebands of the perturbing noise voltage $v(t)$. A general procedure for computing the latter quantities and the initial modulation rates will now be given.

3-1 Excitation of the Active Element

The equivalent oscillator circuits in Figs. 2-1a and 2-1b suggest that the noise source voltage or current could be computed from the appropriate equations of the active element which is either open- or short circuited. Under small-signal conditions, the noise mechanism can be considered "classical", i.e., independent of the RF voltages or currents in the circuit, and only the dc level needs to be considered. Under large-signal conditions, we must find a way of simulating the effect of large RF currents and voltages present at the active element when the circuit is oscillating. This can be achieved by driving the active element from a deterministic current source (if the open-circuit

noise voltage $v(t)$ is to be determined), or by a voltage source [if the short-circuit noise current $i(t)$ is to be determined] at that amplitude and frequency at which it would normally oscillate. Circuits corresponding to this desired situation are shown in Figs. 3-1a and 3-1b. Note that they are non-oscillatory circuits. In singly-tuned oscillators with quality factors that are not too small, either the current or the voltage at higher harmonics of ω_c will be relatively small and one of the circuits in Fig. 3-1 will be applicable. Clearly, the circuit in Fig. 3-1a (3-1b) must be used in conjunction with the oscillator model in Fig. 2-1a (2-1b). The subscripts s and d refer to stochastic and deterministic quantities, respectively.

One point worth mentioning is that the bias circuits in Figs. 3-1a and 3-1b are not open- or short circuited. This is so because we wish to take into account the possible effect of bias circuit impedance on the open-circuit noise voltage (or short-circuit noise current) at high frequencies. This effect, if it exists, might be called "initial modulation" as distinct from the modulation mechanism mentioned in the previous chapter. As a side note, it is suggested that the often encountered term "up-conversion" should perhaps be used in a broader sense than is typically accepted; namely, to include modulation, initial modulation and the conversion which takes place even if the bias circuit in Fig. 3-1a (3-1b) is open (short)-circuited. This latter effect is due to the mutual correlation between the open-circuit noise voltages (short-circuit noise currents) at various frequencies, under large-signal excitation.

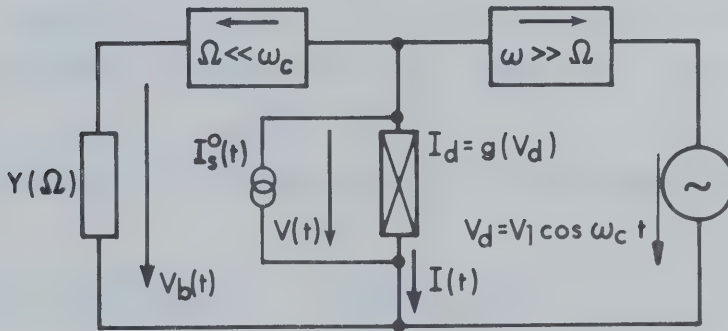


$$V(t) = V_s(t) + V_d$$

$$V_d = \frac{1}{2} \sum_{-\infty}^{\infty} V_n \exp(jn \omega_c t)$$

$$I(t) = I_1 \cos \omega_c t + I_b(t)$$

Fig. 3-1a EXCITATION OF THE ACTIVE ELEMENT BY CURRENT SOURCE



$$I(t) = I_s(t) + I_d$$

$$I_d = \frac{1}{2} \sum_{-\infty}^{\infty} I_n \exp(jn \omega_c t)$$

$$V(t) = V_1 \cos \omega_c t + V_b(t)$$

Fig. 3-1b EXCITATION OF THE ACTIVE ELEMENT BY VOLTAGE SOURCE

3-2 Mathematical Description of the Active Element; Generalized Langevin Equation for Stochastic Quantities

Let us assume that the nonlinear element can be described by the differential equation

$$\begin{aligned}
 & a_m[I(t), V(t)] \frac{d^m I(t)}{dt^m} + b_m[I(t), V(t)] \frac{d^m V(t)}{dt^m} + a_{m-1}[I(t), V(t)] \frac{d^{m-1} I(t)}{dt^{m-1}} + \\
 & + \dots + a_1[I(t), V(t)] \frac{dI(t)}{dt} + b_1[I(t), V(t)] \frac{dV(t)}{dt} + c_0[I(t), V(t)] = F(t) \quad ,
 \end{aligned}
 \tag{3.1}$$

where either $I(t)$ or $V(t)$ is a given periodic driving signal as discussed previously and $F(t)$ represents the internal noise mechanism in the active element (thermal noise, random ionization, etc.). The statistical and spectral properties of $F(t)$ may, in general, be dependent on some controlling parameter related to the power level, i.e., either to the average of $|V(t)|^2$ or of $|I(t)|^2$.

Under non-oscillatory conditions, it is reasonable to write

$$I(t) = I_d(t) + I_s(t) \quad I_s(t) \ll I_d(t) \tag{3.2}$$

$$V(t) = V_d(t) + V_s(t) \quad V_s(t) \ll V_d(t) \quad , \tag{3.3}$$

where $V_d(t)$ and $V_s(t)$ ($I_d(t)$ and $I_s(t)$) are the deterministic and stochastic components of voltage (current), respectively. It may sometimes be convenient or even necessary to formulate Eq. (3.1) in terms of other

electric quantities (e.g. electric field) or to include the latter in Eq. (3.1) in addition to voltage and current. This does not basically change the procedure outlined here; the linearization in stochastic quantities indicated in Eqs. (3.2), (3.3) is simply carried out for all time dependent variables in Eq. (3.1). Eq. (3.1) can then be decomposed into two equations;

- 1) deterministic, which is of the same form as Eq. (3.1) except that the right-hand side is zero
- 2) stochastic, with the second- and higher order products neglected:

$$\begin{aligned}
 & a_m[I_d(t), V_d(t)] \frac{d^m I_s(t)}{dt^m} + \left[\frac{\partial a_m}{\partial I_d} I_s(t) + \frac{\partial a_m}{\partial V_d} V_s(t) \right] \frac{d^m I_d(t)}{dt^m} + b_m[I_d(t), V_d(t)] \\
 & \times \frac{d^m V_s(t)}{dt^m} + \left[\frac{\partial b_m}{\partial I_d} I_s(t) + \frac{\partial b_m}{\partial V_d} V_s(t) \right] \frac{d^m V_d(t)}{dt^m} + \dots + \frac{\partial C_0}{\partial I_d} I_s(t) + \\
 & + \frac{\partial C_0}{\partial V_d} V_s(t) = F(t) \quad .
 \end{aligned} \tag{3.4}$$

This is a generalized version of the Langevin equation.

3-3 Fourier Transform of Langevin Equation; Open-Circuit Noise Voltage (Short-Circuit Noise Current)

The Langevin equation (3.4) is, in general, a nonlinear differential equation since the coefficients a_m , b_m and their derivatives with respect to I_d or V_d are functions of the latter and therefore general functions of time. However, the specific excitation of the active element, as introduced in Section 3-1, enables us to simplify the above-mentioned

equation to a linear differential equation with periodically time-varying coefficients. Since one of the quantities I_d and V_d is enforced as a periodic, sinusoidal quantity, the other may be approximated by Fourier series as indicated in Figs. 3-1a and 3-1b. Thus we have either

$$I_d = I_1 \cos \omega_c t \quad ; \quad V_d = \frac{1}{2} \sum_{-\infty}^{\infty} V_n \exp(jn\omega_c t) \quad , \quad (3.5)$$

or

$$V_d = V_1 \cos \omega_c t \quad ; \quad I_d = \frac{1}{2} \sum_{-\infty}^{\infty} I_n \exp(jn\omega_c t) \quad . \quad (3.6)$$

The coefficients a_m , b_m and their derivatives are then also approximated by Fourier series

$$a_m = \sum_{n=-\infty}^{\infty} a_{m,n} \exp(jn\omega_c t) \quad ; \quad b_m = \sum_{n=-\infty}^{\infty} b_{m,n} \exp(jn\omega_c t) \quad , \quad (3.7)$$

etc.

The coefficients $a_{m,n}$, $b_{m,n}$, ... are functions of the harmonic components of voltage V_d and current I_d :

$$a_{m,n} = a_{m,n}(I_1, V_1, V_{-1}, V_2, V_{-2}, \dots) \quad (3.8)$$

or

$$a_{m,n} = a_{m,n}(V_1, I_1, I_{-1}, I_2, I_{-2}, \dots) \quad , \quad (3.9)$$

$$b_{m,n} = b_{m,n}(I_1, V_1, V_{-1}, V_2, V_{-2}, \dots) \quad (3.10)$$

or

$$b_{m,n} = b_{m,n}(V_1, I_1, I_{-1}, I_2, I_{-2}, \dots) \quad , \quad (3.11)$$

etc.

The substitution of Eqs. (3.5) - (3.11) into Eq. (3.4) leads to an equation of the form

$$\begin{aligned} & \sum_{n=-\infty}^{\infty} C_{m,n} \exp(jn\omega_c t) \frac{d^m I_S(t)}{dt^m} + \sum_{n=-\infty}^{\infty} D_{m,n} \exp(jn\omega_c t) \frac{d^m V_S(t)}{dt^m} + \\ & + \sum_{n=-\infty}^{\infty} C_{m-1,n} \exp(jn\omega_c t) \frac{d^{m-1} I_S(t)}{dt^{m-1}} + \sum_{n=-\infty}^{\infty} D_{m-1,n} \exp(jn\omega_c t) \frac{d^{m-1} V_S(t)}{dt^{m-1}} + \\ & + \dots + \sum_{n=-\infty}^{\infty} C_{0n} \exp(jn\omega_c t) I_S(t) + \sum_{n=-\infty}^{\infty} D_{0n} \exp(jn\omega_c t) V_S(t) = F(t) \quad . \end{aligned} \quad (3.12)$$

On making the assumption that $I_S(t)$, $V_S(t)$ and $F(t)$ are truncated sample functions of a random process, the Fourier transform can be applied, resulting in an equation of the form

$$\sum_{n=-\infty}^{\infty} A_n V_S(\omega + n\omega_c) + B_n I_S(\omega + n\omega_c) = F(\omega) \quad , \quad (3.13)$$

where the coefficients A_n , B_n are functions of ω , $\omega + n\omega_c$ and of the Fourier components $V_0, V_1 \dots V_n, I_0, I_1 \dots I_n$ of the deterministic voltage and current. The latter can be determined from a separate large-signal analysis using Eq. (3.1), where $F(t) = 0$, in conjunction with the excitation diagrams in Figs. 3-1. $V_S(\omega + n\omega_c)$, $I_S(\omega + n\omega_c)$ and $F(\omega)$ are the Fourier transforms of $V_S(t)$, $I_S(t)$ and $F(t)$, respectively, at the

frequencies indicated.

Since we are interested only in the spectra at the frequencies

$$\omega = \Omega + \ell \omega_c \quad |\Omega| \ll \omega_c, \quad \ell = \text{integer} \quad , \quad (3.14)$$

we can substitute Eq. (3.14) into Eq. (3.13), and obtain

$$\sum_{n=-\infty}^{\infty} A_n(\Omega + \ell \omega_c) V_S[\Omega + (n+\ell)\omega_c] + B_n(\Omega + \ell \omega_c) I_S[\Omega + (n+\ell)\omega_c] = F(\Omega + \ell \omega_c) \quad , \quad (3.15)$$

which, introducing $p = n+\ell$, can be rewritten in the more useful form

$$\sum_{p=-M}^M A_{p-\ell, \ell} V_S(\Omega + p\omega_c) + B_{p-\ell, \ell} I_S(\Omega + p\omega_c) = F(\Omega + \ell \omega_c), \quad -M \leq \ell \leq M, \quad (3.16)$$

because in actual computations, p will be limited to a finite range.

Incorporating the relations (c.f. Figs. 3-1)

$$V_S(\Omega) = Z_T(\Omega) I_S(\Omega) \quad , \quad (3.17)$$

and either $I_S(\Omega + n\omega_c) = 0; \quad n \neq 0$ or $V_S(\Omega + n\omega_c) = 0; \quad n \neq 0$

$$I_n = 0 \quad ; \quad |n| > 1 \quad \quad V_n = 0 \quad ; \quad |n| > 1 \quad , \quad (3.18)$$

we obtain a system of linear equations of the form

$$\sum_{p=-M}^M C_{p-\ell, \ell} V_S(\Omega + p\omega_c) = F(\Omega + \ell \omega_c); \quad -M \leq \ell \leq M \quad , \quad (3.19)$$

or a similar system for current. An inversion of Eq. (3.19) yields, in matrix form

$$[V_{sp}] = [C_{p-l, l}^i] \cdot [F_l] ; V_{sp} = V_s(\Omega + p\omega_c), F_l = F(\Omega + l\omega_c) . \quad (3.20)$$

If the above procedure is oriented so as to obtain Eqs. (3.19) and (3.20) in terms of a stochastic quantity other than voltage or current, the corresponding relation between the quantity used and the open circuit voltage (or short-circuit current) must be substituted into Eq. (3.20) to obtain the latter. This will only modify the coefficients $C_{p-l, l}^i$. Then, for a particular $p = \pm q$ we obtain the upper- and lower sidebands

$$V_s(\Omega + q\omega_c) = \sum_{l=-M}^M C_{q-l, l}^i F(\Omega - l\omega_c) \quad (3.21)$$

$$V_s(\Omega - q\omega_c) = \sum_{l=-M}^M C_{-q-l, l}^i F(\Omega + l\omega_c) , \quad (3.22)$$

and for the noise voltage at baseband frequencies

$$V_s(\Omega) = \sum_{l=-M}^M C_{-l, l}^i F(\Omega + l\omega_c) . \quad (3.23)$$

The form of Eqs. (3.21), (3.22) and (3.23) clearly indicates potential conversion in the active element.

3-4 Fourier Transform and Power Spectral Densities of the Initial Modulation Rates

It will now be postulated that the Fourier transform of the perturbing noise voltage $v^\omega(t)$ in the oscillator model in Fig. 2-1a is approximately equal to that of $V_s(t)$ in the vicinity of ω_c :

$$v(\omega_c \pm \Omega) = V_s(\omega_c \pm \Omega) \quad . \quad (3.24)$$

Similarly, the Fourier transform of the perturbing noise voltage $v^\Omega(t)$ is now postulated to be approximately equal to that of $V_s(t)$ at baseband frequencies:

$$v(\Omega) = V_s(\Omega) \quad . \quad (3.25)$$

Hence, the Fourier transforms of the initial noise modulation rates at frequency Ω , from Eqs. (2.27) and (3.21), (3.22), are

$$m(\Omega) = \sum_{\ell=-M}^M (C_{1-\ell,\ell}^i / V_c + C_{-1-\ell,\ell}^i / V_c^*) F(\Omega + \ell \omega_c) \quad (3.26)$$

$$b_v(\Omega) = \sum_{\ell=-M}^M (C_{-\ell,\ell}^i / V_0) F(\Omega + \ell \omega_c) \quad (3.27)$$

$$\phi(\Omega) = -j \sum_{\ell=-M}^M (C_{1-\ell,\ell}^i / V_c - C_{-1-\ell,\ell}^i / V_c^*) F(\Omega + \ell \omega_c) \quad . \quad (3.28)$$

In most cases, $F(t)$ in Eq. (3.1) will belong to a wide-sense stationary process with an almost white spectrum so that, on applying Eqs. (2.28) -

(2.30),

$$\lim_{T \rightarrow \infty} E\{F(\Omega + m\omega_c)F^*(\Omega + n\omega_c)/2T\} = 0 \quad \text{if } m \neq n. \quad (3.29)$$

The power spectral densities of $m(t)$, $b_v(t)$ and $\phi(t)$ are then

$$S_{mm}(\Omega) = \sum_{\ell=-M}^M |C_{1-\ell, \ell}^i/V_c + C_{-1-\ell, \ell}^i/V_c^*|^2 S_{FF}(\Omega + \ell\omega_c) \quad (3.30)$$

$$S_{bb}(\Omega) = \sum_{\ell=-M}^M |C_{-\ell, \ell}^i/V_0|^2 S_{FF}(\Omega + \ell\omega_c) \quad (3.31)$$

$$S_{\phi\phi}(\Omega) = \sum_{\ell=-M}^M |C_{1-\ell, \ell}^i/V_c - C_{-1-\ell, \ell}^i/V_c^*|^2 S_{FF}(\Omega + \ell\omega_c), \quad (3.32)$$

where $S_{FF}(\Omega)$ is the power spectral density of $F(t)$.

In a similar way, the cross spectra $S_{m\phi}(\Omega)$, $S_{mb}(\Omega)$ and $S_{\phi b}(\Omega)$ can be determined by applying Eqs. (2.31) - (2.33) on Eqs. (3.26) - (3.28), using the property (3.29):

$$S_{m\phi}(\Omega) = 2 \sum_{\ell=-M}^M \left\{ \text{Im} \left(\frac{C_{1-\ell, \ell}^i C_{-1-\ell, \ell}^{i*}}{V_c^2} \right) + j \left[\left| \frac{C_{1-\ell, \ell}^i}{V_c} \right|^2 - \left| \frac{C_{-1-\ell, \ell}^i}{V_c} \right|^2 \right] \right\} S_{FF}(\Omega + \ell\omega_c) \quad (3.33)$$

$$S_{mb}(\Omega) = \sum_{\ell=-M}^M \frac{C_{-\ell, \ell}^{i*}}{V_0} \left(\frac{C_{1-\ell, \ell}^i}{V_c} + \frac{C_{-1-\ell, \ell}^i}{V_c^*} \right) S_{FF}(\Omega + \ell\omega_c) \quad (3.34)$$

$$S_{\phi b}(\Omega) = -j \sum_{\ell=-M}^M \frac{C_{-\ell, \ell}^{i*}}{V_0} \left(\frac{C_{1-\ell, \ell}^i}{V_c} - \frac{C_{-1-\ell, \ell}^i}{V_c^*} \right) S_{FF}(\Omega + \ell\omega_c). \quad (3.35)$$

Finally, it may be useful to compute the spectra of the open-circuit noise voltage at the sidebands. From Eqs. (3.21), (3.22), (3.24) and (3.29) we have

$$S_{VV}(\omega_c + \Omega) = \sum_{\ell=-M}^M |C_{1-\ell, \ell}^i|^2 S_{FF}(\Omega + \ell\omega_c) \quad (3.36)$$

$$S_{VV}(\omega_c - \Omega) = \sum_{\ell=-M}^M |C_{-1-\ell, \ell}^i|^2 S_{FF}(\Omega + \ell\omega_c) \quad , \quad (3.37)$$

where $S_{VV}(\omega)$ denotes the power spectral density of the open-circuit noise voltage $v(t)$ at the frequencies indicated.

It is seen that all the auto- and cross spectral densities required in the general expression (2.60) for the amplitude and phase spectra of an oscillator, can be obtained by means of the power spectrum of the basic noise process and the coefficients in Eq. (3.20), which characterizes the frequency response of the active element to its basic noise process.

3-5. Computation of Oscillator Noise: General Procedure

The derivations in the previous sections and in Chapter II resulted in a considerable number of equations as well as of expressions to be substituted into those equations, to obtain the noise at the oscillator output. The purpose of this short section is to consolidate the fundamental results and to show the procedure for computing the oscillator output spectra, given the spectrum of the basic noise process in the active element.

First of all, it would be obviously convenient to complement the

"interaction diagram" of Fig. 2-2, since it is now known how the perturbing noise voltage is obtained from the basic noise process in the active element. Such a complete conversion diagram is shown in Fig. 3-2. The basic noise process first passes through the stage of initial conversion caused by the nonlinearity of the active element and the presence of an RF signal. The resulting noise voltage and the corresponding initial noise modulation rates are then again subject to conversion when the active device is allowed to oscillate freely.

It is immediately seen from Fig. 3-2 that the simplest and most elegant method for calculating the output spectra is as follows. Firstly the Fourier transforms of the output spectra are obtained from the Fourier transform of the basic noise process via all the matrices involved:

$$\begin{aligned}
 \begin{bmatrix} M(\Omega) \\ B_I(\Omega) \\ \phi(\Omega) \end{bmatrix} &= \begin{bmatrix} P^i \end{bmatrix} \cdot \begin{bmatrix} m(\Omega) \\ b_V(\Omega) \\ \phi(\Omega) \end{bmatrix} = \begin{bmatrix} P^i \end{bmatrix} \cdot \begin{bmatrix} I \end{bmatrix} \cdot \begin{bmatrix} v(\omega_C + \Omega) \\ v(\Omega) \\ v(\omega_C - \Omega) \end{bmatrix} = \\
 &= \begin{bmatrix} P^i \end{bmatrix} \begin{bmatrix} I \end{bmatrix} \begin{bmatrix} C^i \end{bmatrix} \begin{bmatrix} F(\Omega + M\omega_C) \\ \vdots \\ F(\Omega + \omega_C) \\ F(\Omega) \\ F(\Omega - \omega_C) \\ \vdots \\ F(\Omega - M\omega_C) \end{bmatrix}
 \end{aligned}$$

= continued on p. 51

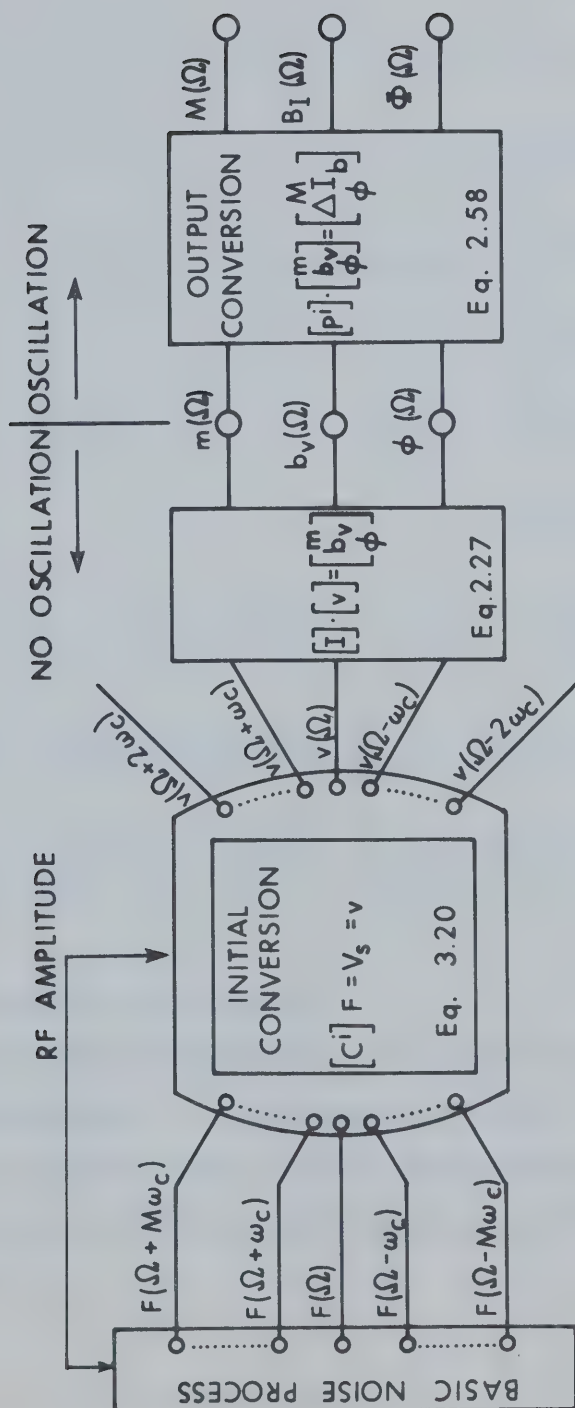


Fig. 3-2 COMPLETE OSCILLATOR NOISE CONVERSION DIAGRAM

continued
from p. 49

$$= \begin{bmatrix} R_{1,-M} & \cdot & \cdot & \cdot & \cdot & R_{1,M} \\ \cdot & & R & & \cdot & \\ R_{3,-M} & \cdot & \cdot & \cdot & \cdot & R_{3,M} \end{bmatrix} \cdot \begin{bmatrix} F(\Omega + M\omega_c) \\ \vdots \\ F(\Omega + \omega_c) \\ F(\Omega) \\ F(\Omega - \omega_c) \\ \vdots \\ F(\Omega - M\omega_c) \end{bmatrix} \quad (3.38)$$

The output spectra are then calculated from the following formulas:

$$S_{MM}(\Omega) = \lim_{T \rightarrow \infty} E\{M(\Omega)M^*(\Omega)/2T\} = \sum_{\ell=-M}^M |R_{1,\ell}|^2 S_{FF}(\Omega + \ell\omega_c) \quad (3.39)$$

$$S_{\Phi\Phi}(\Omega) = \lim_{T \rightarrow \infty} E\{\Phi(\Omega)\Phi^*(\Omega)/2T\} = \sum_{\ell=-M}^M |R_{3,\ell}|^2 S_{FF}(\Omega + \ell\omega_c) \quad , \quad (3.40)$$

where the property (3.29) is used.

It may sometimes be desirable to know the initial spectra along with the output spectra. In this case, Eqs. (3.30) - (3.35) are used to compute all the initial auto- and cross spectra, which in turn can then be inserted into Eq. (2.60) to obtain the output spectra.

CHAPTER IV

APPLICATION OF THE NOISE THEORY TO IMPATT DIODE OSCILLATORS

The large-signal theory of oscillator noise, developed in the previous chapters in a general form, will now be applied to IMPATT diode oscillators. Two decisions must be made at this stage in order to be able to achieve a reasonable compromise between simplicity of application and sufficient accuracy of the results. First, a suitable mathematical model of the IMPATT diode must be selected so that the procedure for calculating the initial spectra (c.f. Chapter III) can be carried out. The initial spectra are of particular interest in this study because of the possibility of comparing their large-signal behaviour with the usual small-signal assumptions imposed on the perturbing noise source. Having obtained the initial spectra, the modified quasistationary perturbation theory described in Chapter II is used for the computation of the measurable output noise spectra. Depending on the accuracy desired and on the associated complexity (i.e., the tolerable computer expense), this may be obtained by using either the most general perturbation matrix in Sec. 2-4 or one of the two simpler approximations in Sections 2-4 and 2-5. The problem of computing time is very real here because of the number of time-consuming auxiliary calculations and the large number of combinations of the parameters involved in computing both the initial and output spectra.

4-1 IMPATT Diode Model

4-1-1 Avalanching p-n Junction

In the reverse biased p-n junction diode, very small reverse saturation currents of electrons and holes flow across the junction. As the reverse voltage is increased, the maximum kinetic energy of the particles carrying this saturation current increases also. When a certain critical electric field intensity has been reached near the junction, the electrons and holes become capable of producing other electron-hole pairs by impact ionization and the phenomenon of rapid carrier multiplication, called avalanche multiplication and/or breakdown ensues. This effect can be controlled and even utilized for high-frequency generation. The avalanche buildup has associated with it a certain delay time; further, after the electrons and holes have passed through the region near the junction, an additional transit delay time is introduced as the carriers drift through the remaining part of the diode. Thus, negative resistance can be produced at certain frequencies, typically in the microwave region. The diodes utilizing this phenomenon are called IMPATT diodes, an acronym IMPact ionization Avalanche Transit Time.

In general, the fundamental equations describing the avalanche process form a rather complex system and the existing analytical solutions have been obtained by making various simplifying assumptions. From these approaches the most general deterministic (i.e., noise excluding) solution known to this author is that of Kuvás and Lee²⁴. The differential equation which they obtained can be considered to be a generalization of the results

of Read²⁵ and Lee *et al.*,²⁶ which were developed for a device somewhat more complicated in structure, but easier to handle mathematically than a general p-n junction. This structure, the Read diode, has been used almost exclusively in various small- and large signal analyses of IMPATT diodes, as well as in noise studies of the latter. Although there exist various structures, the majority of devices used in actual practice are simple one-sided abrupt junctions, for which the Read diode structure is the closest approximation that lends itself to simple mathematical description. We shall, therefore, choose it as the mathematical model of the IMPATT diode.

4-1-2 The Read Diode

This structure, first suggested by Read²⁵ is shown in Fig. 4-1 with its doping profile and electric field distribution. Its most important feature is the division of the diode into two regions. In the high-field region, called the avalanche region, intensive avalanche multiplication takes place when a certain electric field is reached, whereas in the lower-field region, called the drift region, the injected carriers drift across under the influence of the electric field.

The fundamental quantities for the mathematical description of avalanche breakdown are the so called electron and hole ionization rates α_n and α_p and the electron and hole multiplication factors M_n and M_p , respectively. The former are defined as the number of electron-hole pairs generated by an electron (hole) per unit distance. They are strongly dependent on the electric field and this dependence is often approximated by

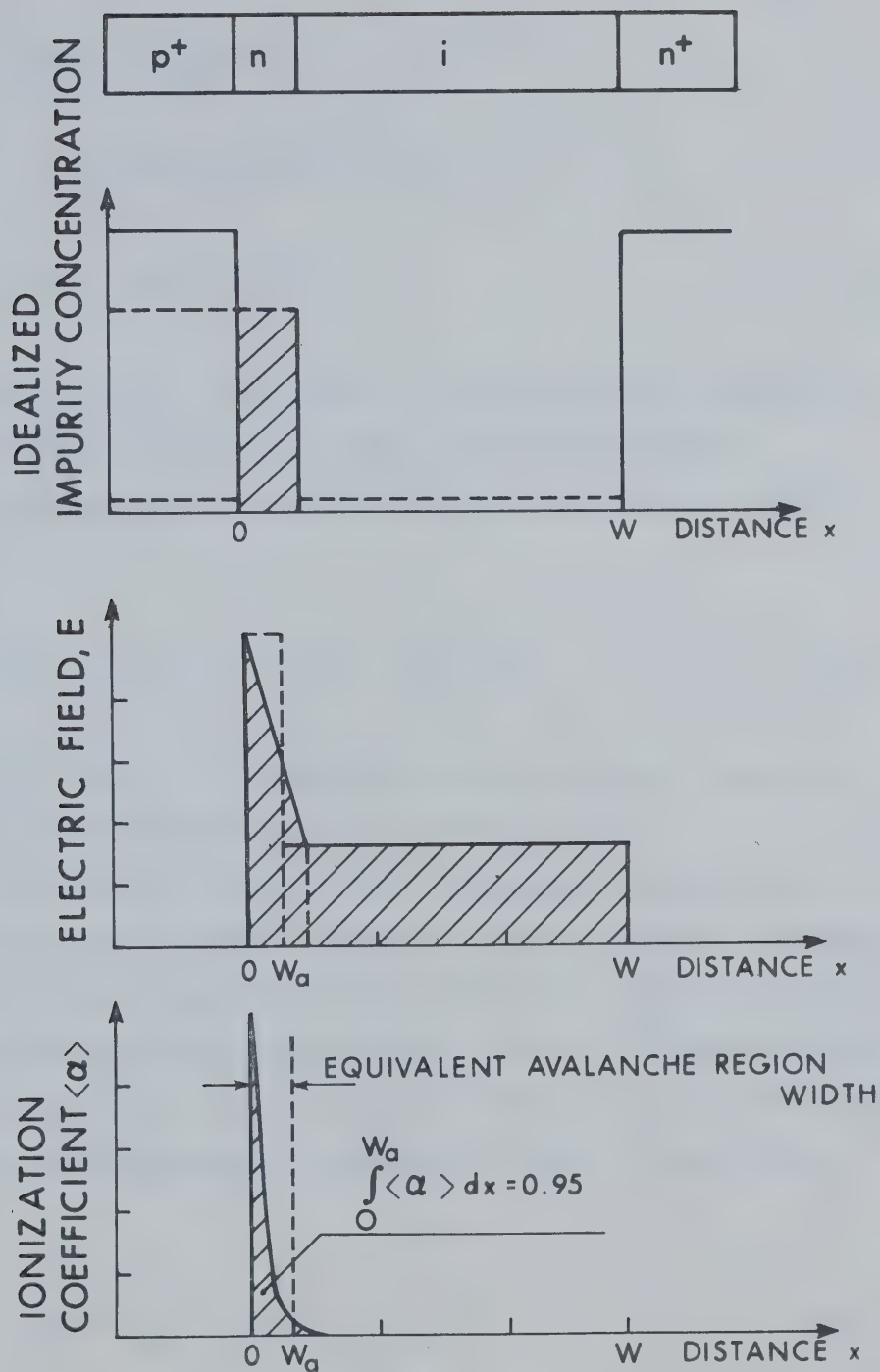


Fig. 4-1 READ DIODE: STRUCTURE, DOPING PROFILE, ELECTRIC FIELD DISTRIBUTION AND AVALANCHE REGION DEFINITION

$$\alpha_n \text{ or } \alpha_p = \alpha_0 \left(\frac{E}{E_0} \right)^m, \quad (4.1)$$

where α_0 , E_0 are constants and $m = 3-9$, or by

$$\alpha_n \text{ or } \alpha_p = A \exp[-(b/E)^m] \quad (4.2)$$

with the values of A , b and m given in tables for various semiconductor materials (typically Germanium, Silicon and Gallium arsenide).

The multiplication factors of electrons and holes are defined as follows:

$$M_p = I_p(w)/I_p(0) \quad ; \quad M_n = I_n(0)/I_n(w), \quad (4.3)$$

where $I_p(0)$ and $I_n(0)$ are the hole and electron currents, respectively, at the boundaries of the depletion layer of total width w .

The differential equation for the generated avalanche current has been derived first by Read²⁵. The most important assumptions were equal ionization rates and drift velocities for electrons and holes and neglect of space charge in the avalanche region. Lee *et al.*²⁶ generalized Read's analysis to different ionization rates and drift velocities while keeping the same form of differential equation; the latter can be written as follows

$$[\partial/\partial t + (M\tau)^{-1}]I_c(t) = I_s/\tau, \quad (4.4)$$

where $I_c(t)$ is the conduction (particle) current at $x = w_a$ i.e., the current flowing out of the avalanche region and consisting of the electron current $I_{cn}(t)$ and of the hole current $I_{cp}(t)$

$$I_c(t) = I_{cn}(t) + I_{cp}(t) \quad , \quad (4.5)$$

and where I_s is the total reverse saturation current consisting of the saturation current of electrons, I_{sn} and holes, I_{sp} :

$$I_s = I_{sn} + I_{sp} \quad . \quad (4.6)$$

The quantities M and τ in Eq. 4.4 are the "equivalent" multiplication factor and the so called intrinsic response time, respectively, which are given by the following relations²⁴:

$$MI_s = M_n I_{sn} + M_p I_{sp} \quad (4.7)$$

$$I_s/\tau = I_{sn}/\tau_n + I_{sp}/\tau_p \quad (4.8)$$

$$M_n^{-1} = 1 - \int_0^{w_a} \alpha_n \exp\left(-\int_x^{w_a} (\alpha_n - \alpha_p) dx'\right) dx \quad (4.9)$$

$$\tau_n = \int_0^{w_a} \exp\left(-\int_x^{w_a} (\alpha_n - \alpha_p) dx'\right) \frac{dx}{v_n + v_p} \quad (4.10)$$

and

$$M_n/M_p = \tau_n/\tau_p = \exp\left(\int_0^{w_a} (\alpha_n - \alpha_p) dx\right) \quad . \quad (4.11)$$

In the above expressions, v_n (v_p) is the electron (hole) velocity and τ_n (τ_p) is the electron (hole) intrinsic response time.

In addition to Eq. 4.4, another relation is needed to account for the influence of the displacement current through the device:

$$I_{ex}(t) = I_c(t) + \epsilon A \frac{dE_a(t)}{dt}, \quad (4.12)$$

where I_{ex} is the external (terminal) current, ϵ is the dielectric permittivity, A is the cross-sectional area of the diode and E_a is the electric field in the avalanche region.

In the noise problem, it has been generally assumed in the literature that the strongest contribution to the overall diode noise comes from the random ionization in the avalanche region. Other sources such as generation-recombination noise, flicker noise and noise due to the imperfections in contacts or the junction itself have been neglected. The first noise analysis of the dc-excited diode was published by Tager⁸, in which a driving noise source term was added to the right-hand side of Eq. (4.4) and its spectral properties were derived from the statistical considerations of the avalanche process. Other analyses^{9,10,11} followed, with some modifications, but all under the condition of the pure dc excitation of the diode. A more general derivation was given recently by Kuvás²⁰. The resulting equation for the conduction current is of the form of Eq. (4.4) with an added stochastic term whose spectral properties were derived for a combined dc and ac excitation of the diode:

$$[\partial/\partial t + (M\tau)^{-1}]I_c(t) = [I_s + F(t)]/\tau. \quad (4.13)$$

The statistical average of $F(t)$ is given by²⁰

$$\frac{\langle F(t)F(t+\sigma) \rangle_{Av}}{\tau^2} = \frac{e\delta(\sigma)I_c(t)}{\tau_n^2} \frac{\alpha_p}{\alpha_n} \left[1 - \frac{\alpha_p + \alpha_n}{2\alpha_p M_n} + \frac{\alpha_n - \alpha_p}{2\alpha_p M_n^2} \right] \quad (4.14)$$

Here e is the electronic charge and $\delta(\sigma)$ is the Dirac delta function. As can be seen from Eqs. (4.9) and (4.1) or (4.2), M_n is a function of electric field. Under the combined dc and ac excitation of the diode, M_n can be expanded in Fourier series²⁰. Also, $I_c(t)$ as a large-signal solution of the deterministic equation (4.4) (see Appendix-B) can be inserted into Eq. (4.14) and, after taking the time average of Eq. (4.14) and Fourier transforming the result, the power spectral density $S_{FF}(\omega)$ of $F(t)$ has the form²⁰

$$\frac{S_{FF}(\omega)}{\tau^2} = \frac{\langle |F(\omega)|^2 \rangle_{Av}}{\tau^2} = \frac{eI_o}{\tau_n \tau_p} \left[1 + \frac{\alpha_n - \alpha_p}{4\alpha_p} (\omega_c \tau_n D_1)^2 (1 - K_2) \right] \quad (4.15)$$

where I_o is the dc (bias) current through the diode, ω_c is the fundamental frequency of oscillation and D_1, K_2 come from the expansions of M_n described in Ref. 20. Since D_1 is proportional to E_1 ; i.e., to the electric field component at the fundamental frequency, the second term in parenthesis on the right-hand side of Eq. (4.15) represents a correction due to the presence of an ac signal.

According to Kuvás, this correction is small for reasonable signal levels so that

$$S_{FF}(\omega)/\tau^2 \approx eI_o/\tau_n \tau_p \quad (4.16)$$

which for $\tau_n = \tau_p = \tau$ (i.e., $M_n = M_p$, $\alpha_n = \alpha_p$, etc.) reduces to Tager's result⁸

$$S_{FF}(\omega) \triangleq eI_0 \quad (4.17)$$

Eqs. (4.13), (4.16) or (4.17) and (4.12) will be used for the application of the analysis presented in Chapter III.

4-1-3 Approximation of Real IMPATT Diodes by Read Diode Equations

As mentioned in Sec. 4-1-1, the majority of actual IMPATT devices are one-sided p-n junctions and the description by Eqs. (4.12) and (4.13) is only a coarse approximation for these. Yet many reasonable results have been obtained in the computation of various IMPATT diode properties with even the simplest form of Eq. (4.13), namely that resulting from the assumptions of equal ionization rates and drift velocities for both electrons and holes. Employing these assumptions in Eqs. (4.9) - (4.11) and substituting into Eq. (4.13), we obtain

$$\frac{\tau_a}{2} \frac{dI_c(t)}{dt} - I_c(t) \left(\int_0^w \alpha(E_a) dx - 1 \right) = I_s + F(t) \quad (4.18)$$

where τ_a is the transit time across the avalanche region:

$$\tau_a = w_a/v \quad (4.19)$$

Eq. (4.18) is the original Read equation and although it is strictly valid only for Germanium, it has been used for the analysis of Silicon diodes,

which are most commonly used in practice and for which the ionization rates α_n and α_p are different. In the latter case, the ionization integral in Eq. (4.18) can be approximated as follows⁸:

$$\int_0^w \alpha dx = \int_0^w \bar{\alpha} dx \quad (4.20)$$

with

$$\bar{\alpha} = (\alpha_p - \alpha_n) / \ln(\alpha_p / \alpha_n) \quad , \quad (4.21)$$

and where the average ionization coefficient $\bar{\alpha}$ is assumed to have a similar dependence on the electric field as α_p or α_n in Eqs. (4.1) or (4.2). Specifically, we shall later employ the approximation

$$\bar{\alpha}(E_a) = w_a^{-1} (E_a/E_b)^m \triangleq w_a^{-1} [1 + m(E_a - E_b)/E_b] \quad , \quad (4.22)$$

where E_b is the electric field in the avalanche region, at breakdown. Employing the usual assumption of E_a being independent of position in the narrow avalanche region, the ionization integral is simply

$$\int_0^w \bar{\alpha}(E_a) dx = \bar{\alpha}(E_a) w_a \triangleq [1 + m(E_a - E_b)/E_b] \quad . \quad (4.23)$$

As pointed out in Ref. 24, the intrinsic response time τ generally differs from the value $\tau_a/2$, which in a realistic diode must be corrected to account for the influence of space charge in the avalanche region and that of the drift region. These corrections depend on the ratio of ionization coefficients and drift velocities for electrons and holes in a complicated manner²⁴. The corresponding formulas would not be practical to

use for our purpose; instead, Eq. (4.18) will be rewritten as follows (also using Eq. (4.23)):

$$k\tau_a \frac{dI_c(t)}{dt} - I_c(t)(\bar{\alpha}(E_a)w_a - 1) = I_s + F(t) \quad , \quad (4.24)$$

and the correction factor k will be calculated from the data given by Kuvás²⁰, which are based on measurements of representative diodes at 6 GHz. These data are summarized in Table 4-1, Sec. 4-3-1.

Also, if Eq. (4.24) is to be used for a p-n junction, the effective avalanche region width must be evaluated from the electric field distribution^{27,28}; Table 4-1 gives Kuvás' values for w_a and also w , the total diode length.

Finally, for one-sided abrupt p-n junctions, the following relation holds between the voltage V_b across the diode at breakdown and the maximum electric field in the avalanche region E_{\max} ²⁷:

$$V_b \approx E_{\max} w / 2 \quad . \quad (4.25)$$

Eqs. (4.12), (4.17), (4.24) together with the data in Table 4-1 and Eq. (4.25) are believed to represent typical IMPATT diodes and will be used in the actual computations.

4-2 Derivation of the Open-Circuit Noise Voltage

4-2-1 Excitation of the Diode

In order to properly apply the mathematical procedure described in

Chapters II and III, the appropriate equivalent circuit must be chosen for the specific oscillator under investigation. Experiments have shown that, in singly-tuned IMPATT diode oscillators, negligible power is delivered to the external circuit at higher harmonics, and Kuvàs²⁰ gave a simple theoretical proof that the external current components at higher harmonics of the oscillation frequency can be neglected. This implies that the equivalent circuits of Fig. 2-1a and 3-1a are suitable models; the mathematical procedure will be oriented towards obtaining an equation of the form (3.20), for the open-circuit noise voltage rather than short-circuit noise current.

Furthermore, the deterministic large-signal analysis which gives the dc and periodic voltages and currents and is necessary in the actual evaluation of the coefficients in Eq. (3.20) is also affected by this choice of the equivalent circuit. The external deterministic current is assumed to consist only of a dc component plus a periodic one at frequency ω_c , the frequency of oscillation. The results of the corresponding large-signal theory of IMPATT diodes, as derived by Kuvàs²⁰, are given in Appendix-B.

4-2-2 Langevin Equation for Stochastic Quantities

If Eqs. (4.12) and (4.22) are substituted into Eq. (4.24), a non-linear differential equation results, similar in form to Eq. (3.1):

$$k\tau_a \left[-\varepsilon A \frac{d^2 E_a(t)}{dt^2} + \frac{dI_{ex}(t)}{dt} \right] + m \frac{E_a(t) - E_b}{E_b} \left[\varepsilon A \frac{dE_a(t)}{dt} - I_{ex}(t) \right] +$$

$$- I_s = F(t) \quad . \quad (4.26)$$

Using

$$E_a(t) = E_{ad}(t) + E_{as}(t) \quad ; \quad E_{as}(t) \ll E_{ad}(t) \quad (4.27)$$

$$I_{ex}(t) = I_{exd}(t) + I_{exs}(t) \quad ; \quad I_{exs}(t) \ll I_{exd}(t) \quad (4.28)$$

as in Eqs. (3.2) and (3.3), the stochastic part of Eq. (4.26) becomes

$$\begin{aligned} k\tau_a \left[-\varepsilon A \frac{d^2 E_{as}(t)}{dt^2} + \frac{dI_{exs}(t)}{dt} \right] + m \frac{E_{as}(t)}{E_b} \left[\varepsilon a \frac{dE_{ad}(t)}{dt} - I_{exd}(t) \right] \\ + m \frac{E_{ad}(t) - E_b}{E_b} \left[\varepsilon A \frac{dE_{as}(t)}{dt} - I_{exs}(t) \right] = F(t) \quad , \end{aligned} \quad (4.29)$$

where the stochastic part of the reverse saturation current I_s is neglected, since it is small compared to $F(t)$ ⁸.

4-2-3 Fourier Transform of Langevin Equation; Open-Circuit Noise

Voltage

The deterministic quantities I_{exd} and E_{ad} in Eq. (4.29) will now be expanded into Fourier series as follows:

$$I_{exd}(t) = I_0 + I_1 \cos \omega_c t = \frac{1}{2} \sum_{n=-\infty}^{\infty} I_{exn} \exp(jn\omega_c t) \quad , \quad (4.30)$$

where

$$I_{exn} = 0 \quad \text{for } |n| > 1 \quad (4.31)$$

and

$$E_{ad}(t) = \frac{1}{2} \sum_{n=-\infty}^{\infty} E_{an} \exp(jn\omega_c t) \quad . \quad (4.32)$$

Similar expansions can be written for the conduction current $I_{cd}(t)$ and for the voltage $V_d(t)$:

$$I_{cd}(t) = \frac{1}{2} \sum_{n=-\infty}^{\infty} I_{cn} \exp(jn\omega_c t) \quad (4.33)$$

$$V_d(t) = \frac{1}{2} \sum_{n=-\infty}^{\infty} V_n \exp(jn\omega_c t) \quad (4.34)$$

The substitution of Eqs. (4.30) and (4.32) into Eq. (4.29) leads to an equation similar in form to Eq. (3.12):

$$\begin{aligned} & -k\tau_a \epsilon A \frac{d^2 E_{as}(t)}{dt^2} + \frac{dE_{as}(t)}{dt} \left[\frac{m\epsilon A}{E_b} \left(\frac{1}{2} \sum_{n=-\infty}^{\infty} E_{an} \exp(jn\omega_c t) - E_b \right) \right] + \\ & - \frac{dI_{exs}(t)}{dt} k\tau_a + E_{as}(t) \left\{ \frac{m}{2E_b} \sum_{n=-\infty}^{\infty} (jn\omega_c t \epsilon A E_{an} - I_{exn}) \exp(jn\omega_c t) \right\} + \\ & - I_{exs}(t) \frac{m}{E_b} \left[\frac{1}{2} \sum_{n=-\infty}^{\infty} E_{an} \exp(jn\omega_c t) - E_b \right] = F(t) \quad (4.35) \end{aligned}$$

Applying Fourier transform to Eq. (4.35) and limiting the number of terms yields an equation of the form

$$\sum_{n=-M}^M A_n E_{as}(\omega + n\omega_c) + B_n I_{exs}(\omega + n\omega_c) \doteq F(\omega) \quad (4.36)$$

which corresponds to Eq. (3.13) in Chapter III.

The coefficients A_n and B_n , from Eq. (4.35), are

$$A_0 = j\omega \epsilon A [m(E_{a0} - E_b)/E_b - j\omega k\tau_a] - mI_{o0}/E_b \quad (4.37)$$

$$B_0 = j\omega k\tau_a - m(E_{a0} - E_b)/E_b \quad (4.38)$$

$$A_{n \neq 0} = (j\omega m e A / 2E_b) E_{an}^* - (m/2E_b) I_{exn}^* \quad (4.39)$$

$$B_{n \neq 0} = -(m/2E_b) E_{an}^* \quad (4.40)$$

Substituting

$$\omega = \Omega + \ell\omega_c, \quad |\Omega| \ll \omega_c, \quad \ell = \text{integer} \quad (4.41)$$

(as in Sec. 3-3) into Eq. (4.36) and introducing $p = \ell + n$, we obtain

$$\sum_{p=-M}^M A_{p-\ell, \ell} E_{as}(\Omega + p\omega_c) + B_{p-\ell, \ell} I_{exs}(\Omega + p\omega_c) \triangleq F(\Omega + \ell\omega_c) \quad (4.42)$$

for $-M \leq \ell \leq M$.

Here

$$A_{p-\ell, \ell} = A_{p-\ell}(\omega = \Omega + \ell\omega_c); \quad B_{p-\ell, \ell} = B_{p-\ell}(\omega = \Omega + \ell\omega_c) \quad (4.43)$$

Eq. (4.42) is the equivalent of Eq. (3.16) in Sec. 3-3.

The field and current components E_{an} and I_{exn} , respectively, in Eqs. (4.37) - (4.40) must be determined from a separate large-signal analysis. In Appendix-B, the Fourier components of the conduction current $I_{cd}(t)$ can be calculated from the normalized electric field component E_{a1}/E_b at the fundamental frequency ω_c . It therefore appears advantageous to replace E_{an}^* and I_{exn}^* in Eqs. (4.37) - (4.40) by the

conduction current components I_{cn}^* . The appropriate relations can be derived from Eq. (4.12). This equation also enables us to express $I_{exs}(\omega)$ in terms of $E_{as}(\omega)$ so that Eq. (4.42) may be written in the form

$$\sum_{p=-M}^M a_{p-\ell, \ell} E_{as}(\Omega + p\omega_c)/E_b \doteq F(\Omega + \ell\omega_c)/mI_0$$

$$-M \leq \ell \leq M \quad . \quad (4.44)$$

The above-mentioned relations are given in Appendix-A. The final normalized form of the coefficients $a_{p-\ell, \ell}$ is derived in Appendix-C.

Since we are interested in the open-circuit noise voltage rather than the electric noise field, the corresponding relation between these two quantities must be known; this is also derived in Appendix-A. This relation may be inserted into the matrix system (4.44) to obtain a similar system with modified coefficients

$$\sum_{p=-M}^M c_{p-\ell, \ell} V_s(\Omega + p\omega_c)/V_b \doteq F(\Omega + \ell\omega_c)/mI_0$$

$$-M \leq \ell \leq M \quad , \quad (4.45)$$

from which $V_s(\Omega + p\omega_c)/V_b$ is obtained by inversion. An alternative is to invert Eq. (4.44) first and then compute the open-circuit noise voltage from the electric noise field. These two alternatives may not be equivalent from a computational point of view, as will be mentioned in

the next section.

Once the relation for the Fourier transform of the open-circuit noise voltage is known, the procedure described in Sections 3-4 and 3-5 is applied to compute the initial and output noise spectra.

4-3 Computed Noise Spectra

4-3-1 Computation: Conditions, Input Data, Procedure

The formulas derived in the previous sections are used to compute both the 'initial' (pre-oscillation) and output modulation spectra of IMPATT oscillators employing a simple series resonant circuit. The computations are carried out for Si, Ge, and GaAs abrupt junction diodes with physical parameters as given in Table 4-1 for various values of the electric parameters specifying the operating point. The physical parameters themselves were also varied. This is important, since they are only equivalent parameters that originate, for example, from an effort to fit the Read diode equations to an abrupt junction diode. As such, they are subject to considerable variation as evidenced by the differing data deemed typical found in the literature^{8,10,20,28}. Besides, actual diodes do differ in their structures even if designed for the same frequency. In the calculations the series resistance of the diode is assumed to be included in the external circuit and its effect is taken into account only in the final comparisons of computed and measured spectra, based on the output power rather than diode voltage. No noise sources other than that associated with the random ionization in the avalanche region are

considered.

Since the initial spectra are of considerable interest in this case, the "all-matrix" method suggested in Sec. 3-5 is not used; instead, the initial spectral densities are calculated from the corresponding formulas as given in Sec. 3-4 and then the computation of the output spectra is carried out. In this way, a better insight is obtained into the mechanism of noise increase in IMPATT diodes under large-signal conditions.

We shall now describe the computational procedure step by step, bringing together all the key equations in the proper order and hopefully making the application of the method described in this thesis clear. The procedure makes use of the normalized quantities introduced in Appendices -A and B.

Calculation of the initial spectra:

Step 1: The following parameters (introduced in Appendix-A) characterizing an IMPATT diode, are assigned specific values:

$$m, (\omega_a/\omega_c)^2, k, \omega_c \tau_d, w_a/w_d, \omega_M/\omega_c.$$

From these m and k are fixed as found in Table 4-1, and $\omega_c \tau_d$ and w_a/w_d are varied around the values given in Table 4-1. The parameter $(\omega_a/\omega_c)^2$ is varied in the range 0.1 - 0.7, which is typical for IMPATT diode oscillators. The parameter (ω_M/ω_c) is typically in the range 10^{-4} - 10^{-6} .

TABLE 4-1 SOME PARAMETERS OF REPRESENTATIVE IMPATT DIODES
AT 6 GHz (From Ref. 20)

	GaAs	Ge	Si
$D = m/k\omega_c\tau_a$	12	7	17
$W(\mu\text{m})$	5.0	5.5	6.0
$\omega_c\tau_d$	2.6	2.9	2.6
$E_b(10^5\text{V/cm})$	4.2	2.0	3.6
$v(10^6\text{cm/s})$	6	6	7
$w_a(\mu\text{m})$	0.8	0.8	1.2
w_a/w_d	0.19	0.17	0.25
$\tau(\text{ps})$	22	14	9.6
m	10.4	3.9	6.3
k	1.75	1.10	0.57

Step 2: For a given combination of the above parameters, several consecutive values of the normalized electric field component $|e_{a1}| = |E_{a1}/E_b|$ at the fundamental frequency ω_c are chosen, typically in the range 0.02 - 0.3. This covers the range of electric field magnitudes occurring in practice. To each of these there corresponds a certain conduction current (normalized with respect to the dc current), whose components are computed from (see Appendix-B, Eqs. (B.2) - (B.5))

$$i_{cn} = I_{cn}/I_o = 2(-1)^p \{f_n + (\omega_a/\omega_c)\}^2 \sum_{p=2}^{\infty} (f_{p-n} + f_{p+n} - 2f_n f_p) f_p / p^2 \quad , \quad (4.46)$$

where

$$f_n = I_n(De_{a1})/I_0(De_{a1}) \quad (4.47)$$

with I_n and I_0 being the modified Bessel functions, and

$$D = (m/k)(\omega_c \tau_d w_a/w_d)^{-1} \quad (4.48)$$

The number of components needed must be determined by trial and error, until the result in Step 6 does not change appreciably with the increase in the number of components. It turns out that 5 harmonic components are sufficient for this purpose.

Step 3: The normalized diode voltage component v_1 at frequency ω_c is computed from (see Appendix-B, Eq. (B.8))

$$v_1 = \frac{V_1}{V_b} = 2 \left\{ \frac{i_{c1} [\theta(\omega_c) - 1]}{j(\omega_a/\omega_c)^{-2D(1+w_a/w_d)}} - j|e_{a1}| \right\} \quad (4.49)$$

where

$$\theta(\omega_c) = [1 - \exp(-j\omega_c \tau_d)] / j\omega_c \tau_d \quad (4.50)$$

The normalized output voltage component v_c at frequency ω_c is then computed from (see Appendix-B, Eq. (B.10))

$$v_c = V_c/V_b = \text{Re}(v_1) \quad (4.51)$$

The normalized external current component i_{ex1} at frequency ω_c is determined

from (see Appendix-B, Eq. (B.7))

$$i_{ex1} = I_{ex1}/I_0 = i_{c1} - D(\omega_a/\omega_c)^{-2}|e_{a1}| \quad , \quad (4.52)$$

and the normalized impedance $z(\omega_c)$ of the external circuit, needed to sustain oscillations, is given by (see Appendix-B, Eq. (B.9))

$$z(\omega_c) = \omega_c C_d Z(\omega_c) = (D/2)(\omega_a/\omega_c)^{-2} v_1 / i_{ex1} \quad . \quad (4.53)$$

Step 4: The normalized baseband frequency parameter Ω/ω_c is assigned a value, typically in the range 10^{-8} to 10^{-4} and the normalized impedance of the external circuit at baseband frequencies,

$$z(\Omega) = \omega_c C_d Z(\Omega) \quad , \quad (4.54)$$

is assigned a value in the range 0 to ∞ .

The coefficients $a_{p-l, l}$ in the conversion matrix (4.44),

$$\sum_{p=-M}^M a_{p-l, l} \frac{E_{as}(\Omega + p\omega_c)}{E_b} = \sum_{-M}^M a_{p-l, l} e_{as}(\Omega + p\omega_c) = \frac{F(\Omega + l\omega_c)}{mI_0} \quad , \quad (4.55)$$

are calculated from Appendix-C, Eqs. (C.13), (C.14), (C.15) and (C.16):

For $p-l = 0$

$$a_{p-l, l} = \{ j(\frac{\Omega}{\omega_c} + l)(\frac{\omega_a}{\omega_c})^{-2} [\frac{\omega_M}{\omega_c} + j(\frac{\Omega}{\omega_c} + l)] [\psi(\Omega + l\omega_c) - 1] \quad . \quad (4.56)$$

For $p-l \neq 0$

$$a_{p-l, l} = -\frac{1}{2} i_{c(p-l)}^* \left\{ 1 + \left(\frac{\Omega}{\omega_c} + p \right) \frac{1 - \psi(\Omega + p\omega_c)}{(p-l) \{ \psi^*[(p-l)\omega_c] - 1 \}} \right\} \quad (4.57)$$

The auxiliary parameter $\psi(\omega)$ is computed as follows (see Appendix-C, Eqs. (C.18) - (C.20)):

$$\psi(\Omega) = [j\Omega/\omega_c z(\Omega)]^{-1} \quad (4.58)$$

$$\left. \begin{array}{ll} \psi(\Omega + q\omega_c) & \text{for } |q| > 1 \\ \psi(n\omega_c) & \text{for } |n| > 1 \end{array} \right\} = 0 \quad (4.59)$$

$$\psi(\omega_c) = (1 - i_{c1}/i_{ex1})^{-1} \quad (4.60)$$

Step 5: The matrix of coefficients $a_{p-l, l}$ is inverted:

$$[a_{p-l, l}^i] = [a_{p-l, l}]^{-1} \quad -M \leq p, l \leq M \quad (4.61)$$

In order to obtain a matrix that relates an open-circuit noise voltage, rather than electric field, to the basic noise process $F(\omega)$ (as in Eq. (3.20)), the elements $a_{p-l, l}$ are multiplied by the corresponding relation (see Appendix-A, Eq. (A.25)):

$$c_{p-l, l}^i = -2a_{p-l, l}^i [\theta(\Omega + p\omega_c) + w_a/w_d] (1 + w_a/w_d)^{-1} \quad (4.62)$$

so that an expression for the normalized noise voltage $v_s = V_s/V_b$ is obtained:

$$[v_{sp}] = (1/mI_0)[c_{p-\ell,\ell}^i][F_\ell] \quad , \quad (4.63)$$

where

$$v_{sp} = v_s(\Omega + p\omega_c) \quad ; \quad F_\ell = F(\Omega + \ell\omega_c) \quad . \quad (4.64)$$

The above procedure has been safer computationally than the alternative of changing the original matrix before inversion. The latter alternative often resulted in an ill-conditioned matrix.

Step 6: The initial spectra can now be computed from Eqs. (3.30) - (3.35), where, instead of V_c , its normalized value $v_c = V_c/V_b$ is used, since the matrix coefficients $c_{p-\ell,\ell}^i$ are now also normalized to V_b . Using Eq. (4.17)

$$S_{FF}(\Omega + \ell\omega_c) = eI_0 \quad , \quad (4.65)$$

and choosing the dc current I_0 (typically in the range 10 - 100 mA), we obtain

$$S_{mm}(\Omega) = 2(me/I_0) \sum_{\ell=-M}^M |c_{1-\ell,\ell}^i/v_c + c_{-1-\ell,\ell}^i/v_c^*|^2 \quad (4.66)$$

$$S_{\phi\phi}(\Omega) = 2(me/I_0) \sum_{\ell=-M}^M |c_{1-\ell,\ell}^i/v_c - c_{-1-\ell,\ell}^i/v_c^*|^2 \quad (4.67)$$

$$S_{m\phi}(\Omega) = 4 \frac{me}{I_0} \sum_{\ell=-M}^M \operatorname{Im} \left(\frac{c_{1-\ell,\ell}^i c_{-1-\ell,\ell}^{i*}}{V_C^2} \right) + j \left\{ \left| \frac{c_{1-\ell,\ell}^i}{V_C} \right|^2 - \left| \frac{c_{-1-\ell,\ell}^i}{V_C^*} \right|^2 \right\} . \quad (4.68)$$

Replacing V_0 in Eqs. (3.31), (3.34) and (3.38) by V_b ($V_0 \neq V_b$ in case of IMPATT diodes), we have

$$S_{bb}(\Omega) = 2(me/I_0) \sum_{\ell=-M}^M |c_{-\ell,\ell}^i|^2 \quad (4.69)$$

$$S_{mb}(\Omega) = 2(me/I_0) \sum_{\ell=-M}^M c_{-\ell,\ell}^{i*} (c_{1-\ell,\ell}^i/V_C + c_{-1-\ell,\ell}^i/V_C^*) \quad (4.70)$$

and

$$S_{\phi b}(\Omega) = -j2(me/I_0) \sum_{\ell=-M}^M c_{-\ell,\ell}^{i*} (c_{1-\ell,\ell}^i/V_C - c_{-1-\ell,\ell}^i/V_C^*) . \quad (4.71)$$

The spectra of the normalized open-circuit noise voltage at the sidebands, from Eqs. (3.36) and (3.37), are

$$S_{VV}(\omega_C + \Omega) = 2(me/I_0) \sum_{\ell=-M}^M |c_{1-\ell,\ell}^i|^2 \quad (4.72)$$

$$S_{VV}(\omega_C - \Omega) = 2(me/I_0) \sum_{\ell=-M}^M |c_{-1-\ell,\ell}^i|^2 . \quad (4.73)$$

The additional factor of 2 in formulas (4.66) - (4.73) has been introduced to obtain the magnitude of real spectra with Ω positive only.

Calculation of the output spectra:

In general, all the initial spectra must be inserted into Eq. (2.60).

However, if $S_{\phi\phi} \gg S_{mm}$, the simplified method given in Sec. 2-5 can be used to compute the output spectra. The previously computed initial spectra $S_{mm}(\Omega)$, $S_{\phi\phi}(\Omega)$, $S_{mb}(\Omega)$, $S_{\phi b}(\Omega)$ and $S_{bb}(\Omega)$ are then inserted into the equations (see Ch. II, Eq. (2.69) and (2.70))

$$S_{MM}(\Omega) = |P_{11}^i|^2 S_{mm}(\Omega) + 2\text{Re}\{(P_{11}^i P_{12}^{i*}) S_{mb}(\Omega)\} + |P_{12}^i|^2 S_{bb}(\Omega) \quad (4.74)$$

$$S_{\Phi\Phi}(\Omega) = |P_{33}^i|^2 S_{\phi\phi}(\Omega) + 2\text{Re}\{(P_{32}^{i*} P_{33}^i) S_{\phi b}(\Omega)\} + |P_{32}^i|^2 S_{bb}(\Omega) , \quad (4.75)$$

where the coefficients P^i , given by Eqs. (2.63), (2.64), (2.71) and (2.72), can be written in a normalized form, realizing that

$$A_c^i = I_{ex1} ; R_L = \text{Re}[z(\omega_c)]/\omega_c C_d ; Z_g^\omega = -z(\omega_c)/\omega_c C_d ;$$

$$\left| \frac{dZ_L}{d\omega_c} \right| = R_L \frac{Q_{ex}}{\omega_c} ; \quad \theta \doteq \frac{\pi}{2} . \quad (4.76)$$

Hence

$$P_{11}^i = \left\{ \frac{i_{ex1}}{\text{Re}z(\omega_c)} \left| \frac{\partial z(\omega_c)}{\partial i_{ex1}} \right| \sin\left(\frac{\pi}{2} - \eta\right) \right\}^{-1} \quad (4.77)$$

$$P_{33}^i = \left\{ \left(\frac{\Omega}{\omega_c}\right) Q_{ex} \sin\left(\frac{\pi}{2} - \eta\right) \right\}^{-1} \quad (4.78)$$

$$P_{12}^i = I_o \frac{z_o}{z_T(\Omega)} \frac{\partial z(\omega_c)}{\partial I_o} \sin\left(\frac{\pi}{2} - \psi\right) \left\{ i_{ex1} \frac{\partial z(\omega_c)}{\partial i_{ex1}} \sin\left(\frac{\pi}{2} - \eta\right) \right\}^{-1} \quad (4.79)$$

$$P_{32}^i = I_o \frac{z_o}{z_T(\Omega)} \frac{\partial z(\omega_c)}{\partial I_i} \sin(\eta - \psi) \left\{ \frac{\Omega}{\omega_c} Q_{ex} \text{Re}z(\omega_c) \sin\left(\frac{\pi}{2} - \eta\right) \right\}^{-1} , \quad (4.80)$$

where $z_0 = \omega_c C_d Z_0$.

The expression for $S_{\phi\phi}(\Omega)$ can be greatly simplified by using Vlaardingbroek's condition given by Eq. (2.53) which simply means that for IMPATT diodes

$$\eta - \psi \cong 0 \quad (4.81)$$

and hence $P_{32}^i = 0$.

Therefore only the primary noise remains:

$$S_{\phi\phi}(\Omega) = |P_{33}^i|^2 S_{\phi\phi}(\Omega) \quad (4.82)$$

and the rms frequency deviation is

$$\Delta f_{\text{rms}} = (f_c / Q_{\text{ex}}) [S_{\phi\phi}(\Omega)]^{1/2} \quad (4.83)$$

The expression for $S_{MM}(\Omega)$ can be similarly simplified only if $z_T(\Omega) \rightarrow \infty$ and all modulation noise disappears. Then

$$S_{MM}^0(\Omega) = |P_{11}^i|^2 S_{mm}(\Omega) \quad (4.84)$$

However, for $z_T(\Omega)$ finite, the magnitude of the modulation term in the complete Eq. (4.74) has already been assessed elsewhere¹² and one only has to be concerned about the influence of the cross-spectral term (second term on the right-hand side of Eq. (4.74)). One might speculate that this term could cause a noise minimum at a bias impedance lower than

$z_T(\Omega) \rightarrow \infty$. However, should the cross-spectrum $S_{mb}(\Omega)$ turn out to be smaller than the smaller of $S_{mm}(\Omega)$ and $S_{bb}(\Omega)$, such a compensation is impossible and only the primary noise given by Eq. (4.84) needs to be studied.

Finally, for comparisons of the computed and measured spectra it is advantageous to plot these spectra in dependence on the diode output power rather than voltage since the latter quantity is difficult to measure with reasonable accuracy in an actual oscillator. This is carried out in Chapter V, Sec. 5-3. However, the voltage scale of the computed spectra must first be changed to output power scale, using the known values of series resistance R_s and negative resistance $\text{Re } Z(\omega_c)$ in Eq. (B.12), and using Eq. (B.9) which relates diode impedance and voltage. From the maximum RF power generated by the measured diode at a given dc current, and from the known diode impedance and series resistance at this power level, the corresponding rms voltage across the diode is obtained. This is usually close to the maximum attainable rms voltage which, according to several references^{19,29,30}, is approximately equal to $0.3V_b$ for Silicon abrupt-junction diodes, while for Germanium diodes this maximum is approximately $0.57V_b$ (the latter datum is from Ref. 19). The corresponding value for GaAs abrupt-junction diodes is believed to be between the data for Silicon and Germanium diodes. To the knowledge of this author, no more accurate information is available in the literature. The relative changes in diode impedance for corresponding changes in diode RF voltage can be computed from Eq. (B.9) and, assuming that the series resistance R_s does not change with RF voltage, the power at the oscillator output can be computed for each value of the diode RF voltage. The computed and

measured noise spectra of the oscillator can then be graphically compared, using output power as the x-coordinate and noise spectral density as the y-coordinate.

4-3-2 Plots of Computed Spectra and Discussion

The procedure described in the previous section yielded data for the initial and output noise spectra as a function of the physical and electrical parameters of the IMPATT diode and of the external oscillator circuit. Numerous plots can be constructed using the above mentioned data. The most important of these are shown in Figs. 4-2 to 4-9 in this section. With the exception of Figs. 4-8 and 4-9, which compare the output amplitude and frequency noise spectra of IMPATT diodes made from Si, Ge and GaAs, these graphs are for Si diodes and depict the initial auto- and cross spectra, or the open-circuit noise voltages of these, in dependence on diode and circuit parameters. These are: RF electric field, RF voltage, bias circuit conductance, drift transit angle, relative avalanche region width and avalanche-to-carrier frequency ratio. Corresponding plots for GaAs and Ge diodes are similar and need not be shown here.

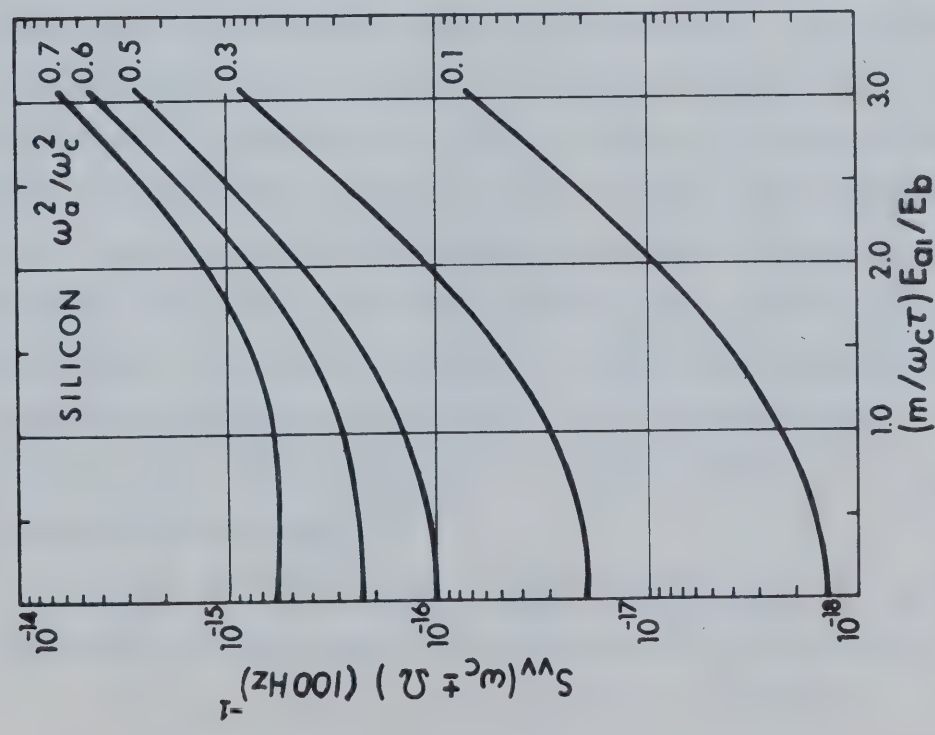
The frequency dependence of the computed initial spectra turned out to be negligible in the baseband frequency range of interest. Hence, the parameter Ω/ω_c is not included in most of the plots. All noise spectra have been computed for a dc bias current of 10 mA. For other currents, the power spectra and the rms frequency deviation must be divided by $I_0(\text{mA})/10$ and by $[I_0(\text{mA})/10]^{1/2}$, respectively.

The range of the diode parameter w_a/w_d (avalanche-to-drift region

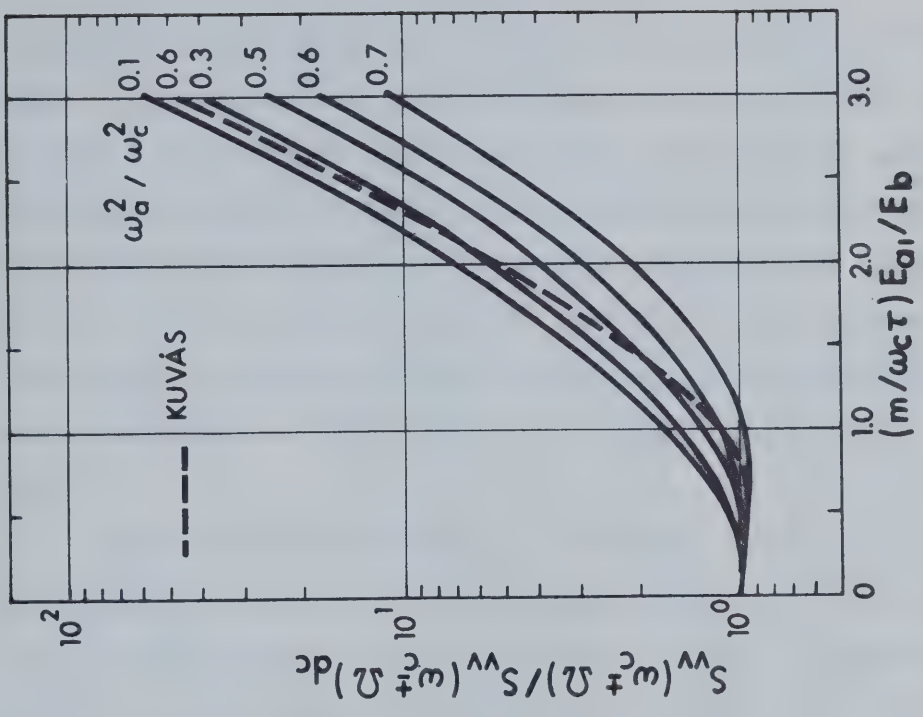
length ratio) has been chosen somewhat arbitrarily around Kuvás' values in Table 4-1. There is no need for great accuracy in this respect, since these values vary from diode to diode, being dependent on diode structure and background doping concentration²⁸. Moreover, the above ratio seems to depend strongly on how the equivalent avalanche region width is defined. For example, the data in Ref. 27 differ completely from those in Ref. 28, where a different definition of avalanche region width is used. Yet, these uncertainties do not detract from the value of the plots given here, since the plots also show how the noise spectra are affected by the changes of the parameter involved.

The drift transit angle $\omega_c \tau_d$ is also affected by the uncertainty in avalanche region width; it further depends on the oscillation frequency and may vary from below 2 to more than 3 for some structures. The value of 3 has been chosen for some of the plots with a fixed $\omega_c \tau_d$ since, according to Ref. 20, this value should be an optimum compromise between good noise performance and reasonable output power.

Fig. 4-2a shows the dependence of the open-circuit noise voltage spectrum on the parameter $(m/\omega_c \tau) E_{a1}/E_b$ for several values of ω_a^2/ω_c^2 . While decreasing ω_a^2/ω_c^2 results in decreasing noise voltage spectral density, it also makes the dependence of the latter on electric field steeper. This can be better seen in Fig. 4-2b, where the open circuit noise voltage spectrum, normalized to its small-signal value, is again plotted as a function of the quantity $(m/\omega_c \tau) \times E_{a1}/E_b$ with ω_a^2/ω_c^2 as a parameter, and a comparison is made for $\omega_a^2/\omega_c^2 = 0.6$ with the curve of Kuvás²⁰. The increasing difference of the two corresponding curves at higher fields may



a) OPEN-CIRCUIT NOISE VOLTAGE SPECTRUM AS A FUNCTION OF RF ELECTRIC FIELD



b) OPEN-CIRCUIT NOISE VOLTAGE SPECTRUM, NORMALIZED TO ITS SMALL-SIGNAL VALUE, AS A FUNCTION OF RF ELECTRIC FIELD

Fig. 4-2

be caused by the different matrix sizes used ($M=5$, compared to $M=2$ of Kuvás). It was found in our calculations that a value of M larger than 5 did not influence the results significantly. Also, there is some experimental evidence³¹ that Kuvás' noise voltage increases too rapidly with increasing electric field. However, its basic behaviour is the same as that of the present data in Fig. 4-2. At low RF fields, the open-circuit noise voltage does not differ appreciably from that existing under pure dc excitation; at higher fields, it increases rapidly with increasing field.

Fig. 4-3 shows the dependence of the initial modulation spectra on the normalized RF diode voltage, for various values of ω_a^2/ω_c^2 as a parameter. At very low RF voltage, the amplitude- and phase spectra are almost equal; to this, there corresponds an open-circuit noise voltage in Fig. 4-2 almost equal to that existing under pure dc excitation. With increasing RF voltage (and electric field) the difference between the initial amplitude- and phase spectra increases also. Figs. 4-2 and 4-3 thus confirm the general considerations in Chapter II; the perturbing noise voltage source is amplitude-dependent and its orthogonal components $v_c(t)$ and $v_s(t)$, which are directly related to the initial modulation rates have, in general, non-equal spectra. Also shown in Fig. 4-3 is the RF voltage dependence of the cross-spectrum of amplitude and phase, $S_{m\phi}(\Omega)$, in absolute value. It is seen that, for a high impedance in the bias circuit, $Z(\Omega) \rightarrow \infty$, this cross-spectrum is insignificant.

In Fig. 4-4, the normalized baseband spectrum $S_{bb}(\Omega)$ and the absolute value of the amplitude-baseband cross spectrum $S_{mb}(\Omega)$ are plotted as

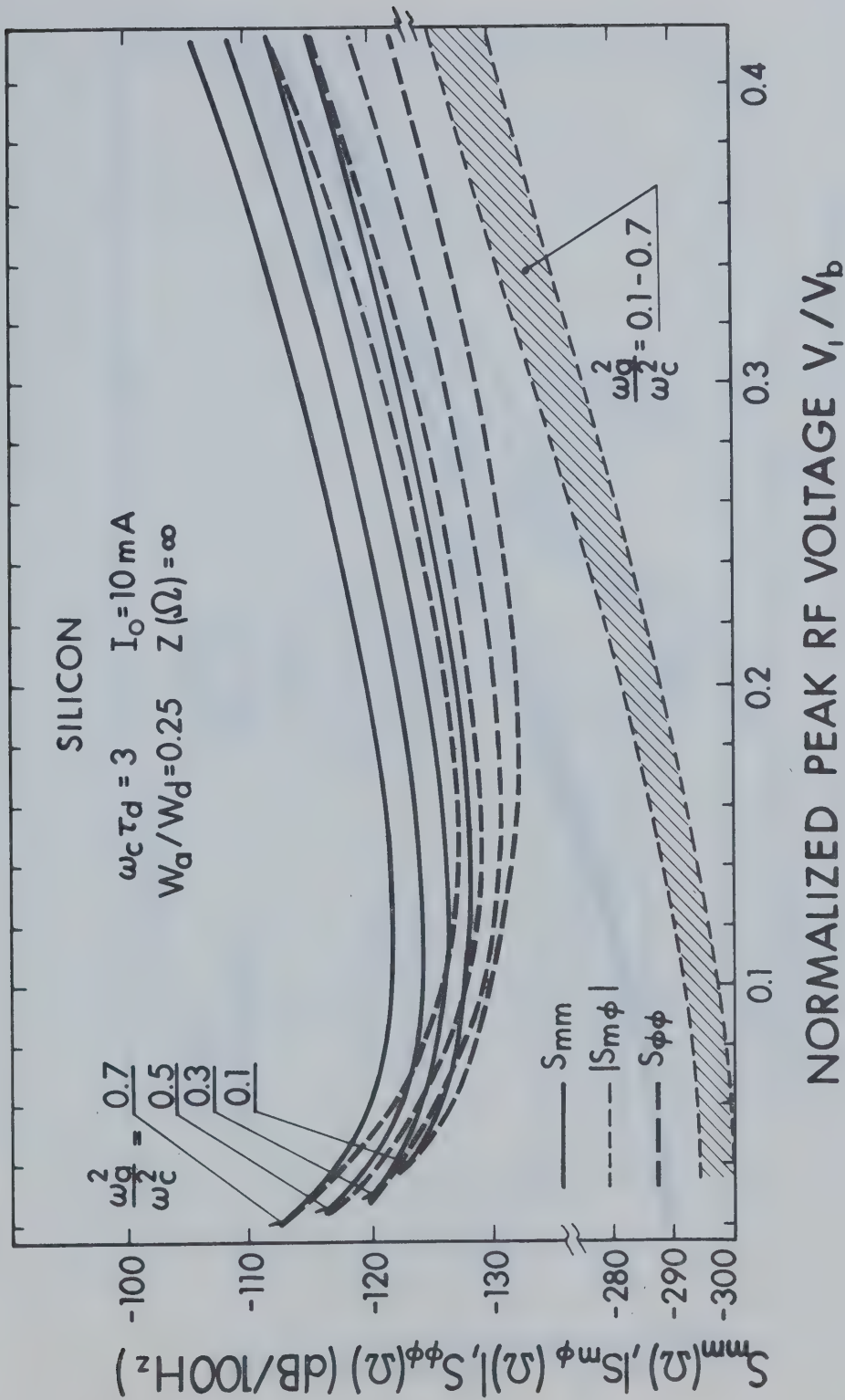


Fig. 4-3 DEPENDENCE OF INITIAL SPECTRA ON DIODE RF VOLTAGE

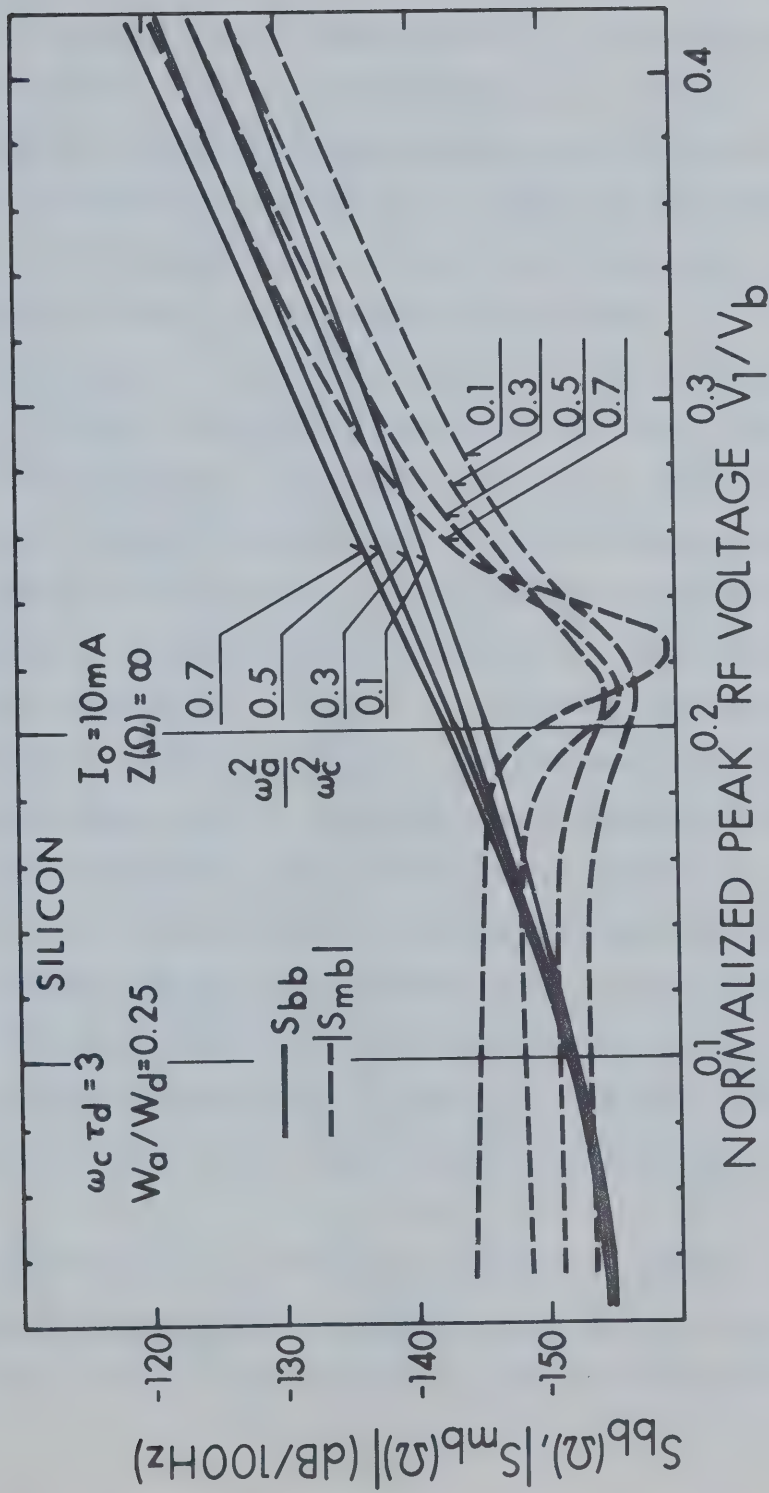


Fig. 4-4 DEPENDENCE OF THE SPECTRA S_{bb} and $|S_{mb}|$ ON DIODE RF VOLTAGE

functions of the normalized RF diode voltage V_1/V_b , for infinite impedance in the bias circuit. Two inter-related phenomena are indicated: 1) even for infinite bias circuit impedance there exists some correlation between amplitude fluctuations and baseband noise voltage, and this correlation increases with increasing RF diode voltage, and 2) the baseband noise voltage spectral density also increases with the latter.

Figs. 4-5 and 4-6 show the dependence of all the initial noise spectra of interest on bias circuit conductance, at a high RF diode voltage. The conductances to the right of the vertical dashed line are not physically realizable because of the thermal resistance of IMPATT diodes. The position of this line has been derived from the data on thermal resistance and chip capacitance of typical Si IMPATT diodes designed for operation at 6 - 12 GHz. It is an average position and there may be deviations in both directions for each individual diode. The minima of initial AM noise, $S_{mm}(\Omega)$, in Fig. 4-5 cannot be observed in practice since, at the corresponding values of bias circuit conductance, the "modulation noise", given by the third term on the right-hand side of Eq. (4.74), completely dominates the oscillator output. This is easily seen by inspecting the magnitude of the coefficients P_{11}^i and P_{12}^i in Eq. (4.74) and that of the noise spectra S_{mm} , S_{bb} and S_{mb} in Figs. 4-5 and 4-6. Hence it is concluded that the output amplitude noise is minimum at $Z(\Omega) = \infty$, as expected.

As mentioned in Sec. 4-3-1, the output phase-or frequency noise is not influenced by modulation. The slight increase in FM noise with increasing bias circuit conductance, which is sometimes observed¹⁶, may

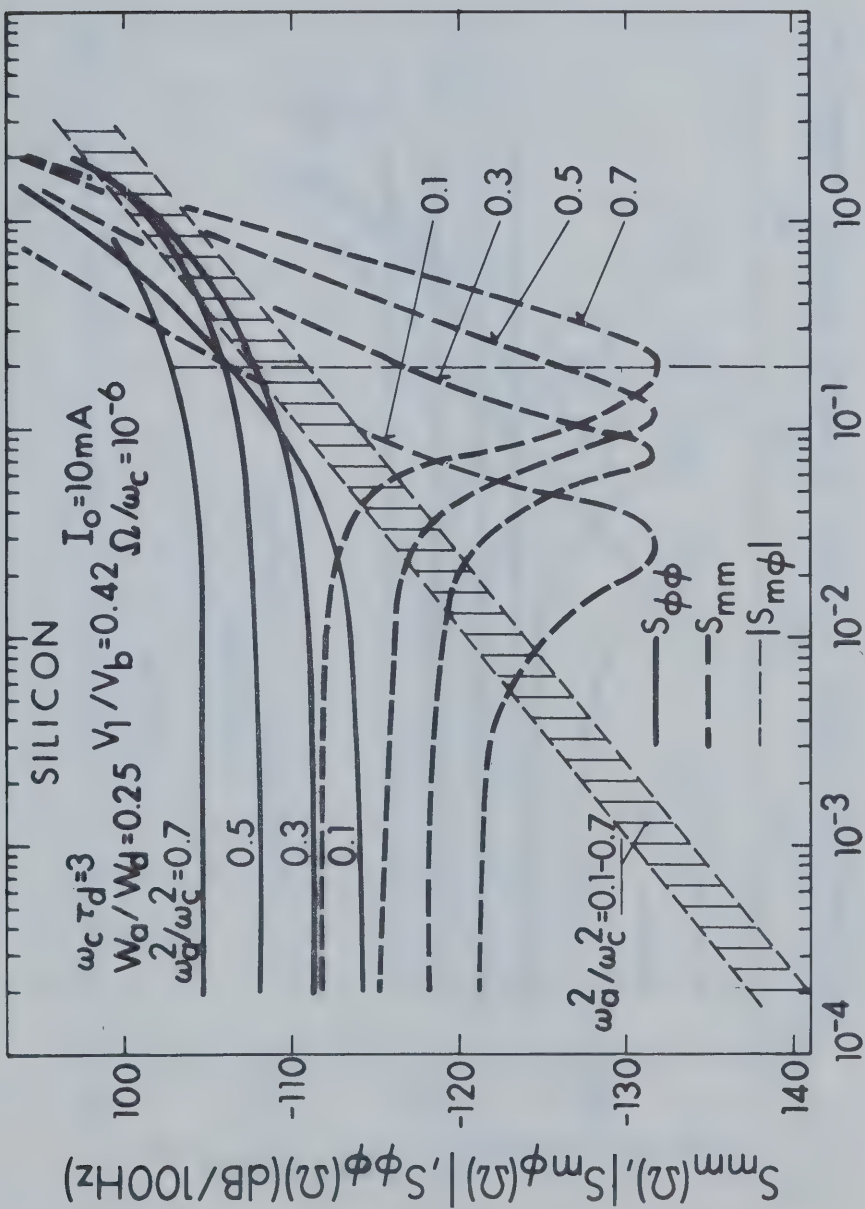


Fig. 4-5 DEPENDENCE OF INITIAL SPECTRA ON BIAS CIRCUIT CONDUCTANCE

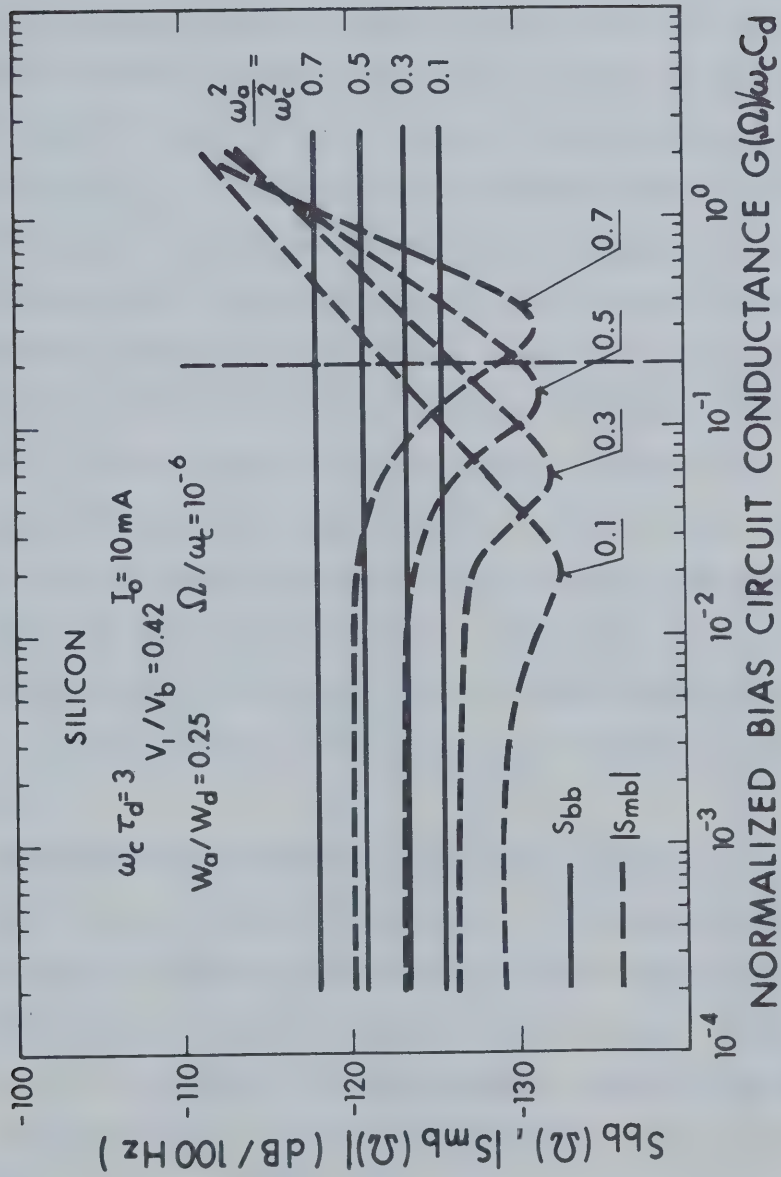


Fig. 4-6 DEPENDENCE OF THE SPECTRA S_{bb} AND $|S_{mb}|$ ON BIAS CIRCUIT CONDUCTANCE

be caused by the increase in the initial spectrum $S_{\phi\phi}(\Omega)$ indicated in Fig. 4-5.

Figs. 4-7 shows the influence of the diode drift transit angle and that of the avalanche-to-drift region ratio on the initial amplitude- and phase noise spectra, for three values of the RF diode voltage. An optimum range of $\omega_c\tau_d$, 4.5 to 5.5 radians, is indicated in Fig. 4-7a for $S_{mm}(\Omega)$ and $S_{\phi\phi}(\Omega)$. A deviation from this optimum range results in a rapid increase in noise, especially at large RF voltages. Note also that $\omega_c\tau_d$ influences the relative magnitudes of the two initial spectra. The above optimum range of 4.5 - 5.5 radians is not in agreement with the optimum value of 3.6 radians resulting from the power/noise considerations of Kuvás²⁰, but agrees well with the optimum of Goedbloed²¹ who, from a small-signal theory, derived a curve similar to those in Fig. 4-7a. However, an actual diode operated at a transit angle in the range 4.5 - 5.5 radians will generate low RF power, as the optimum of the latter is approximately at $\omega_c\tau_d = 2.3$. From this additional consideration, the value of $\omega_c\tau_d = 3.6$, given by Kuvás²⁰, will thus likely be an acceptable compromise.

The dependence of the initial amplitude- and phase noise spectra on the ratio w_a/w_d is more straightforward. It is clearly seen that a long avalanche region is desirable for low noise, as both amplitude and phase noise spectra increase rapidly at small values of w_a/w_d . However, the validity of this conclusion is limited somewhat because of the Read model used.

Finally, in Figs. 4-8 and 4-9 a comparison is given between the noise performance of Si, Ge and GaAs IMPATT diodes. For this comparison, the output amplitude noise spectrum $S_{MM}(\Omega)$ and the rms frequency deviation Δf_{rms} have

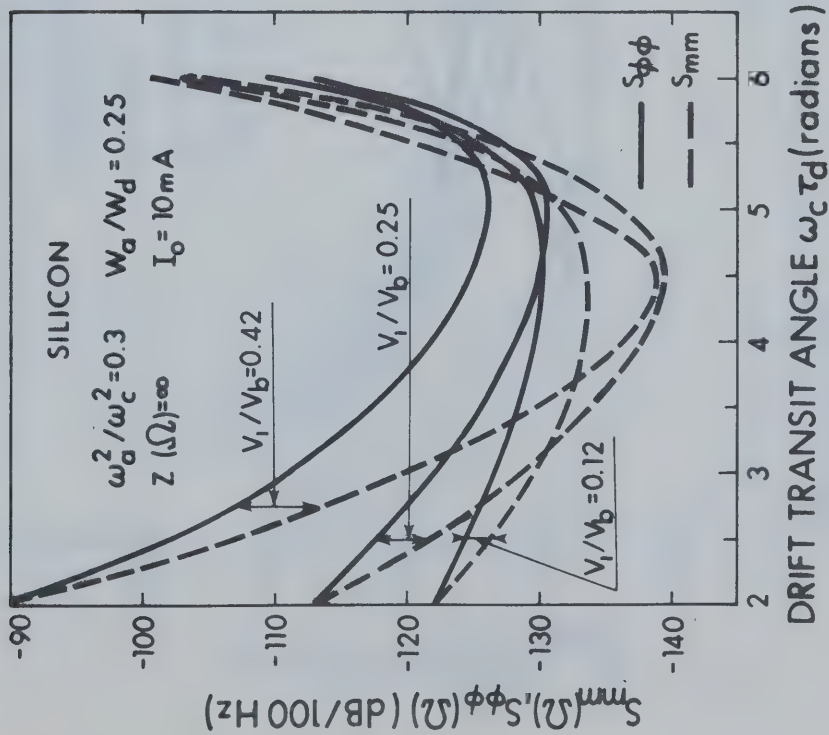
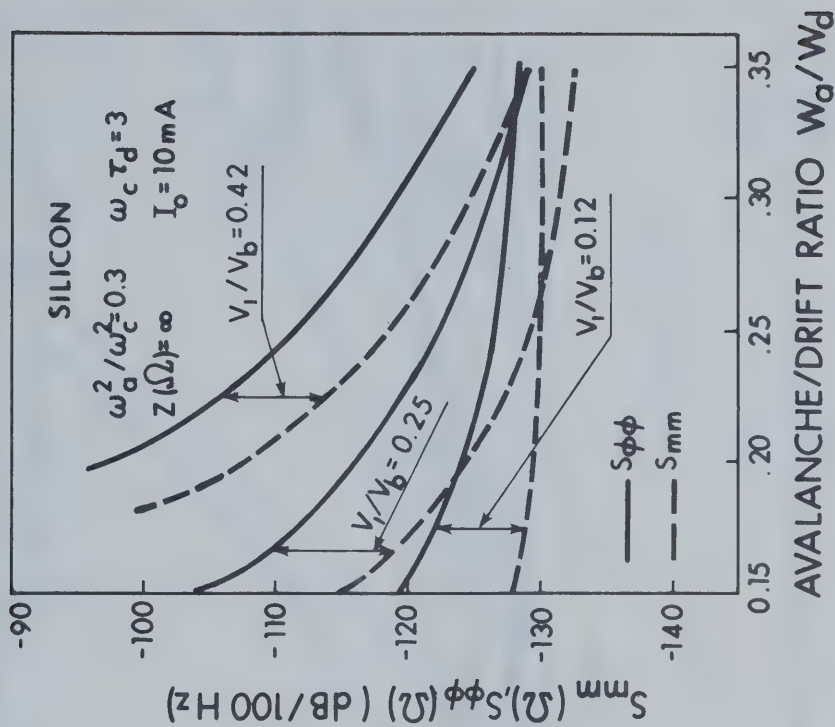


Fig. 4-7 a) INITIAL SPECTRA S_{mm} AND $S_{\phi\phi}$ AS FUNCTIONS OF DRIFT TRANSIT ANGLE



b) INITIAL SPECTRA S_{mm} AND $S_{\phi\phi}$ AS FUNCTIONS OF EQUIVALENT AVALANCHE - TO - DRIFT REGION LENGTH RATIO

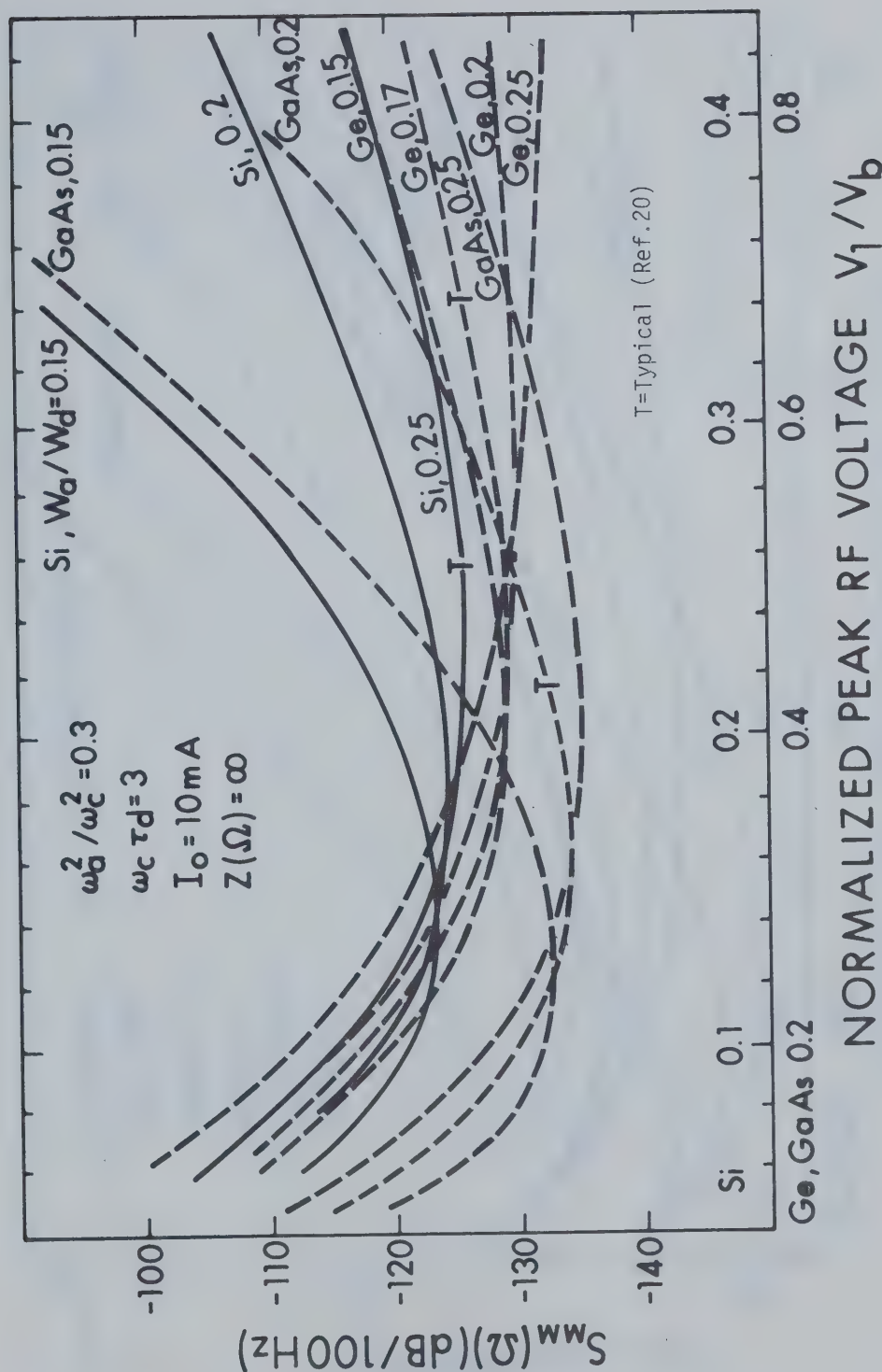


Fig. 4-8 AMPLITUDE NOISE COMPARISON OF Si, Ge AND GaAs IMPATT DIODES

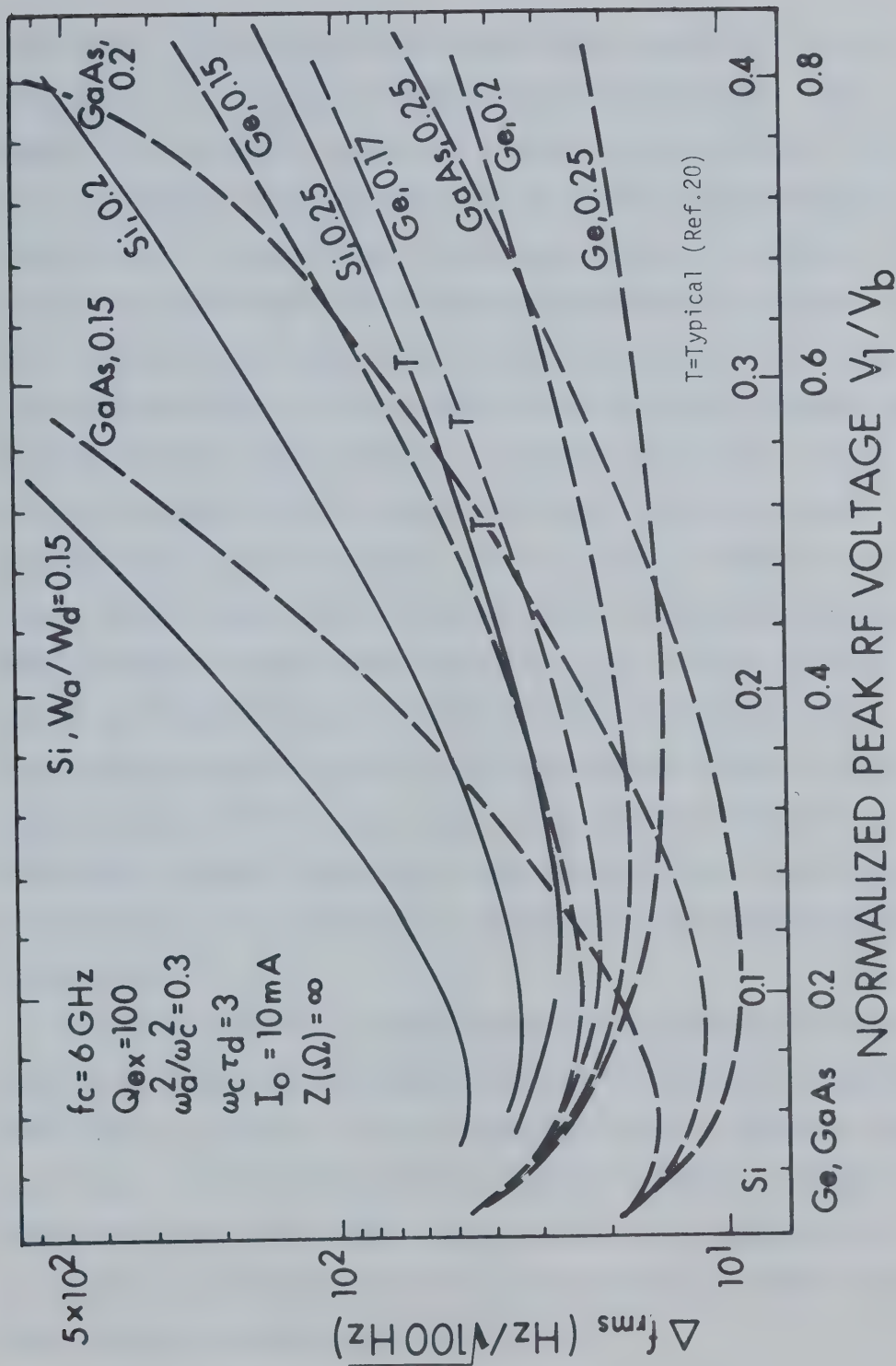


Fig. 4-9 FREQUENCY NOISE COMPARISON OF Si, Ge AND GaAs IMPATT DIODES

been chosen. Unlike the power/noise comparison of Kuvás²⁰, it is not attempted here to relate noise performance to attainable power. The emphasis is on an absolute comparison of noise modulation rates. Also, for a fixed transit angle, the effect of the relative avalanche region width is shown. For Ge and GaAs, the voltage scale differs from that used for Si, since saturation in the former occurs at higher RF voltages. It is seen clearly that information on the noise performance of diodes made from different materials, based on small-signal noise data or theory, may be rather unreliable when applied to a high-level oscillator. The effect of the RF voltage and that of the ratio of w_a/w_d is relatively small for Ge diodes compared to Si and GaAs. Other than that, no generally valid comparison can be made at high RF voltages unless it is understood that the diodes will have certain 'typical' ratios of w_a/w_d . For the ratios of w_a/w_d given in Ref. 20, Figs.4-8 and 4-9 show that at low RF voltages Silicon diodes exhibit a higher noise than Ge and GaAs diodes, in that order; at very high RF voltages, a GaAs diode may exhibit higher noise than a Si diode. A typical GaAs diode is seen to exhibit the lowest noise of all three, if it can be operated at a relatively low RF voltage near the noise minimum.

In order to verify the theory presented in this thesis, the computed output noise spectra must be compared with some measured data of actual IMPATT diode oscillators. For this purpose, no "typical" parameter values can be used. The diodes tested must be examined for these parameters in each specific case so that proper values are used in the computations. The computed spectra obtained in this way are presented, together with the measured data, in Chapter V, Sec. 5-3.

CHAPTER V

NOISE MEASUREMENTS ON IMPATT OSCILLATORS

The emphasis in this project has been on developing a large-signal theory of oscillator noise for a certain class of negative-resistance oscillators. This theory has been applied to IMPATT diode oscillators in order to demonstrate how the general theory can be adapted to a particular device and, at the same time, to obtain specific data which might explain some of the large-signal noise effects observed in IMPATTs or, which may even suggest the existence of some noise phenomena not yet observed.

In this chapter, specific computational results will be compared with the pertinent experimental data on IMPATT oscillator noise. The data of Goedbloed²¹ have been supplemented by additional measurements carried out by the present author. For this purpose, a sensitive noise-measuring system had to be assembled and thoroughly tested for its limiting sensitivity (threshold) and accuracy. A direct-detection noise-measuring system has been chosen. It is described briefly in Section 5-1. The most important data of the IMPATT oscillator and of the diodes used are summarized in Section 5-2, while Section 5-3 contains both the pertinent theoretical results of this study and the available experimental evidence.

5-1 The Noise-Measuring System

5-1-1 Small-Signal Measuring Principles

Direct-detection noise-measuring microwave systems have become well

established lately because of such advantages as better sensitivity (if sufficient input power is available) and the avoidance of complications arising from the use of a local oscillator in a superheterodyne system. A spectrum analysis is obtained separately for AM and for FM noise modulation, so that the AM detector is required to not respond to FM, and vice versa.

A good discussion of small-signal measuring principles is found in Refs.32 and 33. Basically, the waveform is assumed to be expressible in the form

$$v(t) \triangleq V_c[1 + m(t)]\cos[\omega_c + \Delta\omega(t)]t \quad (5.1)$$

for $\Delta\omega(t)$ small and changing slowly with time (quasi-stationarity). An AM detector will yield an ac output dependent only on $m(t)$ and will not respond to changes in frequency $\Delta\omega$ if its bandwidth is sufficiently large compared to peaks of $\Delta\omega$. Similarly, an FM detector normally yields an output voltage

$$V(t) = K \cdot V_c[1 + m(t)]^n \Delta\omega(t) \quad , \quad n = 1 \text{ or } 2 \quad (5.2)$$

and thus v will be a measure of $\Delta\omega$ if $m(t) \ll 1$. This condition is usually well satisfied when $m(t)$ is noise modulation only.

The basic direct-detection measuring system described here, analogous to those of Refs.32 and 33, is shown in Fig. 5-1. Its operation is as follows.

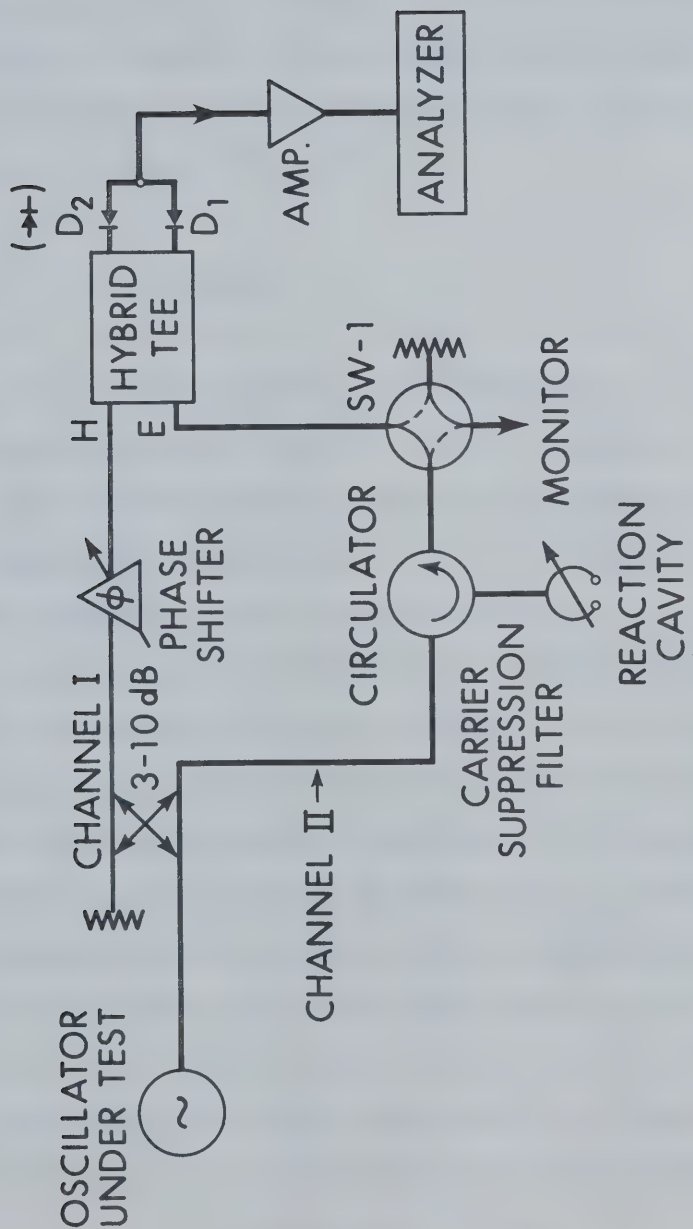


Fig. 5-1 BASIC SYSTEM FOR OSCILLATOR AM-AND FM NOISE MEASUREMENTS

When channel II is interrupted by the switch SW-1 and the E arm of the hybrid tee match-terminated, the hybrid tee and diodes D_1 and D_2 function as an ordinary AM detector (either square-law or linear), if the diodes are connected in phase. If they are connected in opposition, the two diode signals will cancel if the two detector arms are identical electrically. The degree to which this cancellation is achieved is expressed by the suppression factor (SF)

$$SF(\text{dB}) = 20 \log(V_{\text{unbal}}/V_{\text{bal}}) \quad , \quad (5.3)$$

where V_{unbal} is the output voltage in unbalanced condition, and V_{bal} is the output voltage in balanced condition (diodes in opposition). Diode noise that is uncorrelated between D_1 and D_2 will not cancel and will determine, together with the amplifier noise, the AM threshold of the system, if the suppression factor is sufficiently high.

For FM measurements, both channels of the system shown in Fig. 5-1 are used. The carrier suppression filter consists of a circulator and a high-Q reaction cavity. Ideally, the carrier is completely suppressed, which requires that when the cavity is tuned to ω_c , it is exactly critically coupled. If the frequency deviates from ω_c by a small amount $\Delta\omega$, a signal proportional to $Q_0(\Delta\omega/\omega_c)$, shifted in relative phase by $\pm 90^\circ$, will be transmitted to the E arm of the hybrid tee; this signal will be much smaller than the reference signal (containing both carrier and sidebands), transmitted to the H arm of the hybrid tee. With the diodes switched in opposition, this circuit operates as a phase-sensitive

detector, producing an output voltage proportional to (amplitude in channel II) $\cos(\phi_r + \pi/2)$ (for linear detector), or to (amplitude in channel I) (amplitude in channel II) $\cos(\phi_r + \pi/2)$ (for square-law detector), where ϕ_r is the phase difference between the two channels. If ϕ_r is made equal to $\pi/2$ by means of a phase shifter in channel I, we obtain maximum output voltage

$$v(t) = K[1 + m(t)]^n \cdot Q_0 \Delta\omega / \omega_c, \quad (5.4)$$

where $n = 1, 2$ for linear and square-law detectors, respectively. Thus $v(t) \propto \Delta\omega$, if $m(t) \ll 1$.

Once the system has been calibrated, its FM threshold, i.e., the lowest measurable $\Delta\omega$, can be determined from the threshold voltage obtained previously with channel II interrupted.

The detector output voltage, proportional to $m(t)$ or $\Delta\omega(t)$, is amplified and subjected to spectrum analysis. The root-mean-square value of $m(t)$ or $\Delta\omega(t)$ in a given frequency slot (usually 100 Hz or 1 kHz) in the range of modulation frequencies of interest is then measured. For maximum system sensitivity, the spurious noise must be kept at a minimum, since the threshold voltage is determined by the noise added by the detector diodes, the subsequent amplifier, and possible spurious voltages due to ground loops and other extraneous causes.

5-1-2 Threshold and Accuracy

When checking the AM threshold of the system in Fig. 5-1, an unexpected rise in threshold below approximately 10 kHz may be encountered.

As mentioned in Ref. 32, such a rise in threshold in superheterodyne systems is caused in some cases by excessive FM of either the signal under test or of the local oscillator, in conjunction with FM-to-AM conversion in the IF amplifier. A similar phenomenon can occur in the case of a direct-detection system if the FM noise of the oscillator under test is relatively large and the detector used is narrow band. This is the case with some envelope detectors because of their comparatively high $R_j C_j$ product.

A series of experiments has been carried out by this author, which have shown that the threshold at low frequencies can be reduced by broad-banding the detectors. This procedure, together with a more detailed description of the measuring system, is explained in Ref. 34. Since these problems are auxiliary to the main theme of this thesis, only the results will be cited here: with a detector Q of about 20, and an input RF power of some 40 mW, an AM threshold range of -150 to -155 dB/100 Hz has been attained at modulation frequencies from 100 Hz to 50 kHz. With an input power of 15 mW and with the detector frequency response adjusted flat within 1 dB over a 100 MHz range, the AM threshold is approximately -140 dB/100 Hz (at 100 Hz) to -155 dB/100 Hz (at 50 kHz). This is sufficient for noise measurements on IMPATT diode oscillators.

Another problem associated with systems of this type is the effect of their various imperfections on measurement accuracy. The operation of this circuit and its calibration have so far been described in terms of assumed "ideal" conditions; namely, the hybrid tee is perfect, the cavity is tuned precisely to the carrier frequency of the RF signal, and the cavity input impedance is perfectly matched at that frequency, thus

producing no reflection of the carrier. In practical measurement setups, conditions differ significantly from the ideal situation causing various AM-to-FM and FM-to-AM conversions. A computer study of these effects has been carried out by Fikart *et al.*,³⁵ for certain typical values of oscillator AM and FM noise and for a certain typical range of deviations from the above mentioned ideal conditions. This study is explained in more detail in Ref. 35. The results, shown in Fig. 5-2, indicated that FM noise measurements can be made accurately for modulation frequencies within the reflection cavity bandwidth, whereas AM measurements using the "double-channel mode" are highly unreliable. Hence for AM measurements the single-channel mode must be used only.

5-1-3 Complete Measuring System

The complete system for noise measurements at 6 GHz is shown in Fig. 5-3. It is essentially the same system as that in Ref. 33 except that it uses Schottky-barrier diodes as envelope detectors, as in Ref. 32, instead of small-signal backward-diode detectors. Some instruments have been added for convenience: a 4-8 GHz sweeper, an oscilloscope to permit fast adjustment and retuning of the detectors, and a frequency counter for direct frequency observation. The video detector output has been arranged as shown in Fig. 5-4. The two diodes are reversed with respect to each other in their mounts and when threshold measurements are taken (or FM operation required) they are simply connected in a bridge configuration. The two variable resistors facilitate balancing of the bridge since, generally, the detector video impedances are not equal when the voltages

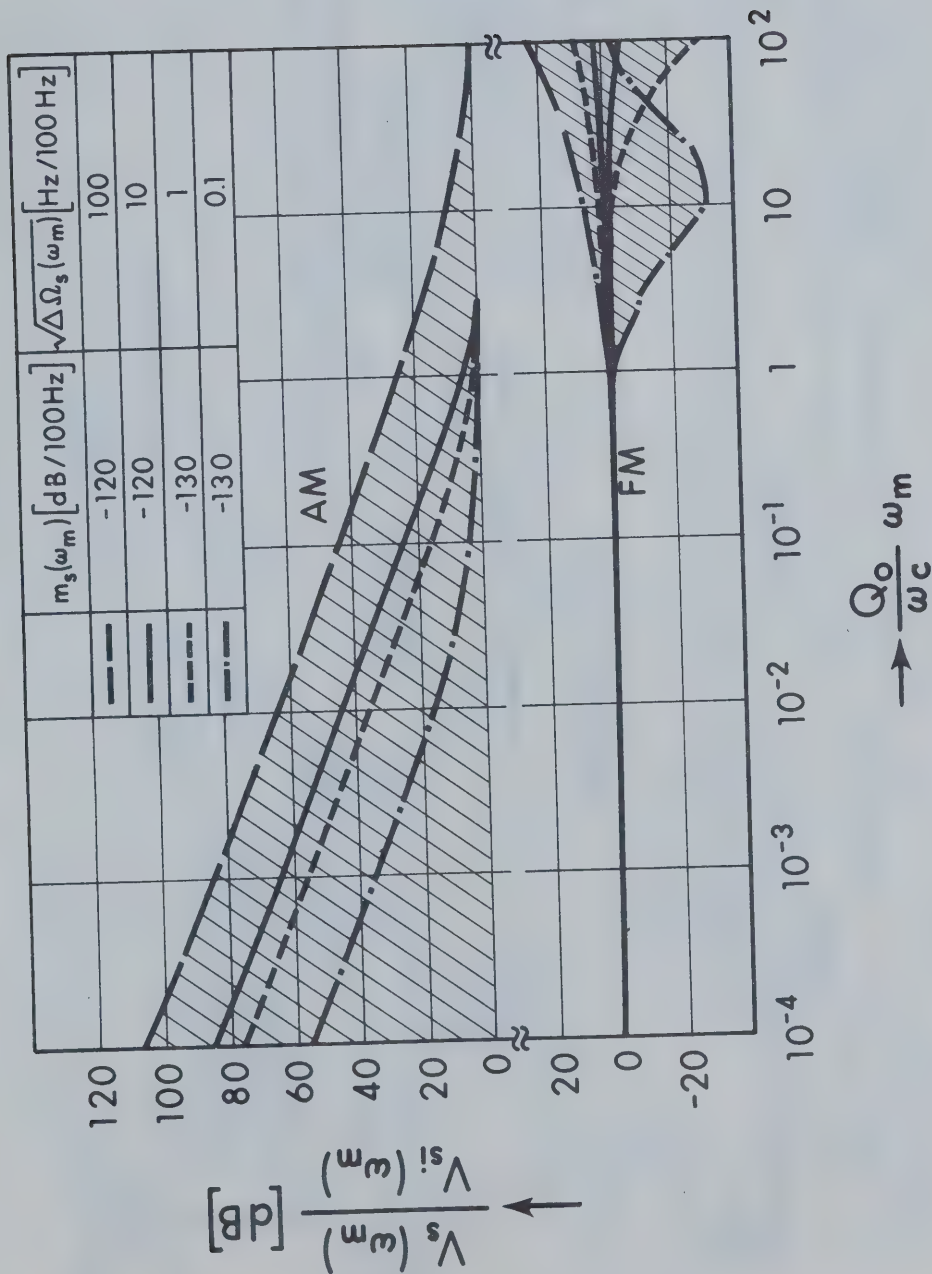


Fig. 5-2 INACCURACY OF NOISE MEASUREMENTS IN THE DOUBLE-CHANNEL MODE, FOR TYPICAL DEVIATIONS OF CIRCUIT PARAMETERS FROM IDEAL AND FOR SEVERAL VALUES OF AM-AND FM OSCILLATOR NOISE

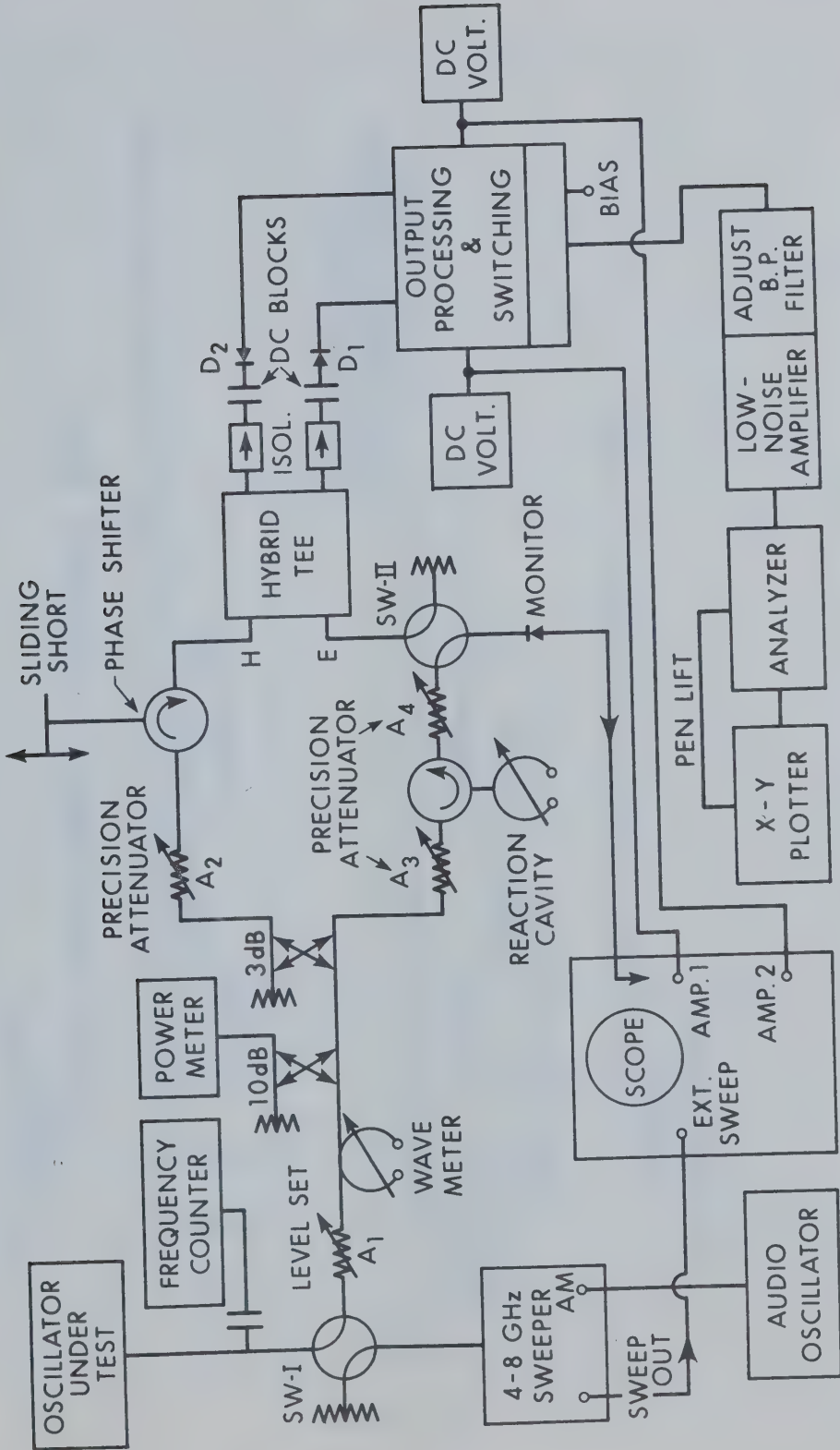


Fig. 5-3 COMPLETE AM-AND FM NOISE-MEASURING SYSTEM

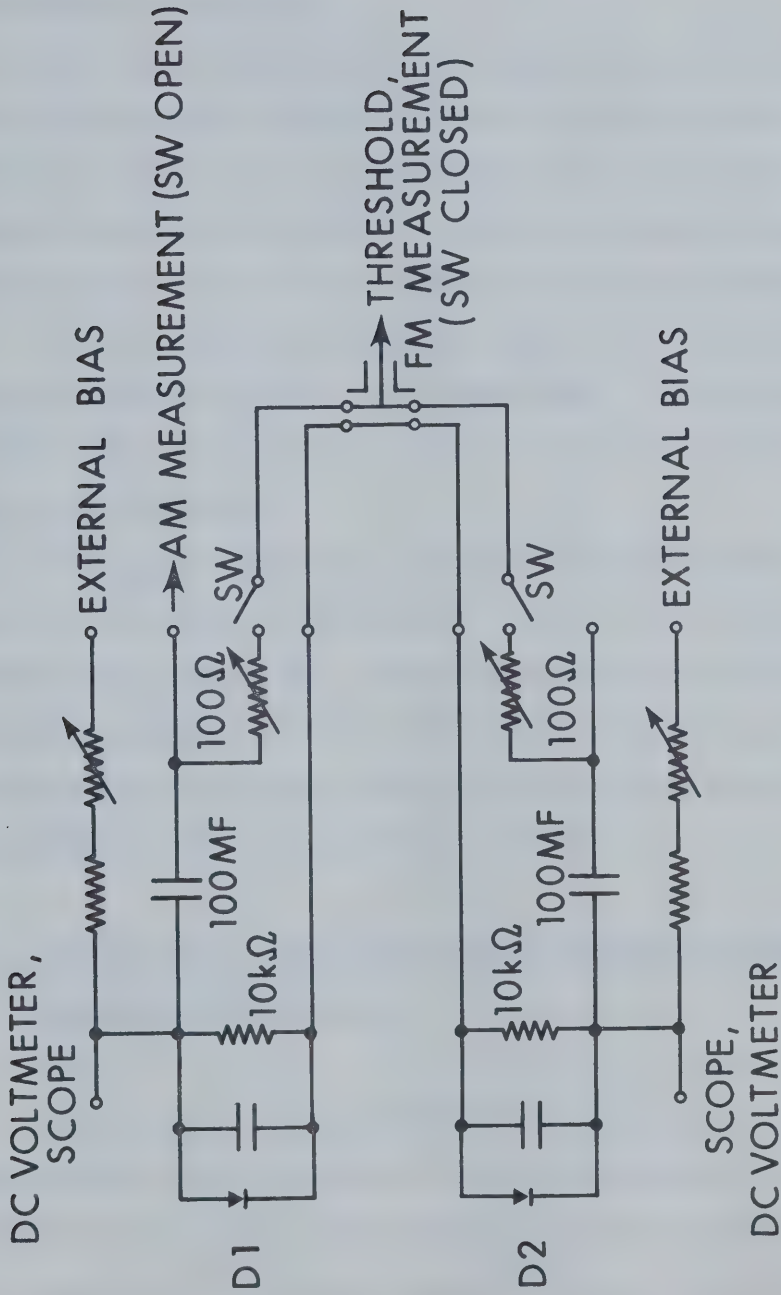


Fig. 5-4 DETECTOR OUTPUT PROCESSING AND SWITCHING

are, and vice versa. Their value is chosen so as not to greatly influence the total noise.

For actual AM measurements only one detector is calibrated and used. This procedure has the advantage of removing spurious low-frequency voltages due to an ungrounded detector mount (when the detectors operate in parallel or in series). Hence, total battery operation is not then required; only the low-noise amplifier is battery operated.

For this system, operating at 6 GHz, a very low-noise Schottky-barrier diode pair HP 5082-2354 has been chosen. The amplifier used has an equivalent rms input-noise voltage of about $0.02 - 0.03 \mu\text{V}$ in a 100 Hz band at low frequencies.

During the measurements, the system has been operated at an input power of 15 mW and with the detectors tuned for a flat response in a 100 MHz range around 6 GHz. The AM threshold was from -140 dB/100 Hz (at modulation frequency 100 Hz) to -155 dB/100 Hz (at 50 kHz). The corresponding FM threshold, using a reflection cavity with $Q = 15000$, was approximately $0.02 - 0.03 \text{ Hz/100 Hz}$ (at 50 kHz).

5-2 Auxiliary Data: IMPATT Diodes, Coaxial Resonator and General Measurement Procedure Used.

Commercial Si and GaAs IMPATT diodes were used in the noise measurements. After completion of the noise measurements, the physical dimensions of the diodes were examined by measuring the semiconductor chip area, and the diode capacitance dependence on reverse voltage. The determination of chip area turned out to be impossible in the case of

the GaAs diodes because of their special contacts, so the data from Ref. 28 were used to calculate the depletion layer width from the known breakdown voltage. The combined physical and electrical parameters of the two types of IMPATT diodes at 6 GHz are given in Table 5-1.

TABLE 5-1 PARAMETERS OF MEASURED IMPATT DIODES AT 6 GHz

DIODE	Mat.	V_b (V)	C_j (pF)	W (μ)	W_a (μ)	w_a/w_d	$\omega_c \tau_d$	AREA
HP 5082-0437	Si	103	0.25	4.8	(Ref.36) 1.2	0.34	2	1.15×10^{-4} cm ²
RAYTHEON MS 804X	GaAs	80	0.35	3.5	(Ref.20) 0.8	0.266	1.86	

The diodes were inserted into a tunable coaxial resonator, a sketch of which is shown in Fig. 5-5. The two movable slugs made possible fine frequency tuning and variable load coupling. The diode holder is of standard design (see, e.g., Ref. 37). Its primary function is that of a good electrical contact with the diode and adequate heat removal.

The diodes were biased by a high-impedance (current) source, typically in the range of bias currents 20 to 30 mA. At a given dc current, the RF power was adjusted by means of the tuning slugs to several different values. The output signal was monitored on a spectrum analyzer to ensure that no spurious oscillations were taking place (these cause a large increase in both AM-and FM noise, compared to single-frequency oscillation).

For each output power adjustment, the external Q of the resonator was measured by the injection locking method³⁸, using an auxiliary

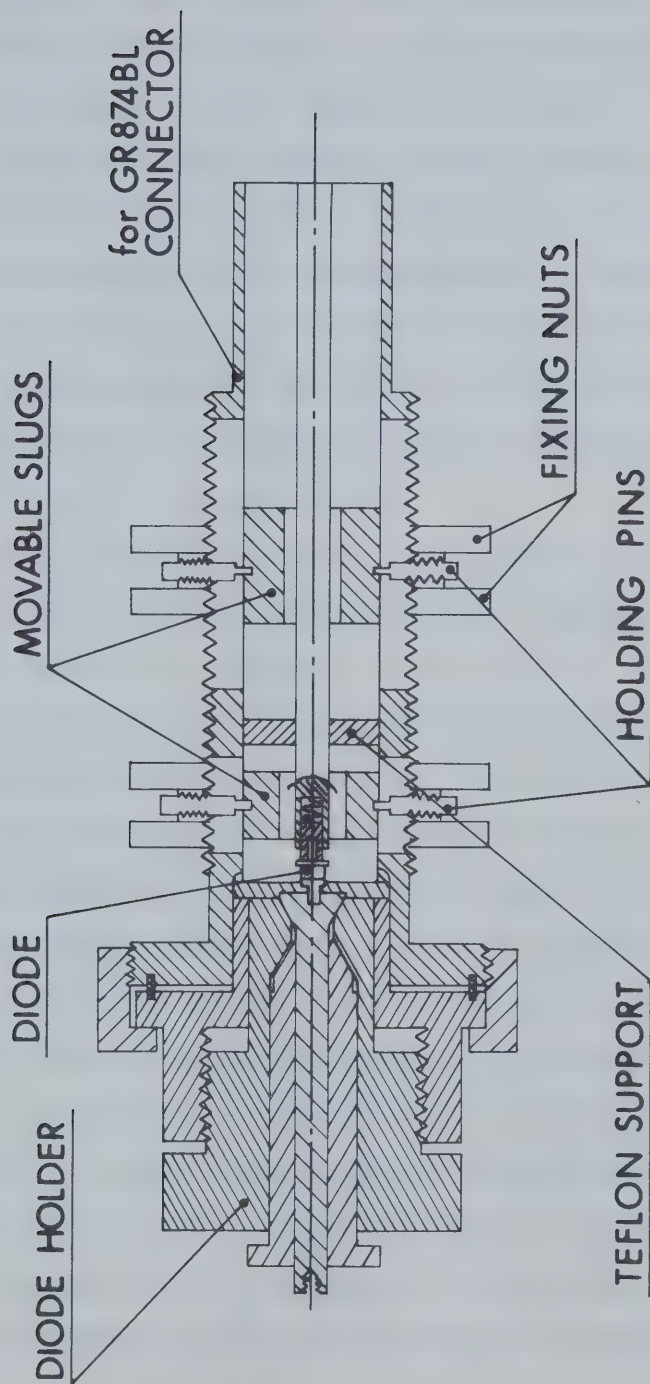


Fig. 5-5 COAXIAL RESONATOR

generator and circulator. After that, the IMPATT oscillator was connected to the noise measuring system and AM-and FM noise measurements taken. The baseband noise voltage across the bias leads was also measured. During these measurements, the oscillation frequency was kept constant, $f_c = 5.94$ GHz. The detected AM-and FM noise spectra, as well as the baseband noise voltage spectrum, were measured in the range of baseband frequencies 100 Hz - 50 kHz. This frequency range enables one to determine if any flicker noise is superimposed on the white noise spectrum, normally expected from IMPATT diodes. The measured spectra are compared with the pertinent computed spectra in the next section.

In the course of measurements, the two GaAs diodes used were found to be somewhat unreliable compared to the Silicon ones. One was damaged at an early stage, apparently by a pulse in the bias circuit, when baseband noise voltage was being measured. Although this particular measurement was made repeatedly in the case of the Si diodes, the latter did not suffer any noticable damage or deterioration. The other GaAs diode, on which baseband noise measurements were not made, lasted through the measurements, but its performance gradually deteriorated, without any apparent external cause. This aging manifested itself mainly in a decreased maximum available RF power at the end of the measurements. On examining this diode, a change in its breakdown voltage was found, from the original value of 80 volts to 60 volts. Also, a relatively poor contact between the semiconductor chip and the metallic stud was discovered; this condition normally causes an excessive junction temperature and contributes to the generation of excess thermal noise¹⁰. This condition is believed to be

partly responsible for the unusually large FM noise measured in this case. Normally, GaAs diodes, if well manufactured, are known to exhibit quite low FM noise³⁹ at not too low baseband frequencies. In any case, the above-mentioned deficiencies appear to be more often encountered in GaAs diodes than in Si diodes, the technology of which is highly developed.

In these circumstances, a comparison of the theoretical- and measured dependence of noise on output power is not representative. For this reason, only the baseband frequency dependence of both AM-and FM noise of the other GaAs diode will be shown, in comparison with the corresponding data of the Si diode measured.

5-3 Comparison of the Computed Noise Spectra with Experimental Data

One of the interesting computational results in Section 4-3-2 is the generally different rate of change of the amplitude-and frequency noise spectra with a change in diode RF voltage. As mentioned in Chapter I, if Kuvás' large-signal analysis were used²⁰, the two noise spectra would exhibit an equal dependence on diode RF voltage. The experimental results of Goedbloed²¹ show clearly that, while FM noise increases relatively rapidly in the high voltage region, the AM noise there almost does not increase at all. Fig. 5-6 shows Goedbloed's results in comparison with the theoretical curves obtained by the present author. Also shown in Fig. 5-6a is a theoretical curve by Goedbloed (small-signal theory). The comparison is not absolute since not all the diode and circuit parameters can be reliably derived from the data given in Ref. 21.

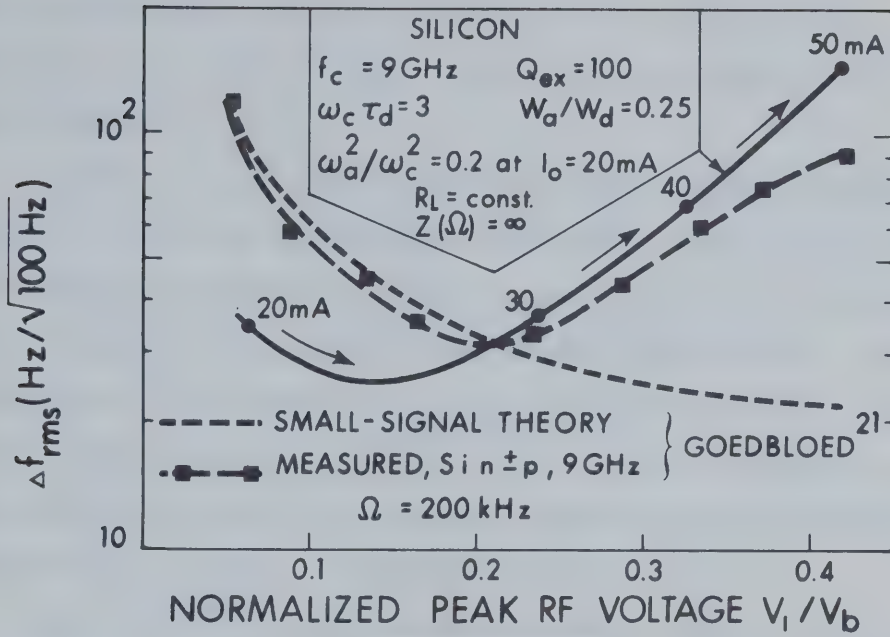


Fig. 5-6a FM NOISE AS A FUNCTION OF RF VOLTAGE

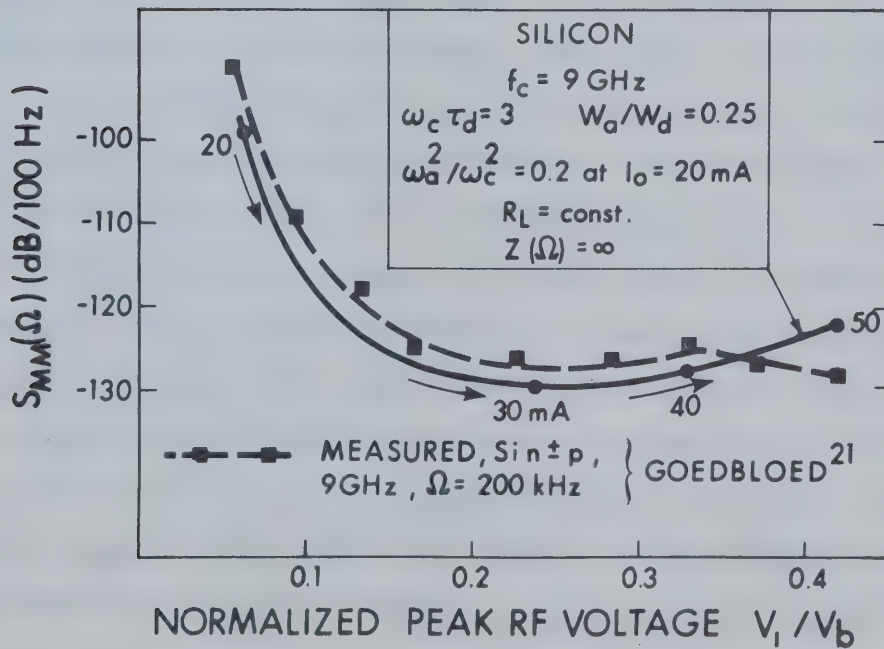


Fig. 5-6b AM NOISE AS A FUNCTION OF RF VOLTAGE

Note that the data in Fig. 5-6 were obtained with a constant load resistance, i.e., the RF voltage across the diode was varied by varying the bias current.

In Fig. 5-7, the influence of drift transit angle on FM noise is shown, as predicted and measured by Goedbloed²¹, and as computed from the large-signal theory of the present author. As before, the comparison is not an absolute one, because of some missing data in Ref. 21. However, the position of the minimum at $4.5 \leq \omega_c \tau_d \leq 5.5$ seems to be little dependent on other diode and circuit parameters. This conclusion can be drawn from the results of Sec. 4-3-2 of this thesis, from Goedbloed's additional observations²¹ and, also, from the data in Ref. 40.

Figs. 5-8 to 5-11 summarize the experimental results of this author, in comparison with the pertinent data obtained from the computations described in Chapter IV. In these figures, the noise spectra are related to output power, a more useful parameter, rather than to diode RF voltage.

Fig. 5-8 shows the theoretical and measured dependence of AM- and FM noise on output power. An important difference of these experimental results with respect to Fig. 5-6 is the tuning procedure used. The data in Fig. 5-8 were taken at a constant bias current, but with variable load resistance. This was achieved by adjusting the tuning slugs to obtain the required RF power, while keeping the frequency constant. It was found that values of relative output power smaller than approximately 0.65 were difficult to obtain without the presence of spurious oscillation. Further, an effect similar to that seen in Fig. 5-6a was observed; namely FM noise was larger than expected from theory at low power levels, with spurious

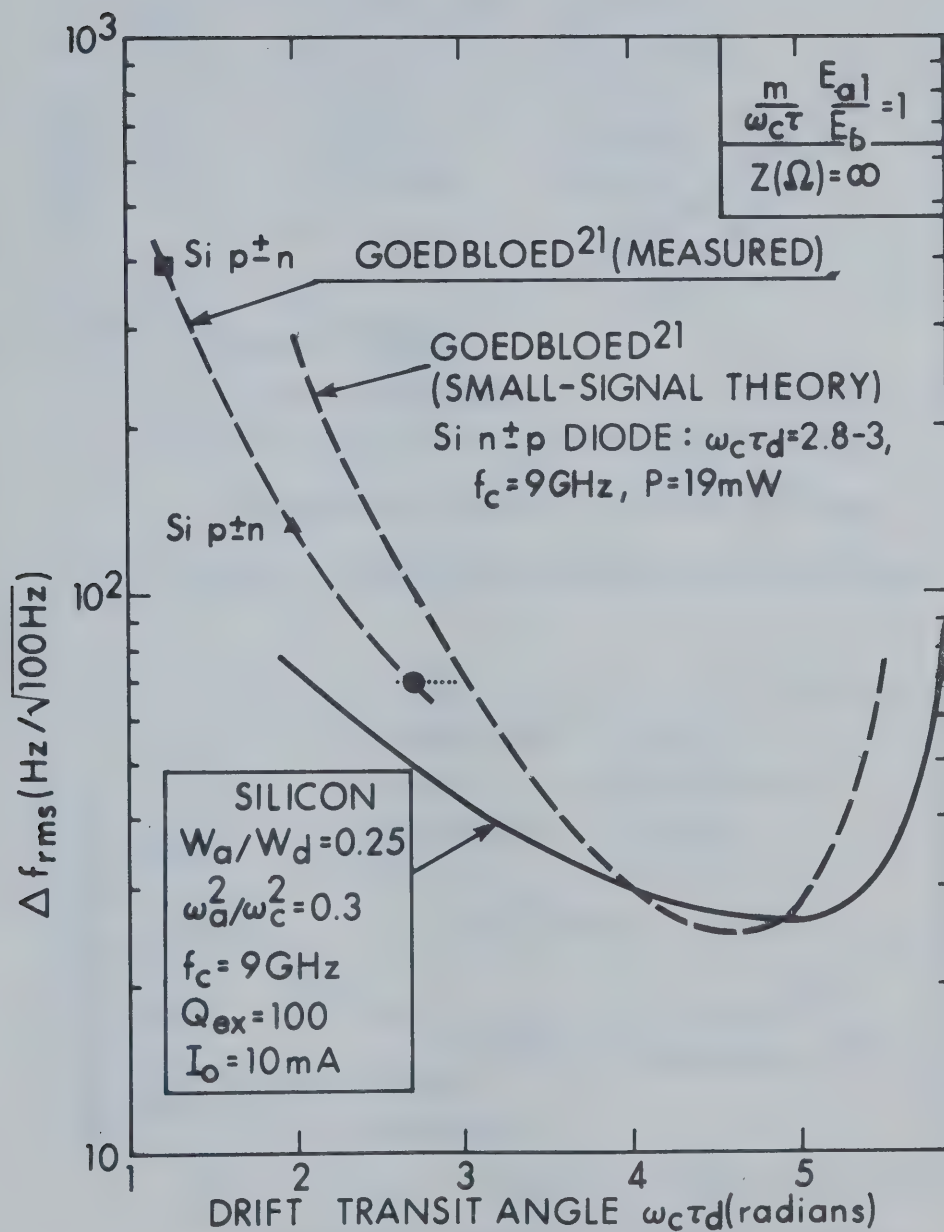


Fig. 5-7 FM NOISE AS A FUNCTION OF DRIFT TRANSIT ANGLE

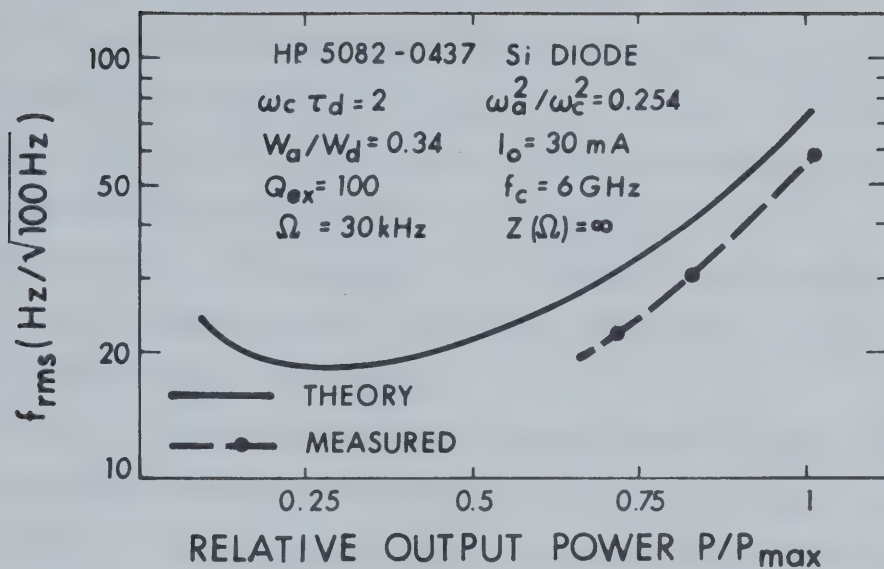


Fig. 5-8a FM NOISE AS A FUNCTION OF OUTPUT POWER

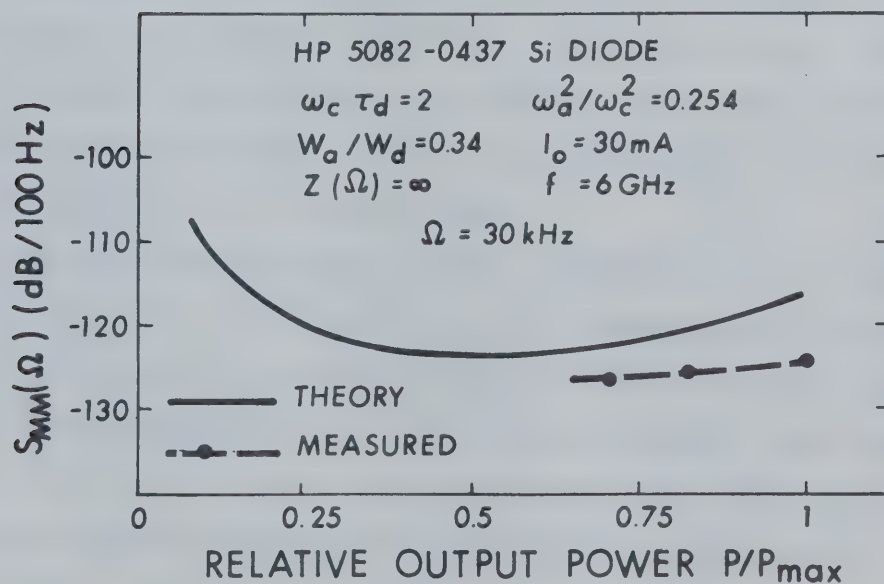


Fig. 5-8b AM NOISE AS A FUNCTION OF OUTPUT POWER

oscillations present. It is possible that the experimental data in Fig. 5-6a were obtained under such condition, since spurious oscillations may, without special attention to them, easily go unnoticed. Fig. 5-8a shows that the measured FM noise increase in the high-output power region is well described by the theoretical curve. The theoretical curve of AM noise exhibits a little steeper rate of increase in the high-power region, than the measured data. On the whole, the agreement between theory and measurement is very good.

The measurements described above were also taken for bias currents of 20 and 30 mA; the results obtained were essentially the same as those in Fig. 5-8. This is illustrated in Fig. 5-9, which shows the FM-and AM noise dependence on bias current, both theoretical and experimental. It must be stressed once again that for each bias current the oscillator was tuned to the same relative output power. The resulting dependence of AM- and FM noise on bias current is very flat, unlike that observed in the case of a constant load resistance, with variable output power. In the latter case, the FM noise has a distinct minimum for a certain bias current (this can be derived, e.g., from Fig. 5-6a).

The baseband noise voltage spectrum is normally of little interest in oscillator noise theory; nevertheless it was measured in this case in order to determine whether the down-conversion predicted from the theory in Sec. 3-4 and indicated in Fig. 4-4, actually takes place. As is seen in Fig. 5-10, this is indeed so, although the theoretical noise voltage spectrum, compared to the measured one, increases more rapidly with RF output power.

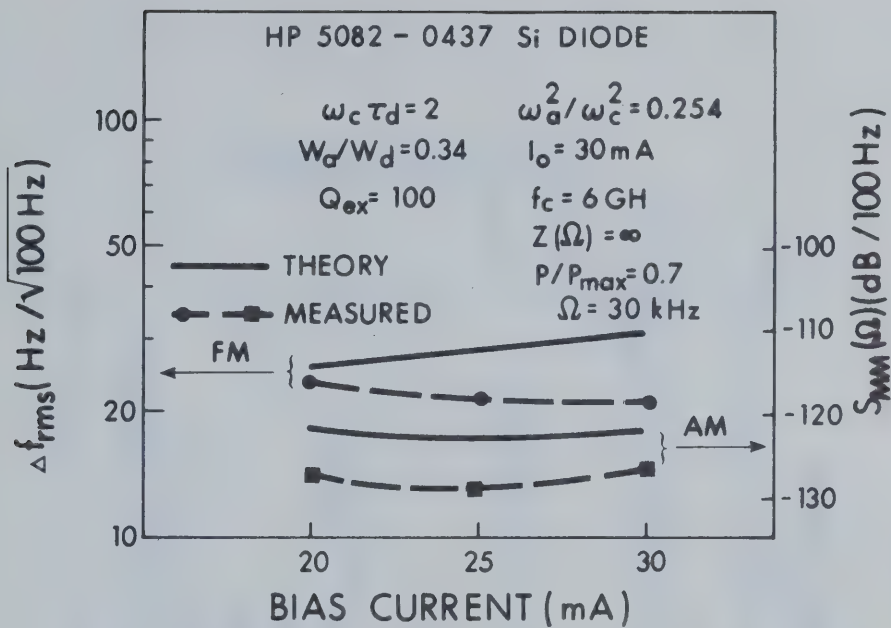


Fig. 5-9 FM-AND AM NOISE AS A FUNCTION OF BIAS CURRENT

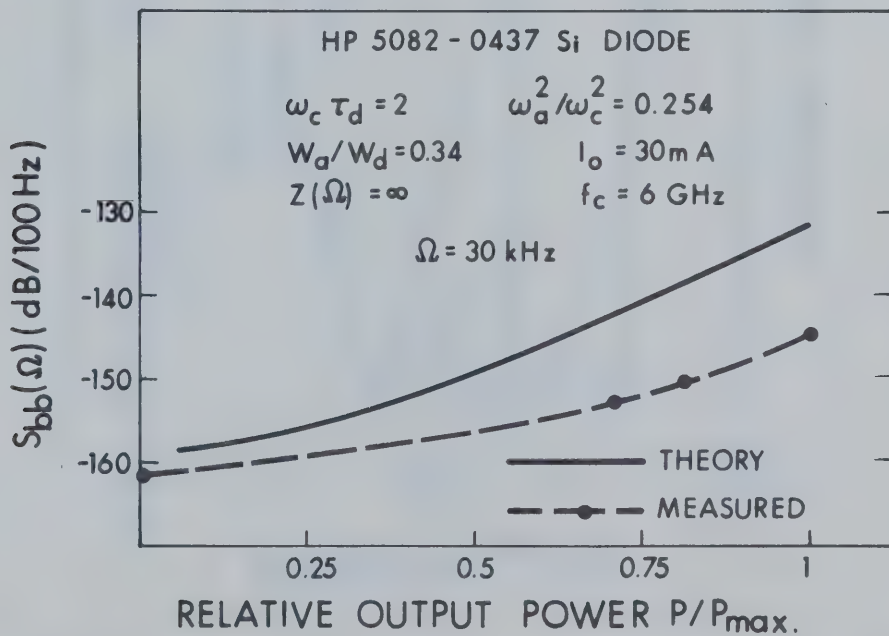


Fig. 5-10 BASEBAND NOISE VOLTAGE SPECTRUM AS A FUNCTION OF OUTPUT POWER

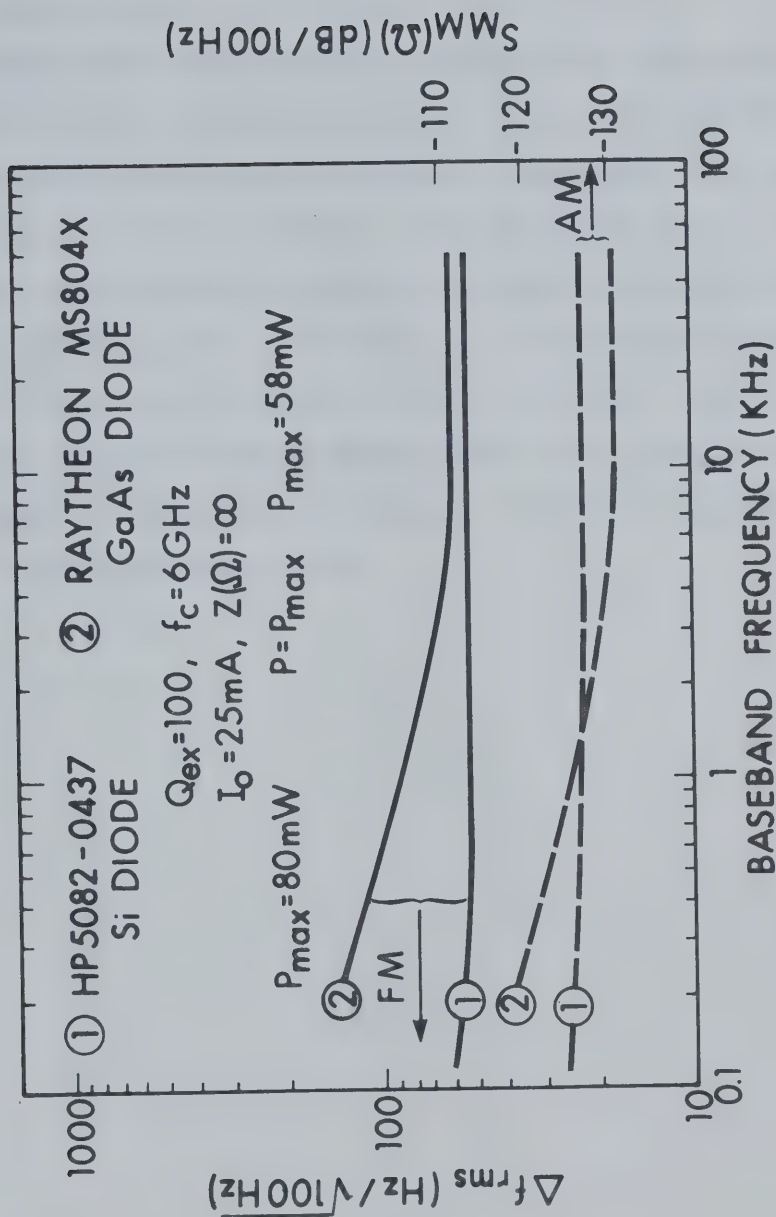


Fig. 5-11 MEASURED AM-AND FM NOISE AS A FUNCTION OF BASEBAND FREQUENCY

Finally, Fig. 5-11 shows how "white" the noise spectra of IMPATT diodes are. Computations based on the present theory resulted in flat noise spectra in the range of baseband frequencies shown in Fig. 5-11. As expected, the Si diodes measured exhibited noise spectra which were effectively flat to a frequency as low as 100 Hz. The GaAs diode produced AM-and FM noise spectra which increased gradually at frequencies lower than approximately 10-20 kHz. This agrees with Ref. 41. This "flicker noise" phenomenon is known to be associated with the quality of the semiconductor surface. At present, a surface quality comparable to that of Si diodes is difficult to achieve in the case of GaAs devices. Therefore, any theory of noise for the latter devices that does not take into account flicker noise, can hold only for baseband frequencies greater than approximately 20 kHz.

CHAPTER VI

SUMMARY AND CONCLUSIONS

In this thesis, a large-signal theory of noise in oscillators has been presented, using a modified quasistationary perturbation theory and an RF-amplitude dependent perturbing noise voltage (current) source. The fluctuations in amplitude and phase are assumed RF-amplitude dependent, but still sufficiently small to permit making the usual quasilinear approximation in the perturbation theory of oscillator noise. The method introduces the concept of initial modulation rates of AM-and FM noise, whose auto- and cross spectra can be determined from a differential equation which described the active element via open-circuit noise voltage or short-circuit noise current at the sidebands about the oscillation frequency. The spectrum of the baseband noise voltage (current) can be also determined in this way, as well as the cross spectra of the latter with the noise voltage (current) sidebands. The above mentioned auto- and cross spectra depend on the magnitude and phase of the periodic voltages and currents present in the circuit as well as on the circuit impedance at baseband frequencies. The AM-and FM noise spectra at the oscillator output are computed from the initial spectra by means of a modified quasistationary perturbation theory. Unlike the large-signal theory of Kuvás²⁰, the present approach makes it possible to separate the computation of the AM-and the FM noise. This is important, since it turns out that the dependence of AM noise on signal level in oscillators is generally different from that of FM noise. The method is suitable for

active elements that can be described by a differential equation in conjunction with a Langevin noise source.

The theory has been applied to IMPATT diode oscillators, using the Read diode equations in the form given by Kuvás²⁰. This reference has also been used for the calculation of several constants needed to approximate the behaviour of abrupt-junction diodes made from Si, Ge and GaAs. Both the initial and output AM- and FM noise spectra have been computed, for various combinations of IMPATT diode and circuit parameters.

A noise-measuring system at 6 GHz has been assembled and tested. Two types of IMPATT diodes were operated as oscillators in a tunable coaxial resonator. The AM- and FM noise spectra of these oscillators were measured by means of the above mentioned system, for different bias currents and output power adjustments.

The computed spectra were compared with the experimental data of Goedbloed²¹ and those obtained by the present author. A good agreement between the theoretical and experimental data has been found. In addition, the following noise properties of IMPATT diode oscillators have been revealed or confirmed:

- 1) The perturbing noise voltage is strongly RF amplitude dependent; its two components, one in-phase and the other in quadrature with the oscillator signal, may, in general, be correlated and have non-equal spectra. The concept of an independent perturbing noise voltage source is valid only at small RF voltage amplitudes.
- 2) Minimum AM- and FM noise at the oscillator output is obtained for a large impedance in the bias circuit.
- 3) Both FM- and AM output noise modulation spectra first decrease and then increase again with increasing RF diode voltage at the frequency of oscillation. Typically, the minimum of the AM noise occurs at a higher

RF voltage amplitude than that of the FM noise, and the subsequent increase in the AM noise is less rapid than that of the FM noise. The rate of increase, positions of the minima and the absolute values of AM- and FM noise spectra depend on the diode material and on the physical and electrical parameters of the diode. Experiments have shown that, for typical commercial Si IMPATT diodes, a decrease of some 30% from the maximum RF power at a given bias current results in a considerable reduction of the FM noise, approximately by 10 dB, while the AM noise typically changes by only a few dB.

4) A low ratio of ω_a/ω_c , large drift transit angle up to approximately 5 radians and a wide avalanche region relative to the drift region reduce both AM- and FM noise. The latter increase very rapidly with decreasing avalanche region width at high RF voltages. For minimum AM- and FM noise, a given diode should be operated at a high oscillation frequency. This decreases the ratio ω_a/ω_c and increases drift transit angle.

5) Comparison of the noise performance of oscillators using IMPATT diodes made from different materials (typically Si, Ge and GaAs) is difficult to carry out in general terms. Small-signal noise theories indicate lowest noise in GaAs diodes, with Ge and Si diodes exhibiting higher noise, in that order. The theory presented in this thesis shows that these conclusions are not necessarily valid under large-signal conditions, where small differences in diode dimensions may have a greater influence than the material itself. For typical IMPATT diode dimensions such as those given in Ref. 20, the theory indicates that, at low RF voltages, GaAs diodes have a lower noise than Ge and Si diodes, in that order; at very high RF voltages, a GaAs diode may exhibit even higher noise than a Si

diode. Finally, the potentially good properties of GaAs diodes at medium RF voltages are somewhat compromised by their relatively high flicker noise at baseband frequencies below approximately 20 kHz.

It is felt that the above results and the corresponding plots are useful as guidelines for the choice of IMPATT diodes and their operating conditions. They may be useful especially in those applications where suppression of FM noise by simple "internal" means would be sufficient, so that such "external" means of noise suppression as injection locking and high Q cavity stabilization need not be used. In this respect, the particular results of this study complement the power/noise considerations of Kuvás²⁰, while the general theory presented in this thesis makes it possible to estimate large-signal AM-and FM noise of some other oscillators as well.

REFERENCES

1. I.L. Berstein, "On fluctuations in the neighbourhood of periodic motion of an auto-oscillating system", Doklad. Akad. Nauk., vol. 20, January 1938.
2. W.A. Edson, "Noise in oscillators", Proc. IRE, vol. 48, pp. 1454-1466, August 1960.
3. J.A. Mullen, "Background noise in nonlinear oscillators", Proc. IRE, vol. 48, pp. 1467-1473, August 1960.
4. K. Kurokawa, "Noise in synchronized oscillators", IEEE Trans. Microwave Theory and Tech., vol. MTT-16, pp. 234-240, April 1968.
5. K. Kurokawa, "Some basic characteristics of broadband negative resistance oscillator circuits", Bell Sys. Tech. J., vol. 48, pp. 1937-1955, July 1969.
6. M. Lax, "Classical noise V: Noise in self-sustained oscillators", Phys. Rev., vol. 160, pp. 290-307, August 1967.
7. R.D. Hempstead and M. Lax, "Classical noise. VI. Noise in self-sustained oscillators near threshold", Phys. Rev., vol. 161, pp. 350-366, September 1967.
8. A.S. Tager, "Current fluctuations in a semiconductor (dielectric) under the conditions of impact ionization and avalanche breakdown", Sov. Phys - Solid State, vol. 6, pp. 1919-1925, February 1965.
9. M.E. Hines, "Noise theory for the Read type avalanche diode", IEEE Trans. Electron Devices, vol. ED-13, pp. 158-163, January 1966.
10. R.H. Haitz, "Noise of a self-sustaining avalanche discharge in silicon: low-frequency noise studies", J. Appl. Phys., vol. 38, pp. 2935-2946, June 1967.
11. H.K. Gummel and J.L. Blue, "A small-signal theory of avalanche noise in IMPATT diodes", IEEE Trans. Electron Devices, vol. ED-14, pp. 569-580, September 1967.
12. E.F. Scherer, "Investigation of the noise spectra of avalanche oscillators", IEEE Trans. Microwave Theory Tech., vol. MTT-16, pp. 781-788, September 1968.

13. M.E. Hines, J.R. Collinet and J.G. Ondria, "FM noise suppression of an injection phase-locked oscillator", IEEE Trans. Microwave Theory Tech., vol. MTT-16, pp. 738-742, September 1968.
14. J.R. Ashley and C.B. Searles, "Microwave oscillator noise reduction by a transmission stabilizing cavity", IEEE Trans. Microwave Theory Tech., vol. MTT-16, pp. 743-748, September 1968.
15. M.S. Gupta, "Noise in avalanche transit-time devices", Proc. IEEE, vol. 59, pp. 1674-1687, December 1971.
16. H.J. Thaler, G. Ulrich and G. Weidmann, "Noise in IMPATT diode amplifiers and oscillators", IEEE Trans. Microwave Theory Tech., vol. MTT-19, pp. 692-705, August 1971.
17. G. Convert, "Sur la theorie du bruit des diodes a avalanche", Revue Technique Thompson-CSF, vol. 3, pp. 419-471, September 1971.
18. D. Delagebeaudeuf, "Analyse grand signal du fonctionnement des diodes a avalanche en mode de transit", Revue Technique Thompson-CSF, vol. 1, pp. 309-337, September 1969.
19. M.T. Vlaardingerbroek, "Theory of oscillator noise", Electron Lett., vol. 7, pp. 648-650, October 1971.
20. R.L. Kuvàs, "Noise in IMPATT diodes: Intrinsic properties", IEEE Trans. Electron Devices, vol. ED-19, pp. 220-233, February 1972.
21. J.J. Goedbloed, "An experimental verification of an analytical theory of the noise of IMPATT diode oscillators", a paper presented at the 1971 European Microwave Conference, Stockholm, Sweden.
22. J.B. Thomas, An Introduction to Statistical Communication Theory, Chapter 3, John Wiley & Sons, Inc., New York, 1969.
23. D. Middleton, An Introduction to Statistical Communication Theory, p. 398, McGraw-Hill Book Co., New York, 1960.
24. R. Kuvàs and C.A. Lee, "Quasistatic approximation for semiconductor avalanches", J. Appl. Phys., vol. 41, pp. 1743-1755, March 1970.
25. W.T. Read, "A proposed high frequency negative resistance diode", Bell Sys. Tech. J., vol. 37, pp. 401-446, March 1958.

26. C.A. Lee, R.L. Batdorf, W. Wiegman and G. Kaminsky, "Time dependence of avalanche process in silicon", J. Appl. Phys., vol. 38, pp. 2787-2796, June 1967.
27. S. Sze, Physics of Semiconductor Devices, Chapters 3 and 5, Willey-Interscience, New York, 1969.
28. W.E. Schroeder and G.I. Haddad, "Avalanche region width in various structure of IMPATT diodes", Proc. IEEE, vol. 59, pp. 1245-1248, August 1971.
29. D.L. Scharfetter and H.K. Gummel, "Large-signal analysis of silicon Read-diode oscillator", IEEE Trans. Electron Devices, vol. ED-16, pp. 64-77, January 1969.
30. A.M. Cowley, Z.A. Fazarinc, R.D. Hall, S.A. Hamilton, C.S. Yen, and R.A. Zettler, "Noise and power saturation in singly tuned IMPATT oscillators", IEEE J. Solid-State Circuits, vol. SC-5, pp. 338-345, December 1970.
31. M.T. Vlaardingerbroek, private communication.
32. J.R. Ashley, C.B. Searles, and F.M. Palka, "The measurement of oscillator noise at microwave frequencies", IEEE Trans. Microwave Theory Tech., vol. MTT-16, pp. 53-60, September 1968.
33. J.G. Ondria, "A microwave system for measurements of AM and FM noise spectra", IEEE Trans. Microwave Theory Tech., vol. MTT-16, pp. 767-781, September 1968.
34. J.L. Fikart and P.A. Goud, "The direct-detection noise-measuring system and its threshold", IEEE Trans. Instrum. Meas., vol. IM-21, pp. 219-224, August 1972.
35. J.L. Fikart, J. Nigrin, and P.A. Goud, "The accuracy of AM and FM noise measurements employing a carrier suppression filter and phase detector", IEEE Trans. Microwave Theory Tech., vol. MTT-20, pp. 702-703, October 1972.
36. R.P. Tetarenko, private communication.
37. "Microwave power generation and amplification using IMPATT diodes", Appl. Note 935, Hewlett-Packard Assoc., Palo Alto, Calif., U.S.A.
38. H.L. Stover and R.C. Shaw, "An experimental study of the basic locking behaviour of Tunnel diode oscillators", Bell Labs Technical Memorandum, July 1965.

39. V.W. Chan and P.A. Levine, "A comparative study of IMPATT diode noise properties", Proceedings of the Third Biennial Cornell Electrical Engineering Conference, vol. 3, pp. 165-174, Cornell University, 1971.
40. H. Statz and H.A. Haus, "The dependence of noise in IMPATT diodes on doping profile", Proceedings of the Third Biennial Cornell Electrical Engineering Conference, vol. 3, pp. 155-164, Cornell University, 1971.
41. J.R. Ashley, private communication.

APPENDIX-A

DERIVATION OF SOME READ DIODE RELATIONS IN NORMALIZED FORM

The purpose of this Appendix is to derive the relations between electric field and external current, conduction current and terminal voltage for the Read diode, in a suitably normalized form.

We shall start with the introduction of the following normalized quantities in the frequency domain:

Normalized conduction current

$$i_c(\omega) = I_c(\omega)/I_0 \quad . \quad (A.1)$$

Normalized external current

$$i_{ex}(\omega) = I_{ex}(\omega)/I_0 \quad . \quad (A.2)$$

Normalized electric field

$$e(\omega) = E(\omega)/E_b \quad . \quad (A.3)$$

Normalized voltage

$$v(\omega) = V(\omega)/V_b \quad . \quad (A.4)$$

In the above, the frequency dependent quantities, denoted by capital letters, are either Fourier transforms or Fourier series components of the corresponding stochastic or deterministic quantities, respectively, in the time domain.

Furthermore, we shall use the "avalanche frequency" parameter

ω_a defined by

$$\omega_a^2 = mI_0/(\epsilon A \tau E_b) = mI_0/(\epsilon A k \tau_a E_b) \quad , \quad (A.5)$$

where I_0 is the dc (bias) current through the diode, E_b is the electric field at breakdown, ϵ is dielectric permittivity, A is the effective cross-sectional area of the diode, τ_a is the transit time through the avalanche region, k is the correction factor as explained in Sec. 4-1-3 and m is the exponent in the approximation of $\alpha(E_a)$ in Sec. 4-1.

A critical parameter for Read diode oscillators is the ratio of the avalanche-to-carrier frequency:

$$\begin{aligned} (\omega_a/\omega_c)^2 &= mI_0/(\epsilon A k \tau_a E_b \omega_c^2) = (m/2k)(1/\omega_c \tau_a)(I_0/\omega_c C_d V_b) \\ &= (D/2)(I_0/\omega_c C_d V_b) \quad , \end{aligned} \quad (A.6)$$

where C_d is the diode geometrical capacitance

$$C_d = \epsilon A/W \quad , \quad (A.7)$$

V_b is the breakdown voltage of the abrupt p-n junction which is to be approximated by the Read model (c.f. Sec. 4-1-3, Eq. (4.25))

$$V_b = E_b W/2 \quad , \quad (A.8)$$

and the parameter D is given by

$$D = m/(k \omega_c \tau_a) \quad . \quad (A.9)$$

D can be more conveniently expressed in terms of other important Read diode parameters; the drift transit angle $\omega_c \tau_d$ where τ_d is the transit time of electrons or holes through the drift region, and the equivalent avalanche-to-drift region length ratio w_a/w_d :

$$D = (m/k)/(\omega_c \tau_d \times w_a/w_d) \quad , \quad (A.10)$$

where w_a and w_d are the avalanche- and drift region length, respectively.

Let us now turn to Eq. (4.12) for the external current:

$$I_{ex}(t) = I_c(t) + \epsilon A \frac{dE_a(t)}{dt} \quad . \quad (A.11)$$

This relation is valid at the boundary of the avalanche and drift regions and is a special case of the more general equation

$$I_{ex}(t) = I_c(t,x) + \epsilon A \frac{dE(t,x)}{dt} \quad . \quad (A.12)$$

Eq. (A.12) can be integrated along the drift region:

$$\frac{1}{w_d} \int_{w_a}^w I_{ex}(t) dx = I_{ex}(t) = \frac{1}{w_d} \int_{w_a}^w I_c(t,x) dx + \frac{\epsilon A}{w_d} \frac{d}{dt} \left(\int_{w_a}^w E(t,x) dx \right) \quad . \quad (A.13)$$

Now the voltage $V(t)$ across the diode is given by

$$V(t) = - \int_0^w E(t,x) dx = -E_a(t)w_a - \int_{w_a}^w E(t,x) dx \quad , \quad (A.14)$$

since the electric field may be assumed to be independent of position in the avalanche region.

Because of the absence of ionization in the drift region and with the assumption of a saturated drift velocity of the carriers, the particle current $I_c(t, x)$ can be expressed as a travelling wave

$$I_c(t, x) = I_c[t - (x - w_a)/v_s, x = w_a] \quad . \quad (A.15)$$

With a new variable

$$t' = t - (x - w_a)/v_s \quad , \quad (A.16)$$

the first integral on the right-hand side of Eq. (A.3) can be rewritten as follows:

$$\frac{1}{w_d} \int_{w_a}^w I_c(t, x) dx = - \frac{v_s}{w_d} \int_t^{t-\tau_d} I_c(t') dt' = \frac{1}{\tau_d} \int_{t-\tau_d}^t I_c(t') dt' \quad , \quad (A.17)$$

where $I_c(t')$ is the conduction current at $x = w_a$.

Eq. (A.13) now becomes

$$I_{ex}(t) = \frac{1}{\tau_d} \int_{t-\tau_d}^t I_c(t') dt' - C_d \frac{w}{w_d} \frac{d}{dt} [V(t) + E_a(t)w_a] \quad . \quad (A.18)$$

Let us Fourier transform Eqs. (A.11) and (A.18):

$$I_{ex}(\omega) = I_c(\omega) + j\omega \epsilon A E_a(\omega) \quad . \quad (A.19)$$

Normalizing and using Eq. (A.6) we obtain

$$\begin{aligned}
 i_{ex}(\omega) &= i_c(\omega) + j(\omega \varepsilon A E_b / I_0) e_a(\omega) = \\
 &= i_c(\omega) + j(\omega / \omega_c) D(\omega_a / \omega_c)^{-2} e_a(\omega) \quad .
 \end{aligned} \tag{A.20}$$

From Eq. (A.18) we have

$$\begin{aligned}
 I_{ex}(\omega) &= \frac{1 - \exp(-j\omega\tau_d)}{j\omega\tau_d} I_c(\omega) - j\omega C_d \frac{w}{w_d} [V(\omega) + E_a(\omega)w_a] \\
 &= \theta(\omega) I_c(\omega) - j(\omega / \omega_c) \omega_c C_d (w/w_d) [V(\omega) + E_a(\omega)w_a] \quad , \tag{A.21}
 \end{aligned}$$

where

$$\theta(\omega) = (1 - \exp(-j\omega\tau_d)) / j\omega\tau_d \quad . \tag{A.22}$$

Normalizing and using Eq. (A.6) again, we obtain

$$\begin{aligned}
 i_{ex}(\omega) &= \theta(\omega) i_c(\omega) - j(\omega / \omega_c) (\omega_c C_d / I_0) (w/w_d) (E_b w / 2) v(\omega) + \\
 &\quad - j(\omega / \omega_c) \omega_c C_d / I_0 (w E_b) (w_a / w_d) e_a(\omega) \\
 &= \theta(\omega) I_c(\omega) - j(\omega / \omega_c) (D/2) (\omega_a / \omega_c)^{-2} (w/w_d) v(\omega) + \\
 &\quad - j(\omega / \omega_c) D(\omega_a / \omega_c)^{-2} (w_a / w_d) e_a(\omega) \quad , \tag{A.23}
 \end{aligned}$$

where $\theta(\omega)$ can also be written in the normalized form

$$\theta(\omega) = \{1 - \exp[-j(\omega/\omega_c)\omega_c\tau_d]\} [j(\omega/\omega_c)\omega_c\tau_d]^{-1} . \quad (\text{A.24})$$

On eliminating $i_c(\omega)$ from Eqs. (A.20) and (A.23) and setting $i_{ex}(\omega) = 0$, an equation is obtained for the normalized open-circuit voltage $v^\infty(\omega)$ in terms of the normalized field $e_a(\omega)$:

$$v^\infty(\omega) = -2[\theta(\omega) + (w_a/w_d)][1 + (w_a/w_d)]^{-1} e_a(\omega) . \quad (\text{A.25})$$

Similarly, eliminating $i_{ex}(\omega)$ from Eqs. (A.20) and (A.23) yields a relation for the normalized voltage $v(\omega)$ in terms of the normalized electric field $e_a(\omega)$ and the normalized conduction current $i_c(\omega)$:

$$v(\omega) = 2 \left\{ \frac{i_c(\omega)[\theta(\omega) - 1]}{j(\omega/\omega_c)D(\omega_a/\omega_c)^{-2}[1 + (w_a/w_d)]} e_a(\omega) \right\} . \quad (\text{A.26})$$

Returning to Eq. (A.21) and using

$$V(\omega) = I_{ex}(\omega)Z(\omega) , \quad (\text{A.27})$$

where $Z(\omega)$ is the impedance of the external circuit, we obtain

$$\begin{aligned} I_{ex}(\omega) = & I_c(\omega)\theta(\omega) - j(\omega/\omega_c)\omega_c C_d (w_a/w_d) w E_a(\omega) + \\ & - j(\omega/\omega_c)\omega_c C_d (w/w_d) I_{ex}(\omega) Z(\omega) . \end{aligned} \quad (\text{A.28})$$

Normalizing and introducing the normalized impedance

$$z(\omega) = \omega_c C_d Z(\omega) \quad (\text{A.29})$$

yields the equation

$$\begin{aligned}
 i_{\text{ex}}(\omega) \left[1 + j \left(\frac{\omega}{\omega_c} \right) z(\omega) \left(1 + \frac{w_a}{w_d} \right) \right] &= i_c(\omega) \theta(\omega) - j \left(\frac{\omega}{\omega_c} \right) \frac{C_d}{I_o} E_b \frac{w_a}{w_d} e_a(\omega) \\
 &= i_c(\omega) \theta(\omega) - j \left(\frac{\omega}{\omega_c} \right) D \left(\frac{w_a}{w_c} \right)^{-2} \frac{w_a}{w_d} e_a(\omega) \quad .
 \end{aligned}
 \tag{A.30}$$

Elimination of $i_c(\omega)$ from Eqs. (A.20) and (A.30) yields

$$i_{\text{ex}}(\omega) = \frac{j(\omega/\omega_c) D(\omega_a/\omega_c)^{-2} [\theta(\omega) + (w_a/w_d)] e_a(\omega)}{\theta(\omega) - \{1 + j(\omega/\omega_c) z(\omega) [1 + (w_a/w_d)]\}} \quad .
 \tag{A.31}$$

Similarly, the elimination of $i_{\text{ex}}(\omega)$ from Eqs. (A.20) and (A.30) results in an expression for $i_c(\omega)$:

$$i_c(\omega) = \frac{j(\omega/\omega_c) D(\omega_a/\omega_c)^{-2} \{1 + j(\omega/\omega_c) z(\omega) [1 + (w_a/w_d)] + (w_a/w_d)\}}{\theta(\omega) - \{1 + j(\omega/\omega_c) z(\omega) [1 + (w_a/w_d)]\}} e_a(\omega) \quad .
 \tag{A.32}$$

Eqs. (A.31) and (A.32) can be formally simplified by introducing

$$\psi(\omega) = \frac{\theta(\omega) + (w_a/w_d)}{\theta(\omega) - \{1 + j(\omega/\omega_c) z(\omega) [1 + (w_a/w_d)]\}} \quad .
 \tag{A.33}$$

On substituting Eq. (A.33) into (A.31) and (A.32), we obtain

$$i_{\text{ex}}(\omega) = j(\omega/\omega_c) (\omega_a/\omega_c)^{-2} D \psi(\omega) e_a(\omega)
 \tag{A.34}$$

and

$$i_c(\omega) = j(\omega/\omega_c) (\omega_a/\omega_c)^{-2} D [\psi(\omega) - 1] e_a(\omega) \quad .
 \tag{A.35}$$

The ratio of the two currents is

$$i_{\text{ex}}(\omega)/i_c(\omega) = \psi(\omega)/[\psi(\omega)-1] \quad . \quad (\text{A.36})$$

APPENDIX-B

LARGE-SIGNAL DESCRIPTION OF THE READ DIODE

In a deterministic analysis, the stochastic term in the Read diode equation (4.13) is deliberately left out so that this equation reduces to Eq. (4.4) which we shall rewrite here, using the symbol $I_{cd}(t)$ to denote the deterministic current:

$$\left[\frac{\partial}{\partial t} + (M\tau)^{-1} \right] I_{cd}(t) = \frac{I_s}{\tau} . \quad (B.1)$$

It has been shown in Ref. 20 that, under usual operating conditions, the conduction current $I_{cd}(t)$ can be expressed by means of the electric field component E_{a1} in the avalanche region in the following manner: Let f_n be defined as the ratio of the Bessel functions of order n and zero, respectively:

$$f_n = I_n(D_1)/I_0(D_1) , \quad (B.2)$$

where

$$D_1 = (m/\omega_c k\tau_a) |E_{a1}/E_b| = D |e_{a1}| . \quad (B.3)$$

Using the expansion

$$i_{cd}(t) = \frac{I_{cd}(t)}{I_0} = 1 + \frac{1}{2} \sum_{n=-\infty}^{\infty} i_{cn} \exp(jn\omega_c t) , \quad (B.4)$$

the normalized conduction current components i_{cn} are given by²⁰

$$i_{cn} = 2(-1)^n \left\{ f_n + \left(\frac{\omega_a}{\omega_c} \right)^2 \sum_{p=2}^{\infty} (f_{p-n} + f_{p+n} - 2f_n f_p) \frac{f_p}{p^2} \right\} \quad n \neq 0. \quad (B.5)$$

This relation has been derived for the electric field phase angle chosen to be equal to $\pi/2$:

$$e_{a1} = j|e_{a1}| \quad (B.6)$$

The normalized electric field e_{a1} is the initial value with which the large-signal calculations are started. Having obtained the normalized conduction current components i_{cn} , the external current component i_{ex1} at the fundamental frequency ω_c is obtained from Eq. (A.19):

$$i_{ex1} = i_{c1} + jD(\omega_a/\omega_c)^{-2}e_{a1} = I_{c1} - D(\omega_a/\omega_c)^{-2}|e_{a1}| \quad (B.7)$$

The normalized diode voltage component v_1 , at the fundamental frequency ω_c is computed from Eq. (A.26):

$$v_1 = \frac{V_1}{V_b} = 2 \left\{ \frac{i_{c1} [\theta(\omega_c) - 1]}{j(\omega_a/\omega_c)^{-2} D [1 + \omega_a/\omega_d]} - j|e_{a1}| \right\} \quad (B.8)$$

In order to sustain oscillations, the external circuit must exhibit the normalized impedance (defined by Eq. (A.29))

$$\begin{aligned}
 z(\omega_c) &= \omega_c C_d Z(\omega_c) = \omega_c C_d V_1 / I_{ex1} = (\omega_c C_d I_o / V_b)(v_1 / i_{ex1}) = \\
 &= (D/2)(\omega_a / \omega_c)^{-2} v_1 / i_{ex1} \quad .
 \end{aligned}
 \tag{B.9}$$

If the external circuit is a simple series combination of a reactance and resistance, the normalized output voltage component v_c at the carrier frequency ω_c is given by

$$v_c = V_c / V_b = R_e(V_1) / V_b = R_e(v_1) \quad . \tag{B.10}$$

The total normalized power obtained at frequency ω_c is calculated from

$$p_T = P_T / V_b I_o = 0.5 v_c i_{ex1} \quad . \tag{B.11}$$

To make comparisons with actual diode measurements, the effect of parasitic series resistance must be taken into account. The ratio of the effective normalized output power and the total normalized power is given by

$$p_{eff} / p_T = 1 - r_s / R_e z(\omega_c) \quad , \tag{B.12}$$

where r_s is the series resistance normalized with respect to $1/\omega_c C_d$.

APPENDIX-C

DERIVATION OF THE COEFFICIENTS $a_{p-l,l}$ IN THE CONVERSION MATRIX (4.44)

Using the normalized electric field and current, introduced in Appendix-A, Eq. (4.36) may be written in the form

$$\sum_{n=-M}^M A_n^0 e^{j(\omega+n\omega_c)t} + B_n^0 e^{-j(\omega+n\omega_c)t} = F(\omega) \quad , \quad (C.1)$$

where the coefficients A_n^0 and B_n^0 , from Eqs. (4.37) - (4.40), are

$$A_0^0 = j\omega \epsilon A E_b [m(E_{ao} - E_b)/E_b - jk\omega\tau_a] - mI_o \quad (C.2)$$

$$B_0^0 = I_o [jk\omega\tau_a - m(E_{ao} - E_b)/E_b] \quad (C.3)$$

$$A_n^0 = j(m\omega \epsilon A/2) E_{an}^* - (m/2) I_{en}^* \quad n \neq 0 \quad (C.4)$$

$$B_n^0 = -(mI_o/2E_b) E_{an}^* \quad n \neq 0 \quad (C.5)$$

Eqs. (C.2) - (C.5) should now be also normalized. First we note that⁸

$$m(E_{ao} - E_b)/E_b = -\bar{M}^{-1} \quad , \quad (C.6)$$

where \bar{M} is the average (dc) multiplication factor. In analogy with Ref. 8 we introduce the parameter

$$\omega_M = (k\tau_a \bar{M})^{-1} , \quad (C.7)$$

which has the dimension of frequency. Now, using the normalizations and parameters introduced in Appendix-A, the coefficients A_n^0 and B_n^0 can be rewritten as follows:

$$\begin{aligned} A_n^0 &= mI_0 \left\{ \frac{j\omega \epsilon A E_b k\tau_a}{mI_0} \left[m \frac{E_{ao} - E_b}{E_b k\tau_a} - j\omega \right] - 1 \right\} = \\ &= mI_0 \{ j(\omega/\omega_a)^2 [-(\omega_M + j\omega)] - 1 \} = \\ &= mI_0 \{ -j(\omega_a/\omega_c)^2 (\omega/\omega_c) [(\omega_M/\omega_c) + j(\omega/\omega_c)] - 1 \} . \end{aligned} \quad (C.8)$$

$$\begin{aligned} B_0^0 &= mI_0 [j\omega k\tau_a/m + k\tau_a \omega_M/m] \\ &= mI_0 [j(\omega/\omega_c)/D + (\omega_M/\omega_c)/D] = \\ &= (mI_0/D) [(\omega_M/\omega_c) + j(\omega/\omega_c)] . \end{aligned} \quad (C.9)$$

$$\begin{aligned} A_n^0 \quad n \neq 0 &= (mI_0/2) [j(\omega \epsilon A E_b / mI_0) m e_{an}^* - i_{exn}^*] \\ &= (mI_0/2) \{ j(\omega \epsilon A E_b k\tau_a / mI_0) (\omega_c^2 m / \omega_c k\tau_a) e_{an}^* - i_{exn}^* \} \\ &= (mI_0/2) [j(\omega/\omega_c) (\omega_a/\omega_c)^{-2} D e_{an}^* - i_{exn}^*] . \end{aligned} \quad (C.10)$$

$$B_n^0 \quad n \neq 0 = -(mI_0/2) e_{an}^* . \quad (C.11)$$

Using Eq. (A.31), Eq. (C.1) may be written in the form

$$\sum_{n=-M}^M a_n(\omega) e_{as}(\omega+n\omega_c) = F(\omega)/mI_0, \quad (C.12)$$

where $a_n(\omega)$ is determined by means of Eqs. (C.8) - (C.11) and (A.33) - (A.36) as follows:

$$\begin{aligned} a_0(\omega) &= [A_0^0 + B_0^0 j(\omega/\omega_c)(\omega_a/\omega_c)^{-2} D\psi(\omega)](mI_0)^{-1} \\ &= -j(\omega_a/\omega_c)^{-2}(\omega/\omega_c)[(\omega_M/\omega_c)+j(\omega/\omega_c)]^{-1} + \\ &\quad D^{-1}[(\omega_M/\omega_c)+j(\omega/\omega_c)]j(\omega/\omega_c)(\omega_a/\omega_c)^{-2} D\psi(\omega) = \\ &= j(\omega/\omega_c)(\omega_a/\omega_c)^{-2}[(\omega_M/\omega_c)+j(\omega/\omega_c)][\psi(\omega)-1]^{-1}. \end{aligned} \quad (C.13)$$

$$\begin{aligned} a_n(\omega) &= \{A_n^0 + B_n^0 j[(\omega+n\omega_c)/\omega_c](\omega_a/\omega_c)^{-2} D\psi(\omega+n\omega_c)\}(mI_0)^{-1} = \\ &= (1/2)[j(\omega/\omega_c)(\omega_a/\omega_c)^{-2} D e_{an}^* + j n(\omega_a/\omega_c)^{-2} D \psi^*(n\omega_c) e_{an}^*] + \\ &\quad -(1/2)\{j[(\omega+n\omega_c)/\omega_c](\omega_a/\omega_c)^{-2} D \psi(\omega+n\omega_c) e_{an}^*\} = \\ &= -\frac{1}{2} j e_{an}^* \left(\frac{\omega_a}{\omega_c}\right)^{-2} D \left\{ \frac{\omega}{\omega_c} + n \psi^*(n\omega_c) - \frac{\omega+n\omega_c}{\omega_c} \psi(\omega+n\omega_c) \right\} \\ &= -\frac{1}{2} \frac{i c n}{n[\psi^*(n\omega_c)-1]} \left\{ \frac{\omega+n\omega_c}{\omega_c} [1-\psi(\omega+n\omega_c)] + n[\psi^*(n\omega_c)-1] \right\} = \\ &= -(i c n^*/2) \{1 + [(\omega+n\omega_c)/\omega_c][1-\psi(\omega+n\omega_c)]/n[\psi^*(n\omega_c)-1]\}. \end{aligned} \quad (C.14)$$

The coefficients $a_{p-l,l}$ in Eq. (4.44), Chapter IV, are obtained as follows:

$$a_{p-l,l} = a_n(\omega=\Omega+l\omega_c), \quad (C.15)$$

with

$$p-l = n \quad . \quad (C.16)$$

The parameter

$$\psi(\omega) = \frac{\theta(\omega) + (w_a/w_d)}{\theta(\omega) - [1 + j(\omega/\omega_c)z(\omega)][1 + (w_a/w_d)]} \quad (C.17)$$

can be somewhat simplified for specific frequencies:

$$\psi(\Omega) = [j(\Omega/\omega_c)z(\Omega)]^{-1} \quad , \quad (C.18)$$

since $\theta(\Omega) = 1$ for $\Omega \ll \omega_c$,

$$\left. \begin{array}{l} \psi(\Omega + q\omega_c) \\ |q| > 1 \\ \psi(n\omega_c) \\ |n| > 1 \end{array} \right\} = 0 \quad \text{since } z(\omega \gg \omega_c) \rightarrow \infty \quad . \quad (C.19)$$

Finally, from Eq. (A.36) we have

$$\psi(\omega_c) = [1 - i_{c1}/i_{ex1}]^{-1} \quad . \quad (C.20)$$

The conduction current components i_{cn} and the external current i_{ex1} , needed in the expressions for the coefficients $a_n(\omega)$, are obtained from the large-signal analysis described in Appendix-B.

B30053